Photocopy and Use Authorization

In presenting this thesis in partial fulfillment of the requirements for an advanced degree at Idaho State University, I agree that the Library shall make it freely available for inspection. I further state that permission for extensive copying of my thesis for scholarly purposes may be granted by the Dean of Graduate Studies, Dean of my academic division, or by the University Librarian. It is understood that any copying or publication of this thesis for financial gain shall not be allowed without my written permission.

Signature:______________________________

Date:__________________________________

Influences of Tectonic and Geomorphic Processes on Fault Scarp Height Variability in an Extensional Tectonic Terrane, Teton Fault, Wyoming

by

Kyla Grasso

A thesis

submitted in partial fulfillment

of the requirements for the degree of

Master of Science in the Department of Geosciences

Idaho State University

Spring 2020

Committee Approval

To the Graduate Faculty:

The members of the committee appointed to examine the thesis of KYLA GRASSO find it satisfactory and recommend that it be accepted.

Dr. Glenn Thackray,
Major Advisor

Dr. Benjamin Crosby,
Committee Member

Dr. Tracy Payne,
Graduate Faculty Representative

Acknowledgements

First and foremost, a big thank you to the community that makes ISU's Geosciences Department so uniquely welcoming and supportive. The faculty, staff, students, and dogs of this department have made my time at ISU more enjoyable than I imagined graduate school might be.

Thank you to my graduate thesis committee as a whole for sharing their guidance, insight, and comments as this project and thesis came together. Thank you to my advisor, Glenn Thackray, for making this project and my time at Idaho State University a reality. I am sincerely grateful for the opportunity to work on a project that included a supportive and encouraging advisor who offered reliable guidance balanced with the freedom to explore ideas. And Ben Crosby, thank you for helping me refine this work, improve my technical skills, and leading me to an incredible employment opportunity after graduation. I'm sure we will cross paths (hopefully on a landslide) in the near future.

Thank you to the researchers who have published so many previous works on the Teton Range, fault dynamics, paleoseismicity, and all of the other topics this project has touched upon.

I would also like to thank the many other folks who gave me help and feedback along the way: Emily Chojnacky for making up "bear songs" and putting up with my zig-zagging, spur of the moment, 45-degree slope climbing whims while working as my field assistant- your dedication to surviving hail storms, lone grizzly bear cubs, and wet logs is commendable. Stacy Henderson for providing the many long conversations, internet memes, and excuses to go trail running that were perhaps not necessary, but were very much needed, distractions from this project. And to the rest of the 2018 graduate student cohort for providing feedback on this project as it came together over the past year and a half.

A grateful thank you goes out to the staff of the American Alpine Club Teton Climbers Ranch for hosting a couple of geologists for several weeks over the summer of 2019, and to the staff of the University of Wyoming National Park Service Research Station for making their bunkhouses a comfortable place to stay while doing field work.

This project was funded by National Science Foundation grant 1755079 to Idaho State University (PI Thackray) with additional contributions from the Career Path Internship Program at Idaho State University, and housing and logistical support provided by the University of Wyoming National Park Service Research Station and the American Alpine Club Climber's Ranch.

Contents

List of Figures

List of Tables

Influences of Tectonic and Geomorphic Processes on Fault Scarp Height Variability in an Extensional Tectonic Terrane, Teton Fault, Wyoming

Thesis Abstract-Idaho State University (2020)

Landscape disturbance events (e.g., earthquakes, slope failures) play key roles in landscape evolution in tectonically active areas. Along the 75-km Teton fault, fault scarps vary in height by up to tens of meters over short (<1 km) distances. LiDAR-based mapping indicates that scarp height is affected by glacial geomorphology, slope failure, and alluvial processes. I propose a four-section model of the Teton fault based on vertical separation across fault scarps and the expected pattern of normal fault behavior. At a broad scale, vertical separation is greatest along the southern portion of the fault. At a finer scale, vertical separation is lower at the ends of the fault and at three locations within the central fault zone, and higher between these areas. The transition zones between these four sections may represent boundaries between fault sections or segments and may have important implications for hazards analysis.

Key words: Teton Range, Teton fault, LiDAR, slope failure

Chapter I: Introduction

Introduction

The Teton fault is expressed at the surface as a 75-km long series of north-northeast trending normal fault scarps on the eastern foot of the Teton Range (Figure 1). This project identifies and characterizes fault scarps and slope failure deposits, analyzes vertical separation across fault scarps, and discusses the implications of variable scarp height as it pertains to fault segmentation and hazards assessment along the Teton fault.

Large-scale landscape disturbance events (e.g., earthquakes, slope failures, and floods) play key roles in landscape evolution in tectonically active areas (Keefer, 1984). Similarly, glacial and alluvial processes alter landscape geomorphology and influence sediment flux in alpine environments (McColl and Davies, 2013). Smaller-scale processes (e.g., alluvial erosion and deposition, hillslope diffusion) also influence landscape geomorphology. These processes alter the surface expression of faults and introduce landscape complexity along range fronts and also play a significant role in shaping landscapes. Along the Teton range front, fault scarps are well-expressed and vary in height by up to tens of meters over short (<1 km) and long distances. The effects of slope failure and other geomorphic processes on fault scarp height along the range front have not previously been addressed, and along-strike, systematic variability in scarp height can be revisited and reanalyzed with detailed LiDAR data and associated digital techniques.

This thesis builds on previous and on-going work centered on building a more complete model and understanding of the paleoseismic activity, surface faulting and offset, and the occurrence and distribution of large-scale landscape disturbance events including slope failures and glacial activity that have led to the modern Teton landscape. It presents the results of detailed fault scarp and slope failure deposit mapping, fault scarp topographic profiling, simple scarp height and vertical separation analyses along the Teton fault and discusses implications for fault segmentation and seismotectonic and slope failure hazard assessments.

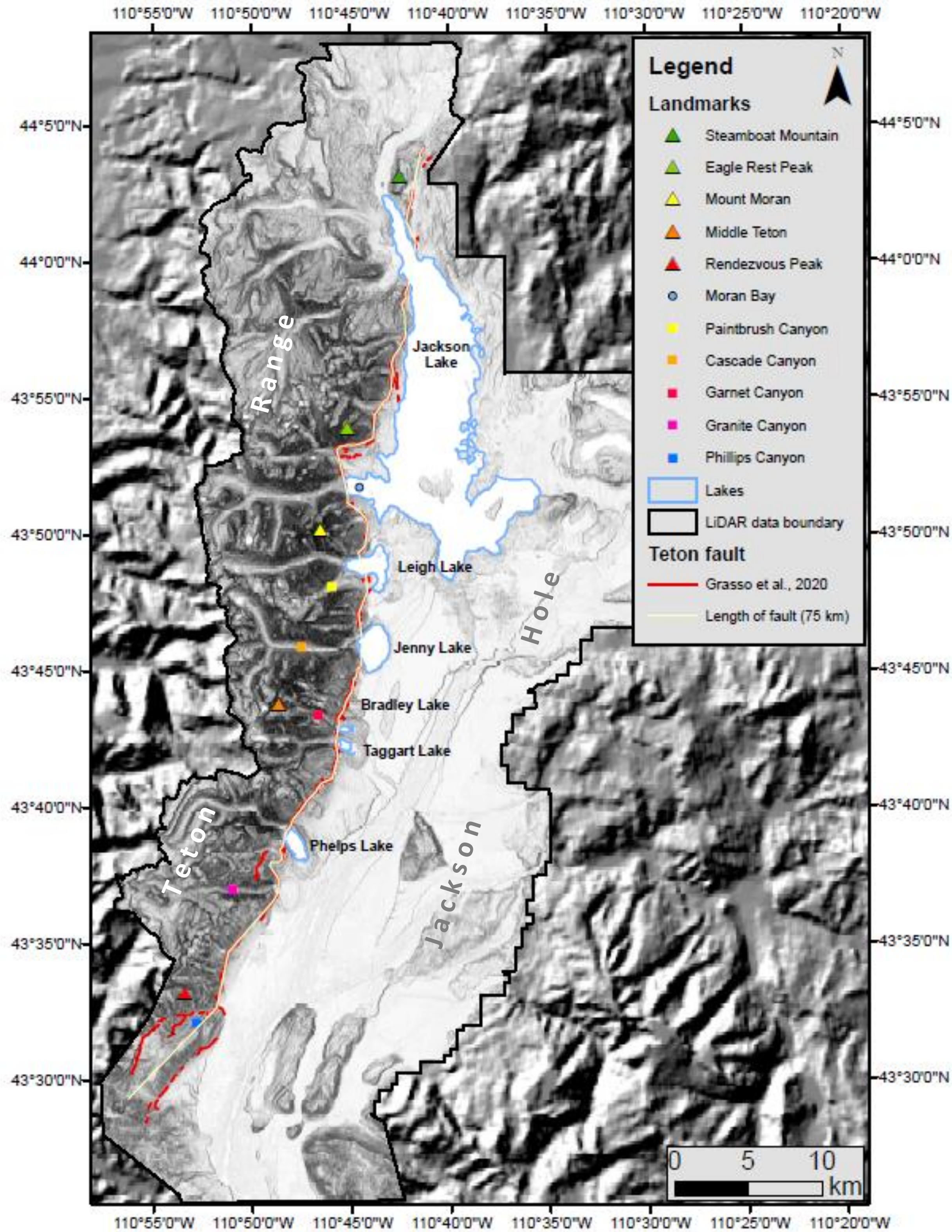

Figure 1. Study area. The study area spans an approximately 1-km wide swath following the Teton fault. A 90-m resolution DEM provides the backdrop to the 1-m resolution LiDAR-derived slope map shown here.

Study area and approach

The study area consists of an approximately 1-km wide zone straddling the Teton fault (Figure 1). Digital and field mapping were used to develop fault scarp profiles and characterize slope failure and other processes that have influenced scarp height along the Teton fault. Light detection and ranging (LiDAR) data were used to generate digital elevation (DEM), hillshade, and slope models of the study area. The LiDAR data was collected in Grand Teton National Park by Woolpert, Inc. under contract to the United States Geological Survey (USGS) over the summer of 2014 (Woolpert, Inc., 2015). Data was provided to USGS in ERDAS .IMG format with 1 m cell size and vertical error ranging from -0.194 m to 0.135 m with an average of 0.027 m after hydrologic flattening was conducted. This dataset provides the basis for digital mapping and scarp profiling used in this project. A 90-m resolution DEM of Wyoming was used as a regional backdrop for mapping (Wyoming Geographic Information Science Center, 1997).

Digital- and field-mapping approaches and fault scarp vertical separation analysis were used to identify and characterize fault scarp geomorphology and slope failure deposits along the Teton range front. Simple scarp height is defined as the vertical distance between the highest and lowest points across the fault scarp, while vertical separation is defined as the restored vertical distance between the tectonically undeformed footwall and hanging wall surfaces. The reader is referred to Chapter II for a detailed description of the methods, findings, and interpretations of the data generated by this project. The LiDAR-derived slope model, Teton fault, and local landmarks are shown in (Figure 1).

Along-strike, variable slip of the Teton fault

Along-strike variation in slip rate (and therefore vertical separation across fault scarps, VS) is expected to increase toward the central portion of normal faults (Cowie and Roberts, 2001; Densmore et al., 2007). Previous authors suggest that the Teton fault has three primary sections that may have contrasting offset rates (Figure 2) (Susong et al., 1987; Smith et al., 1993; Roberts and Burbank, 1993; Byrd et al., 1994). The age of Teton fault initiation, total fault offset, and fault slip rate have been the subject of debate.

Estimates of when uplift initiated on the Teton fault vary from 15-2 Ma. Apatite (U-Th)/He and fission track ages of samples from the footwall of the Teton fault indicate that uplift initiated at the northern end of the fault 15-13 Ma and proceeded southward over time (Brown et al., 2017). However, this timing contrasts with estimates from several other studies. One of the earliest estimates of Teton fault initiation was given by Love (1977), who, based on inferences from the Teewinot Formation stratigraphy (~3 km east of the Teton range front), suggested that the fault must have initiated post ~5 Ma. The 4.45 Ma Kilgore Tuff, erupted from the Heise volcanic field on the Snake River Plain of southeast Idaho, has been mapped in the Jackson Hole valley and its presence may indicate that the Teton Range was not a significant orographic barrier to volcanic ash deposition at the time; hence, uplift on the Teton fault had not produced significant topography by the time of eruption (Morgan and McIntosh, 2005). Lake sediments and pollen data from the Shooting Iron Formation, interpreted as late Pliocene in age, have been used to infer that the Teton fault initiated more recently than ~2 Ma (Leopold et al., 2007). The timing of fault initiation is intimately related to estimates of long-term fault offset rates.

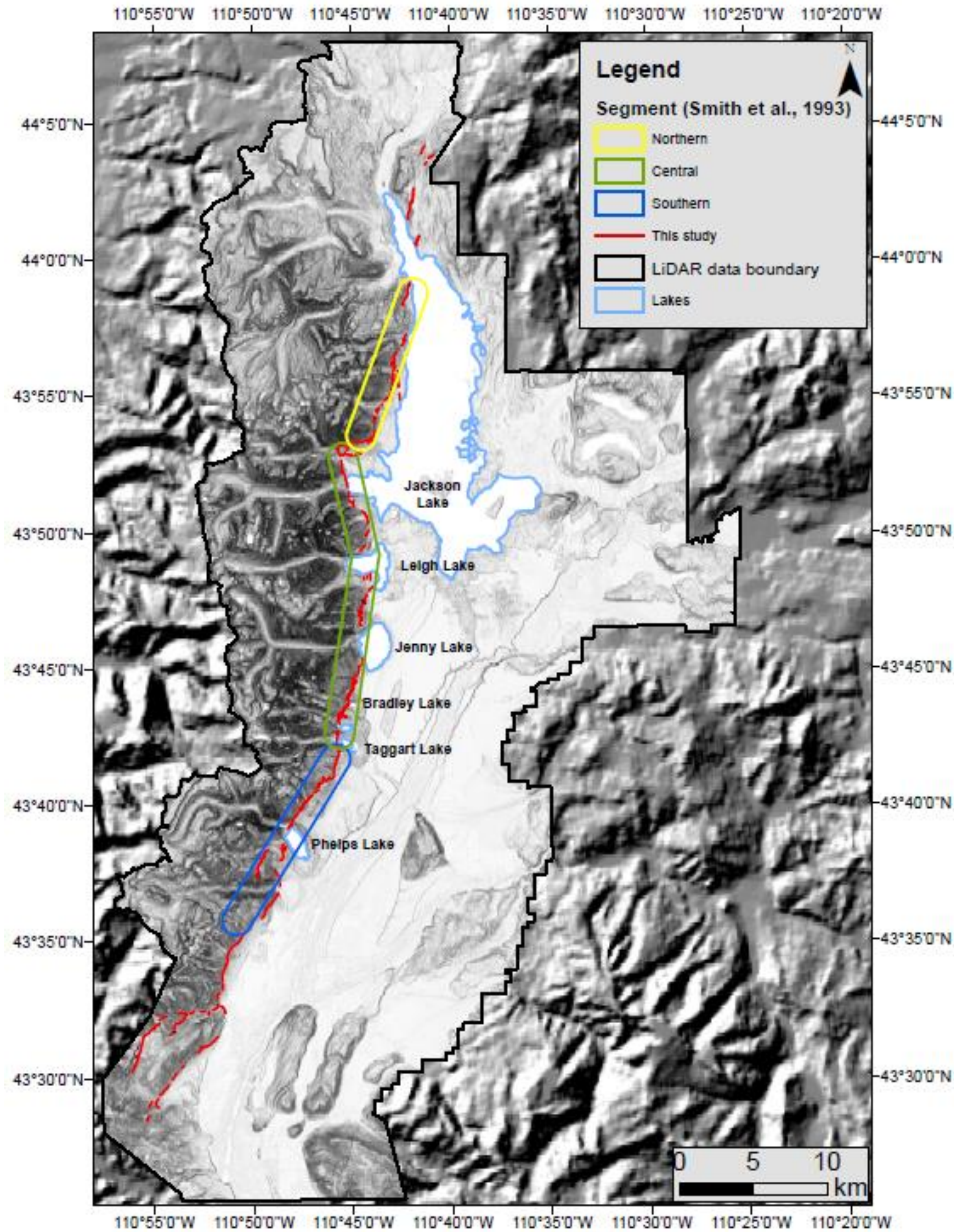

Figure 2. Three-segment model of the Teton fault proposed by Susong et al. (1987) and built upon by Smith et al. (1993). Note that these studies did not span the entire length of the Teton fault and relied on scarp profiling at 17 locations in their three-segment interpretation of the fault. Section boundaries are approximate and based on interpretation from figures in Susong et al. (1987) and Smith et al. (1993).

Fault offset rates have been estimated from paleoseismic trenching studies and vertical separation across deglacial surfaces of known age (Table 1). At Granite Canyon, a rate of ~1.3 mm/yr was calculated for the latest Pleistocene to mid-Holocene (14.4-4.6 ka) (Byrd et al., 1994). This was the earliest studies of fault offset and paleoseismicity along the Teton fault. More recent work at the Buffalo Bowl site, resulted in a Holocene closed-interval vertical slip rate of ~0.9 mm/yr. Using vertical separation across fault scarps and a deglacial surface that dates to 14.7±1.1 ka, Thackray and Staley (2017) calculated an average postglacial vertical separation rate of 0.82±0.13 m/k.y. Paleoseismic trenches across two scarps at Leigh Lake revealed evidence for two Holocene earthquake events at ~5.9 and ~10 ka, which are associated with 1.1-1.7 m and 0.4-1.7 m of vertical displacement, respectively; estimates of fault offset rates were not published with the study (Zellman et al., 2019c). A summary of data from paleoseismic trenching studies is given in (Table 1).

Table 1. Summary of paleoseismic trench data from previous authors. Radiocarbon (^{14}C) and optically-stimulated luminescence (OSL) methods are commonly used to date offset sediments in paleoseismic trenching studies.

Location	Number of trenches	Earthquake event timing	Dating method	Reference
Steamboat Mountain	2	SM1: between 3.8 and 6.1 ka SM2: prior to 7.1 ka	^{14}C radiocarbon and OSL	Zellman et al., 2018
Leigh Lake	2	LL1: 5.9 ka (4.8-7.1 ka) LL2: 10 ka (9.7-10.4 ka)	^{14}C radiocarbon and OSL	Zellman et al., 2019
Granite Canyon	1	GC1: ~4.8-7.0 ka GC2: ~7.9 ka	^{14}C radiocarbon	Byrd et al., 1995
Buffalo Bowl	1	BB1: 4.6 ka (3.9-5.7 ka) BB2: 7.1 ka (5.5-8.8 ka) BB3: 9.9 ka (9.4-10.4 ka)	^{14}C radiocarbon and OSL	DuRoss et al., 2019

Variable erosion of fault scarps by Pleistocene glacial processes

The Pinedale glaciation (~22-13 ka) ended in the Teton-Yellowstone area with glaciers retreating from the study area approximately 15 ka., leaving behind a series of glacially carved valleys and glacial moraines along the eastern range front (Figure 3) (Licciardi and Pierce, 2008; Licciardi et al., 2014b, 2014a; Pierce et al., 2018). Surface exposure dating of lateral and end moraines at Glacier Gulch, Bradley and Taggart Lakes reveals a nuanced history of deglaciation along the Teton range front. Deglaciation from the high lateral moraines is interpreted as taking place at 23-21 ka, while deglaciation from adjacent end moraines dates to ~17-15 ka (Licciardi et al., 2019). The older, and higher, lateral moraines likely did not experience erosion or deposition from later (or smaller) glacial advance and retreat (Figure 3).

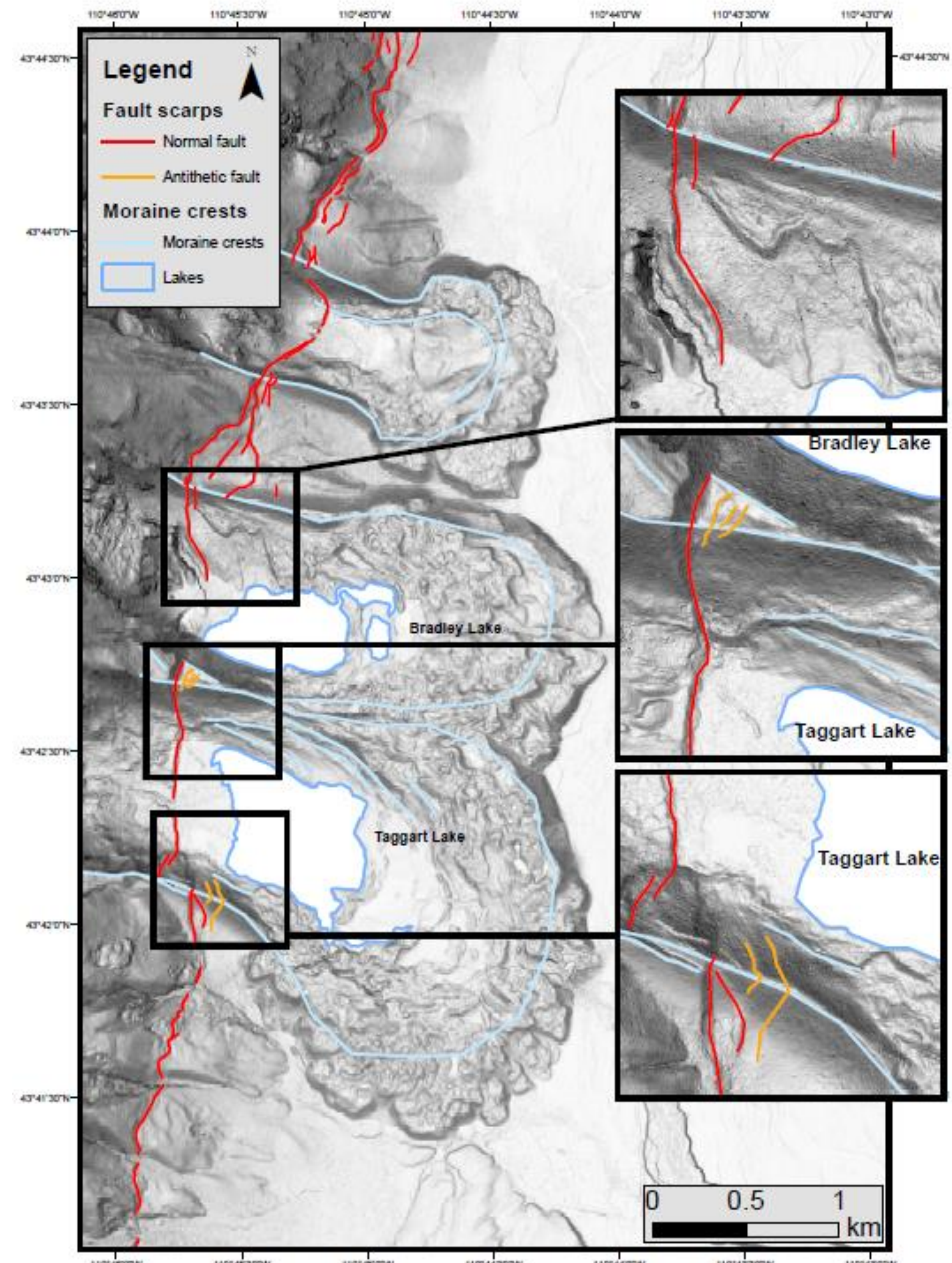

Figure 3. High scarps at Bradley and Taggart Lakes, Pinedale age moraine crests, and antithetic scarps crossing the moraine south of Taggart Lake. Note that the variation in scarp height over short distances along left lateral moraine at Taggart Lake is less than that on the right lateral moraine.

Variable ages of glacial landforms used in previous work on scarp height

The ages of range-front landforms and lake-bottom sediments have been determined from cosmogenic ^{3}He and ^{10}Be surface exposure and radiocarbon dating along the Teton fault (Licciardi and Pierce, 2008; Licciardi et al., 2014b, 2014a, 2015; Larsen et al., 2016; Pierce et al., 2018). Landforms of varying age pose a challenge to addressing fault scarp height variability. Scarps that cross significantly older landforms may have experienced a greater number of slip events, while younger landforms should have undergone fewer slip events. Thus, landform age plays a critical role in addressing fault scarp height variation along the Teton range front.

In their study of fault scarp height and vertical separation, Thackray and Staley (2017) assumed that where valley glaciers crossed pre-existing fault scarps, glacial erosion or deposition reduced the scarp height to the valley floor, effectively erasing the pre-existing vertical separation on the floors of the glacial valleys and on adjacent lateral moraines. High scarps (>10 m vertical separation) cut recessional deposits (e.g., moraines and outwash terraces) in the Taggart and Bradley Lake basins as well as other locations along the range front (Figure 4). Where fault scarps cross these features, glacial advance and retreat may not have fully erased the pre-existing scarp, and high scarps may be the result of inherited offset added to postglacial offset. High scarps crossing the lateral moraines at Taggart and Bradley Lakes may be the result of incomplete scarp erasure resulting in inherited scarp height.

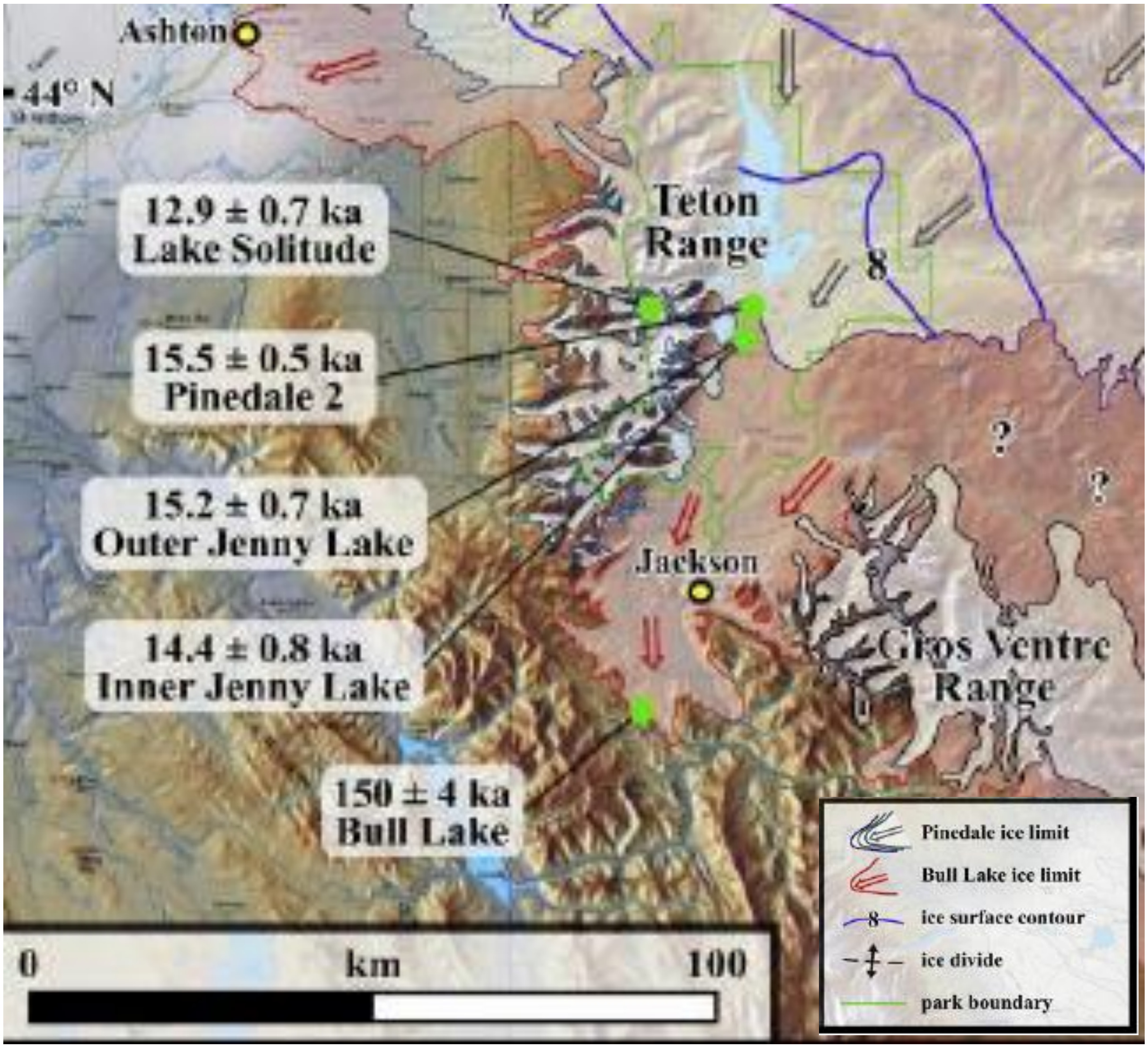

Figure 4. Maximum ice extents of the Bull Lake (~150-120 ka) and Pinedale (~22-13 ka) glaciations in the Yellowstone-Teton region. Retreat of Pinedale-age ice left behind a series of glacial outwash surfaces, lateral and terminal moraines, and drumlinoid features in Jackson Hole and along the Teton range front. Note surface exposure ages of Pinedale glacial deposits (green circles). Modified from Licciardi and Pierce, 2018.

Postglacial erosion and burial by slope failure and alluvial processes

Erosion by large-scale slope failure events (e.g., translational slides, debris flows) has influenced the Teton Range landscape (Foster et al., 2008; Tranel et al., 2011, 2015). Alluvial processes erode and construct landforms that contribute to fault scarp degradation and burial. Peri- and para-glacial rockfalls can contribute large volumes of sediment to the landscape, potentially burying preexisting landforms. Such events are influenced by climatic shifts, glacial debuttressing, and, potentially, seismic events (Ballantyne, 2002; Tranel and Strow, 2017). However, the influences of slope failure, alluvial processes, and other geomorphic processes on fault scarp height have not been the subject of previous studies of the Teton range front.

Combination of these factors, and possibly others

Variable fault offset rates, variable erosion by Pleistocene glacial processes, and erosion by slope failure may all influence the Teton fault individually or in combination. It is also possible that other factors not identified here (e.g., hydrologic cycles) play a role in fault scarp height variability and sediment flux within the fault zone. Slope failures can be triggered by seismic events (Romeo, 2000; Havenith et al., 2003; Valagussa et al., 2019), but the steep slopes of the Teton Range are a primary factor regardless of seismic triggers. Erosion and deposition by alluvial processes can reduce fault scarp height (Wallace, 1977; Brocklehurst and Whipple, 2006).

Geologic Setting

The high peaks of Grand Teton (4,200 m) and Mount Moran (3,800 m) are the backdrop to Grand Teton National Park and adjacent areas in northwestern Wyoming. Slip along the 70-km long, NNE-striking Teton fault combined with inherited Laramide structural influences and erosional processes has resulted in the dramatic range front topography of the Teton Range.

Uplift of the Teton Range began with Laramide thrust faulting in Late Cretaceous and early Paleogene time. Eastward compression of the North American continent resulted in low angle thrust faulting throughout the Rocky Mountain fold and thrust belt, including the modern Teton region. The Laramide Orogeny uplifted Precambrian and overlying Paleozoic and Mesozoic rocks along the Cache Creek thrust fault, creating the Teton-Gros Ventre uplift (Love et al., 2003). Movement along the Cache Creek thrust at the southern end of the modern Teton Range vertically offset Precambrian rocks exposed in the area by approximately 6 km (Smith et al., 1993). As this uplift was taking place, east- and northeast-dipping reverse faults, including the Buck Mountain and Forellen Peak faults, formed across the Teton-Gros Ventre region (Love et al., 2003).

These faults increased the overall vertical displacement of Precambrian, Paleozoic, and Mesozoic rocks in the area and interrupted the north-south and northwest-southeast fabric created during the Sevier Orogeny (Love et al., 2003). The resultant landscape of uplifted and tilted tectonic blocks was further modified by uplift along the Teton fault (Roberts and Burbank, 1993; Love et al., 2003; Brown et al., 2017). The core of the Teton Range is broadly composed of metamorphosed intrusive and metasedimentary rocks which belong to the Archean Webb Canyon Gneiss and Proterozoic Mount Owen Quartz Monzonite and associated pegmatite (Love et al., 1992, 2003). The Paleozoic and Mesozoic strata uplifted during the Laramide Orogeny form key bedrock units at the northern and southern ends of the Teton Range, as well as in the western portion of the range. The early Quaternary Huckleberry Ridge Tuff blanketed much of the region and forms an important marker horizon in the Jackson Hole valley and the Teton Range.

The bedrock units and tuff are blanketed by Quaternary deposits along much of the Teton fault (Love et al., 1992; Pierce and Good, 1992; Pierce et al., 2018). Northeast of Jackson Lake, the Teton fault offsets the Huckleberry Ridge Tuff, which is overlain by Pleistocene glacial deposits. Along the western side of Jackson Lake, glacial deposits overlie siltstone and shale deposits of the

Upper Devonian Darby Formation and Archean gneisses and migmatite. South of Jackson Lake, Archean layered gneiss, migmatite, and metagabbro form the primary bedrock.

The Teton region experienced repeated glaciations during Pleistocene time, providing key markers for estimating fault slip rates. Geomorphic evidence of two of these glaciations, the Bull Lake and Pinedale, is widely preserved throughout the Jackson Hole valley and Teton range front. Ice from two distinct sources impacted Jackson Hole and the Teton fault zone. Outlet lobes of the Greater Yellowstone Glacial System (GYGS) flowed into Jackson Hole, as did mountain glaciers in major valleys of the Teton Range itself (Licciardi et al., 2014b, 2015; Pierce et al., 2018; Licciardi and Pierce, 2018).

Moraines and outwash surfaces extending to the southern end of Jackson Hole record the advance of the GYGS from the north (Licciardi and Pierce, 2008, 2018; Pierce et al., 2011). Moraine boulders at the south end of Jackson Hole have an average surface exposure age of 136+/-13 ka (Licciardi and Pierce, 2008). In southern Jackson Hole, eight episodes of loess deposition and paleosol development were recorded in a 9 m section overlying a Bull Lake age glacial outwash terrace (Pierce et al., 2011). These data, coupled with cosmogenic ^{10}Be dating of moraine deposits, indicate that the Bull Lake glaciation took place during marine isotope stage (MIS) 6, which spanned 190-130 ka (Pierce et al., 2018; Licciardi and Pierce, 2018).

The retreat of Bull Lake age ice was followed by advance and retreat of GYGS-sourced ice during three phases of the Pinedale glaciation, Pinedale-1, -2, and -3, spanning ~22-13 ka and corresponding with MIS 2 (Love et al., 1992; Pierce and Good, 1992; Licciardi and Pierce, 2008).

During Pinedale-1, -2, and -3 advances, Yellowstone ice cap outlet glaciers advanced into Jackson Hole from the east, northeast, and north, respectively, while mountain glaciers descended eastward down glacial valleys in the Teton range to intersect with Yellowstone ice in the Jackson Lake area or to flow into the margins of Jackson Hole to the south of Jackson Lake (Licciardi and Pierce, 2008; Pierce et al., 2018).

Pinedale age glacial ice retreated from the study area approximately 15 ka, leaving behind a sequence of deglacial valley floor deposits, lateral and end moraines, outwash terraces, and drumlins (Licciardi and Pierce, 2008, 2018). In the study area, Pinedale glacial activity is recorded as a series of lateral and terminal moraines along the range front (Licciardi and Pierce, 2008; Pierce et al., 2018) and by deeply eroded valley floors.

Previous work

The Teton fault and range front geomorphology have been the subject of many previous studies. Geologic and fault maps, paleoseismic studies, fault slip rate, earthquake and slope failure hazards have been investigated with varying approaches and at varying scales, but questions of fault sections and segments, slip history, and hazards remain.

Fault mapping

Early mapping of the Teton fault identified Quaternary scarps along 55 km of the fault and inferred three fault segments, each with unique displacement histories (Susong et al., 1987; Smith et al., 1993). These findings and interpretations have been refined by subsequent studies. The most recent and complete maps of the Teton fault include the Geologic Map of Grand Teton National Park (Love et al., 1992) and a lidar-based Teton Fault scarp map (Zellman et al., 2019a). The first of these provides bedrock and surficial deposit distribution throughout Grand Teton National Park and along the Teton range front, while the latter is a detailed map of fault scarps developed from the LiDAR dataset used in this study.

Segmentation

Along-strike variability in fault scarp height has been well documented by previous authors (Smith et al., 1993; Byrd, 1995; Thackray and Staley, 2017). Faults zones may be comprised of individual faults that rupture in separate events, or segmented faults in which segments may rupture individually or in unison (DuRoss et al., 2016). Ruptures on a single segment may also cross over a segment boundary, affecting part of a neighboring segment in a “spillover rupture”, or may rupture only part of a single segment (“partial-segment rupture”) (DuRoss et al., 2016). As fault zones develop, segments undergo displacement and, over time, can become linked components of a system that is longer than the individual segments (King, 1983; Faulds and Varga, 1998; Fossen and Rotevatn, 2016).

Fault zone growth occurs by two primary end-member mechanisms which have been modeled: 1) simple fault tip propagation, in which once-isolated fault strands grow toward one another, eventually becoming linked (‘isolated fault growth model’), or 2) by rapid establishment of the full length of the fault without significant fault tip propagation (‘coherent fault growth model’) (Walsh et al., 2003). A relationship between strain and fault propagation develops in structurally mature normal fault systems (Fossen and Rotevatn, 2016). Thus, the identification of fault segments and the processes affecting fault development over time are important factors in understanding fault behavior. These factors should also be considered in assessing seismotectonic hazards.

The characteristics that define fault segments have been debated in the literature. Fault scarp height variability, changes in fault trend, changes in range crest topography, lateral variations in fault strike and footwall structures, and inferences from gravity anomaly data are all considered potential indicators of fault segmentation (Crone and Machette, 1984; DePolo et al., 1991; Smith et al., 1993; Faulds and Varga, 1998; Walsh et al., 2003; DuRoss et al., 2016). Two- and three-segment models have been proposed for the Teton fault, and the three-segment model is commonly referred to by previous authors. It is important to note that many of the commonly referred to indicators of segmentation are distinctly two-dimensional in nature. The two-dimensional nature of geologic maps and the limited ability of many study approaches to portray three-dimensional conditions at depth along a fault may contribute to misunderstandings of fault growth and segmentation (Walsh et al., 2003). It should also be noted that both the criteria used to identify fault or segments and the scale at which those criteria are assessed both need to be considered in fault segment interpretations.

A three-segment model based on surface displacement across the fault scarp, with boundaries south of Taggart Lake and at Moran Bay, was proposed by Susong et al. (1987). The model is based on interpretation of vertical separation across the fault scarp at 17 locations, the extent of similarly aged faulting, changes in fault trend, changes in range topography, lateral variations in fault strike and footwall structures, and inferences from gravity anomaly data (Susong et al., 1987) (Figure 2). Other authors have generally agreed with the three-segment interpretation and suggested that each segment of the fault may have unique offset rates (Roberts and Burbank, 1993; Byrd et al., 1994). However, this interpretation is contrasted by that of Ostenaa (1988), who suggested that gravity anomaly interpretations are not concurrent with a fault segment boundary and that the fault may be consist of two segments rather than three.

Fault scarp height

Studies of fault scarp height have primarily focused on scarp degradation rates and applications for estimating the time of rupture from scarp geomorphology (Wallace, 1977; Bucknam and Anderson, 1979; Pierce and Colman, 1986; Arrowsmith et al., 1998; Phillips et al., 2003). The morphological degradation of fault scarps was documented by Wallace (1977), who made inferences of scarp age from geomorphological characteristics of scarps, and later followed up with theoretical work by Nash (1984), who suggested that the geomorphic diffusion equation could be used to date fault scarps.

Normal fault scarps rapidly adjust to reach a stable angle of repose following a surface rupturing earthquake. Scarps then degrade through diffusive and erosive processes (Gilbert, 1909; Wallace, 1977; Andrews and Hanks, 1985; Arrowsmith et al., 1998; Hilley et al., 2010). At the time of initial rupture, fault scarps dip 50-90˚ (typically ~60˚) away from the uplifted block (Wallace, 1977). Fresh scarp faces are typically covered in unconsolidated material, and soil and roots often overhang the scarp crest. After rupture, scarps begin degrading by frost heaving and other hillslope transport processes. The fresh slope of a newly formed scarp becomes muted as lose clasts fall down the slope face, and hillslope processes move material downslope. Over time, water erosion becomes the dominant factor controlling scarp slope morphology (Wallace, 1977). Slopes may be gravity-controlled, with debris removed by the effect of gravity; wash-controlled, with debris carried downslope by alluvial slope wash; or some combination of these factors depending on their steepness and material components (Cooke and Warren, 1973). More recent work has highlighted the need to couple these approaches with modern dating techniques so that models can be calibrated to specific field areas (Phillips et al., 2003; Tucker et al., 2011). Previous authors have not focused on the effects of slope failure on fault scarp height.

Applications of the diffusion equation to fault scarp degradation and inferences of scarp age are common, but variations in lithologic conditions, scarp height, aspect, climate zone, determinations of sediment flux, and other factors introduce uncertainty to the age estimates and require models to be calibrated to each study site (Nash, 1984; Pierce and Colman, 1986; Arrowsmith et al., 1998; Phillips et al., 2003). Slope failure processes influence landscape evolution and sediment flux in actively uplifting areas (Keefer, 1984; Burbank et al., 1996; Highland and Bobrowsky, 2008) but few, if any, studies have looked at the effects of slope failure on fault scarp height.

Slip rate and paleoseismology

The Teton fault is the principal source of large magnitude seismic events on the eastern flank of the Teton Range (Smith et al., 1993; O'Connell et al., 2003; Petersen et al., 2014). The Pleistocene to mid-Holocene slip rate and paleoseismic history of the Teton fault has been investigated by a series of paleoseismic trenching studies at four locations and a vertical separation analysis focusing on the fault scarps at Taggart Lake.

At Steamboat Mountain, preliminary radiocarbon dates from two trenches across the fault indicate surface rupturing earthquakes between 3.8 and 6.1 ka (event SM1) and prior to 7.1 ka (event SM2) (Zellman et al., 2018). Trenches across two of the three scarps mapped south of Leigh Lake record evidence of two surface rupturing events which took place at ~5.9 ka (LL1; 4.8-7.8 ka) and ~10 ka (LL2; 9.7-10.4 ka) which are associated with 1.1-1.7 m and 0.4-1.7 m of vertical displacement, respectively (Zellman et al., 2019c). Three paleoseismic events have been interpreted from the paleoseismic trenching study at Buffalo Bowl, having taken place at ~4.6, ~7.1, and ~9.9 ka based on radiocarbon and optically-stimulated luminescence (OSL) dating (DuRoss et al., 2019b). The Buffalo Bowl study provide evidence for a Holocene closed-interval vertical slip rate of ~0.9 mm/yr (DuRoss et al., 2019b). The earliest paleoseismic trenching study, at Granite Canyon, resulted in a calculated offset rate of ~1.3 mm/yr between latest Pleistocene and mid-Holocene time (14.4-4.6 ka) (Byrd et al., 1994). The findings from paleoseismic trenching studies are summarized in Table 1.

The offset rates inferred from paleoseismic studies is generally in agreement with the vertical separation rate of 0.82±0.13 mm/yr calculated by Thackray and Staley (2017) for scarps at Taggart Lake. However, the high scarps and vertical separation rate of the southern range front remain enigmatic. Several authors have inferred that about two-thirds of postglacial offset along the southern fault took place prior to 8 ka (Hampel et al., 2007). It has been hypothesized that melting of the Yellowstone ice cap and Teton valley glaciers may have contributed to rapid uplift as surface unloading allowed rapid isostatic rebound (Hampel et al., 2007).

These studies document a well-preserved record of Pleistocene and Holocene surface rupturing earthquake events and indicate that the Teton fault, although apparently seismically quiescent at moment magnitude (M_L) >3, is active and a potentially significant source of seismic and related hazards in the area (White, 2006).

Larsen et al. (2019) interpret the paleoseismic record from turbidite deposits found in sediment cores taken from Jenny Lake. A continuous 14,000-year record of paleoseismic and slope failure events has been interpreted from the core record. At least seven fault rupturing events are evident in the sediment core record, occurring at 14.0 ±0.4 ka, 12.9 ± 0.1 ka, 11.6 ±0.2 ka, 10.3 ±0.2 ka, 9.1 ± 0.1 ka, 8.3 ±0.1 ka, and 7.7 ±0.1 ka. The events are separated in time by ~1,050 years (±~250 years) but are followed by >5,000 years of apparent inactivity. The most recent event has been correlated to the turbidite deposits from sediment cores at Leigh, Bradley, and Phelps Lakes. Additionally, cosmogenic ^{10}Be exposure ages from boulders and bedrock surfaces constrain the timing of two deep-seated slope failures on the western shore of Jenny Lake. The slope failures appear to have been triggered by earthquake events that occurred at ~14.0 ka and 8.1 ka (Larsen et al., 2019).

Hazards analysis

The 2014 National Seismic Hazard Map data, modeling, and paleoseismic studies of the Teton fault indicate that the fault could produce earthquakes with M_L >6.5 (Smith et al., 1993; Byrd et al., 1994; Petersen et al., 2014). Seismicity and earthquake modeling indicates that the Teton-Yellowstone region encompasses one of the greatest seismic hazards in the western United States (White et al., 2009). Taken together, paleoseismic data and historic seismicity in the Intermountain

Seismic Belt (ISB) indicate the Teton fault is a potentially significant source of seismic hazard for the region. Earthquake hazard assessments of the Teton region have primarily focused on ground shaking-related hazards, and we emphasize here that the potential for slope failure, either induced by seismic activity or other triggers, is also a major hazard along the range front.

Hazards assessments of the Teton fault have primarily focused on earthquake shaking hazards but have also indicated the potential for slope failure, subsidence, seiche and other hazards. Gilbert et al. (1983) compiled the first seismic hazards study for the region and presented one of the first formal analyses of hazards associated with earthquake activity on the Teton fault (O'Connell et al., 2003). More recent studies have emphasized the evidence for Quaternary faulting in the area and the recurrence interval of a few hundred to a few thousand years for large magnitude earthquakes in the Intermountain Seismic Belt (ISB), which includes the Teton fault (Smith et al., 1993).

Earthquakes can cause seismically induced slope failures (Havenith et al., 2003; Rodríguez-Peces et al., 2014; Kim et al., 2016). Although no large earthquakes have occurred on the Teton fault in historic times, the Hebgen Lake area, north of the Teton Range, ruptured with a M 7.3 earthquake in 1959 and has generated several $M \geq 6.0$ historic events (Doser and Smith, 1983; Barrientos et al., 1987). The 1959 Hebgen Lake earthquake triggered the Madison Canyon rockslide, which resulted in 20×10^6 m^3 of rock being displaced (Hadley, 1978). Large earthquakes on the Teton fault could lead to seismically induced slope failures along the range front, impacting trail systems, local communities, and other infrastructure. Identifying range front areas that are prone to slope failure is a key step in hazard mitigation and planning.

Efforts to identify areas of the Teton Range that are prone to slope failure began in the 1980s. Early landslide mapping across Wyoming was carried out by Case (1989), and more recent work has improve initial interpretations in the Teton Range (Shroder and Weihs, 2017). Here, I map slope failure deposits and characterize the areas where they are found (refer to Chapters II, III, IV and V for results and interpretation).

Noting that the patterns and controls on slope failure phenomena in GTNP were poorly documented or understood, Marston et al. (2010) mapped fall, slide, and flow deposits along Paintbrush, Cascade, Garnet, Death, and Granite Canyons using digital and field mapping approaches. They found that slides occurred with the greatest frequency where the Teton fault was between 1,300 and 4,100 m away, and the slope gradient was greater than 49˚. Falls were most likely to occur in areas where the slope aspect is north facing, the distance from the Teton fault is between 1,300 and 3,700 m, and the slope gradient is between 56˚ and 62˚. In contrast, flows were found to occur with the greatest frequency in areas where the slope aspect is south facing, the Teton fault is <3,400 m away, and the slope gradient is between 28˚ and 54˚ (Marston et al., 2010). The authors also found that slope failures interact with between 18% and 52% of the trail systems through the surveyed canyons (Marston et al., 2010).

This thesis is divided into five chapters. Chapter I introduces the study area, relevant literature, and problem statement. Chapter II is prepared as a stand-alone summary of the work completed and is in manuscript format in preparation for future submission to a peer-reviewed journal for publication. The remaining chapters discuss the results, interpretations, and the implications of this work as it applies to seismotectonic and slope failure hazards.

Problem statement

The geomorphic evolution of the Teton fault zone has been studied in detail by several previous workers but remains insufficiently understood. Specifically, variations in scarp height are well documented but the reasons for that variability have not been thoroughly explored. Variable fault slip, and variable erosion and burial by glacial, slope failure, and alluvial processes may all contribute to variations in scarp height.

Along the fault, glacial and alluvial landform sequences are offset by active faulting, creating diachronous and synchronous markers of fault movement (Byrd, 1995; McCalpin, 1996; Thackray et al., 2013; Thackray and Staley, 2017). Spatial and temporal variations of fault motion have been identified from paleoseismic trench observations and landform geomorphology along the Teton range front (Figure 5) (Byrd, 1995; Thackray and Staley, 2017; Zellman et al., 2018, 2019c; DuRoss et al., 2019b).

However, the influences of glacial, alluvial, and slope failure processes on scarp height variability need to be better understood. Variable fault scarp height may be explained by 1) along-strike, variable offset rates of the Teton fault; 2) variable erosion of the fault scarp by Pleistocene glacial processes; 3) variable ages of glacial landforms; 4) postglacial erosion and burial by slope failure and alluvial processes; or 5) some combination of these factors, and possibly others.

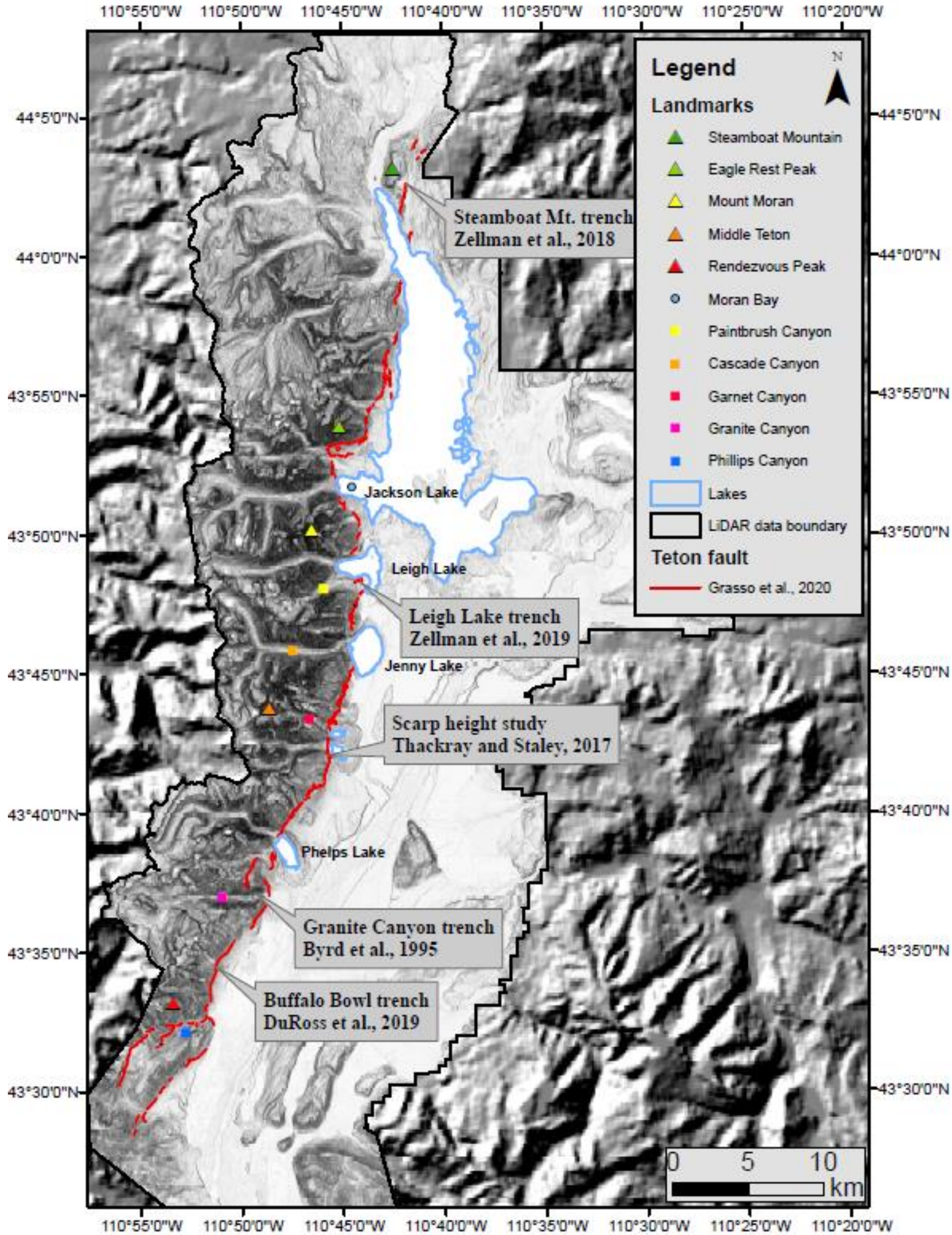

Figure 5. Paleoseismic trenching study sites and associated publications. Note: Thackray and Staley (2017) examined fault scarp height within a limited area along the central range front and compared results with data from previous paleoseismic trenching studies.

Chapter II: Vertical separation across fault scarps and implications for fault section boundaries in an extensional tectonic terrane, Teton fault, Wyoming, USA (manuscript for journal submission)

Abstract

Landscape disturbance events (e.g., earthquakes, slope failures, floods) play key roles in landscape evolution in tectonically active areas. Similarly, glacial and alluvial processes introduce landscape complexity on many range fronts. Along the 75-km Teton range front, fault scarps are well-expressed geomorphically and vary in vertical separation by up to tens of meters over short distances (<1 km) and longer distances (1 to 20 km) in a geomorphically complex setting.

Light detection and ranging (LiDAR) based mapping of the fault zone indicates that fault scarp height is affected by glacial geomorphology, slope failure, and alluvial processes. Vertical separation across well-preserved fault scarps varies along the fault. At a broad scale, vertical separation across is greatest in the central portion of the fault. At a finer scale, however, vertical separation of scarps is less in the floors of deglaciated valleys than on neighboring lateral moraines (e.g., Phelps Lake). The lower scarps on valley floors likely reflect younger landform age. Anomalously high scarps (>15 m vertical separation; e.g., the left lateral moraine at Phelps Lake) are likely artifacts of greater landform age.

On the basis of vertical separation patterns along the strike of the fault and changes in strike direction, we propose a four-section model of the Teton fault, contrasting with the previous, three-segment interpretations. These four sections are (N to S) the Eagle Rest Peak (ERP), Mount Moran

(MM), Middle Teton (MT), and Rendezvous Peak (RP) sections. The ERP section spans the northern 27 km of the fault and is characterized by vertical separation of 1.0 to 21.3 m based on scarp profiles at 18 locations. The MM section extends from north of Moran Bay to the south end of Jenny Lake and is characterized by vertical separation ranging from 1.6 to 32.0 m based on measurements from seven profiles spanning 12 km of the fault. The MT section reaches from south Jenny Lake to Granite Canyon and is characterized by vertical separation ranging from 6.6 to 20.9 m based on measurements at 11 scarp profiles along 16 km of the fault. The RP section extends from Granite Canyon to the south end of the fault at Teton Pass, and vertical separation ranges from 12.9 to 54.4 m based on measurements at 6 locations.

Vertical separation is greatest toward the central portion of each of these sections, following the expected pattern of normal fault behavior (Cowie and Scholz, 1992; Cowie and Roberts, 2001). The anomalously high scarps in the Rendezvous Peak section, where the geochronology is limited, may be the result of greater landform age or high offset rates. The transition zones between these four sections may represent boundaries between fault sections or segments.

Introduction

The Teton fault is expressed at the surface as a 75-km long series of north-northeast trending normal fault scarps on the eastern flank of the Teton Range (Figure 1). This project identifies and characterizes fault scarps and slope failure deposits, analyses patterns of vertical separation across fault scarps, and discusses the implications of variable scarp height as it pertains to fault segmentation and hazards assessment along the Teton fault.

Landscape disturbance events (e.g., earthquakes, slope failures, and floods) play key roles in landscape evolution in tectonically active areas (Keefer, 1984). Similarly, glacial and alluvial processes alter landscape geomorphology and influence sediment flux in alpine environments (McColl and Davies, 2013). Smaller-scale processes (e.g., alluvial erosion and deposition, hillslope diffusion) also influence landscape geomorphology. These processes alter the surface expression of faults and introduce landscape complexity along range fronts.

Along the Teton fault, fault scarps are well-exposed and vary in height by up to tens of meters over short distances (<1 km) and longer distances (1 to 20 km). High-resolution light-detection and ranging (LiDAR) data, clear expression of fault scarps, and accessibility make the Teton range front an ideal location to study the influences of glacial, alluvial, and slope failure processes on scarp height variability.

Along the fault, glacial and alluvial landform sequences are offset by fault scarps, providing diachronous and synchronous markers of fault movement (Byrd, 1995; McCalpin, 1996; Thackray et al., 2013; Thackray and Staley, 2017). Spatial and temporal variations of fault motion are reflected in paleoseismic trench observations and landform geomorphology (Byrd, 1995; Thackray and Staley, 2017; Zellman et al., 2018, 2019c; DuRoss et al., 2019b). Variable fault scarp height may result from by 1) along-strike, variable offset rates of the Teton fault; 2) variable erosion of the fault scarp by Pleistocene glacial processes; 3) variable ages of glacial landforms used in previous work on scarp height; 4) postglacial erosion and burial by slope failure and alluvial processes; or 5) some combination of these factors, and possibly others. The influences of these processes on fault scarp geomorphology, and the influences of fault slip on these processes and their resultant landforms, are the subject of this study.

Geologic Setting

Uplift of the Teton Range began with Laramide thrust faulting in Late Cretaceous and early Paleogene time. The Laramide Orogeny uplifted Precambrian and overlying Paleozoic and Mesozoic rocks along the Cache Creek thrust fault, creating the Teton-Gros Ventre uplift (Love et al., 2003). Movement along the Cache Creek thrust at the southern end of the modern Teton Range vertically offset Precambrian rocks exposed in the area by approximately 6 km (Smith et al., 1993). As this uplift was taking place, east- and northeast-dipping reverse faults, including the Buck Mountain and Forellen Peak faults, formed across the Teton-Gros Ventre region (Love et al., 2003). These faults increased the overall vertical displacement of Precambrian, Paleozoic, and Mesozoic rocks in the area and interrupted the north-south and northwest-southeast fabric created during the Sevier Orogeny (Love et al., 2003). The resultant landscape of uplifted and tilted tectonic blocks was further modified by uplift along the Teton fault (Roberts and Burbank, 1993; Love et al., 2003; Brown et al., 2017).

The core of the Teton Range is broadly composed of metamorphosed intrusive and metasedimentary rocks which belong to the Archean Webb Canyon Gneiss and Proterozoic Mount Owen Quartz Monzonite and associated pegmatite (Love et al., 1992, 2003). The bedrock units are blanketed by Quaternary deposits along much of the Teton fault (Love et al., 1992; Pierce and Good, 1992; Pierce et al., 2018). Northeast of Jackson Lake, the fault offsets the early Quaternary Huckleberry Ridge Tuff, which is overlain by Pleistocene glacial deposits. Along the western side of Jackson Lake, glacial deposits overlie siltstone and shale deposits of the Upper Devonian Darby Formation and Archean gneisses and migmatite. South of Jackson Lake, Archean layered gneiss, migmatite, and metagabbro form the primary bedrock.

Glacial History

The Teton region experienced repeated glaciations during Pleistocene time, generating key markers for estimating fault slip rates. Geomorphic evidence of the two most recent glaciations, the Bull Lake and Pinedale, is widely preserved along the Teton range front. During Bull Lake and Pinedale time, ice from two distinct sources impacted Jackson Hole and the Teton range front. Outlet lobes of the Greater Yellowstone Glacial System (GYGS) flowed into Jackson Hole from the north and northeast, and mountain glaciers in major valleys of the Teton Range flowed easterly down major valleys, to and across the range front (Licciardi et al., 2014b, 2015; Pierce et al., 2018; Licciardi and Pierce, 2018).

Moraines and outwash surfaces extending to the southern end of Jackson Hole record the advance of the GYGS from the north (Licciardi and Pierce, 2008, 2018; Pierce et al., 2011). Moraine boulders at the south end of Jackson Hole have an average surface exposure age of 136+/-13ka

(Licciardi and Pierce, 2008). These data indicate that the Bull Lake glaciation in Jackson Hole took place during marine isotope stage (MIS) 6, which spanned 190-130 ka and was succeeded by glacial events predating Pinedale time (Pierce et al., 2018; Licciardi and Pierce, 2018).

The retreat of Bull Lake age ice was followed by advance and retreat of GYGS-sourced ice during three phases of the Pinedale glaciation, Pinedale-1, -2, and -3, spanning ~22-13 ka and corresponding with MIS 2 (Love et al., 1992; Pierce and Good, 1992; Licciardi and Pierce, 2008, 2018). During Pinedale-1, -2, and -3 advances, Yellowstone ice cap outlet glaciers advanced into Jackson Hole from the east, northeast, and north, respectively, while mountain glaciers descended eastward down glacial valleys in the Teton range to intersect with Yellowstone ice in the Jackson Lake area or to flow into the margins of Jackson Hole to the south of Jackson Lake (Licciardi and Pierce, 2008; Pierce et al., 2018).

Pinedale-age glacial ice retreated from the study area approximately 15 ka, leaving behind a sequence of deglacial valley floor deposits, lateral and end moraines, outwash terraces and fans, and drumlins (Licciardi and Pierce, 2008, 2018). In the main range-front study area, Pinedale glacial activity is recorded as a series of lateral and terminal moraines along the range front (Licciardi and Pierce, 2008; Pierce et al., 2018), by alluvial landforms, and by deeply eroded valley floors.

Methods

Digital mapping

The study area was digitally mapped using 1-m resolution LiDAR data and ArcGIS version 10.7.1 software. The LiDAR-based slope map was draped over the hillshade model and used to map fault scarps and slope failure deposits within the study area. Scarps were mapped based on geomorphic characteristics including length, height, cross-sectional shape and slope angle, and cross-cutting relationships with other surficial landforms. Slope failure deposits were mapped from slope and hillshade models following the general guidelines of Burns and Madin (2009). Slope failure deposits mapped in the study area fall into two categories: translational slides and debris flows. Lateral moraines, moraine crests, and drumlin crests were mapped from slope and hillshade models based on geomorphic characteristics. LiDAR-derived digital elevation (DEM), hillshade, slope, and topographic models were used to construct a geomorphic map of the fault zone using methods similar to those employed by Harding (2000), Burns and Madin (2009), and Crawford (2012).

Scarp profiling

This project relies on measurements of fault scarps derived from topographic profiles. Topographic profiles across fault scarps were measured using the ArcGIS profiler tool. Profiles were measured perpendicular to the strike and at approximately 1 km intervals along the fault. Profiling sites were selected where landform surfaces on either side of the scarp appear to be synchronous (Figure 6). The placement of profile lines was adjusted slightly along the fault to capture data across the highest scarps with similar surface slope angles on the hanging wall and footwall sides of the fault, reflecting the highest recorded vertical separation while minimizing the effects of erosion and other height-reducing processes. Scarps impacted by slope failures or other erosive events were not profiled. In an idealized model where the surface slope angles are equal, uncertainties in calculated vertical separation are minimized. In order to address questions of scarp profiling uncertainty, five parallel scarp normal profiles were generated from the DEM along a ~85 m long section of the fault in the Phelps Lake valley. Vertical separation was calculated at each profile location and ranged from 7.1 m to 8.2 m, with an average of 7.6 m, with a standard deviation of 0.4 m.

The LiDAR data was collected in Grand Teton National Park by Woolpert, Inc. under contract to the United States Geological Survey in 2014 (Woolpert, Inc., 2015). Data was provided to USGS in ERDAS .IMG format with 1 m cell size and vertical error ranging from -0.194 m to 0.135 m with an average of 0.027 m after hydrologic flattening was conducted. This dataset provides the basis for digital mapping and scarp profiling used in this project. A 90-m resolution DEM of Wyoming was used as a regional backdrop for mapping (Wyoming Geographic Information Science Center, 1997).

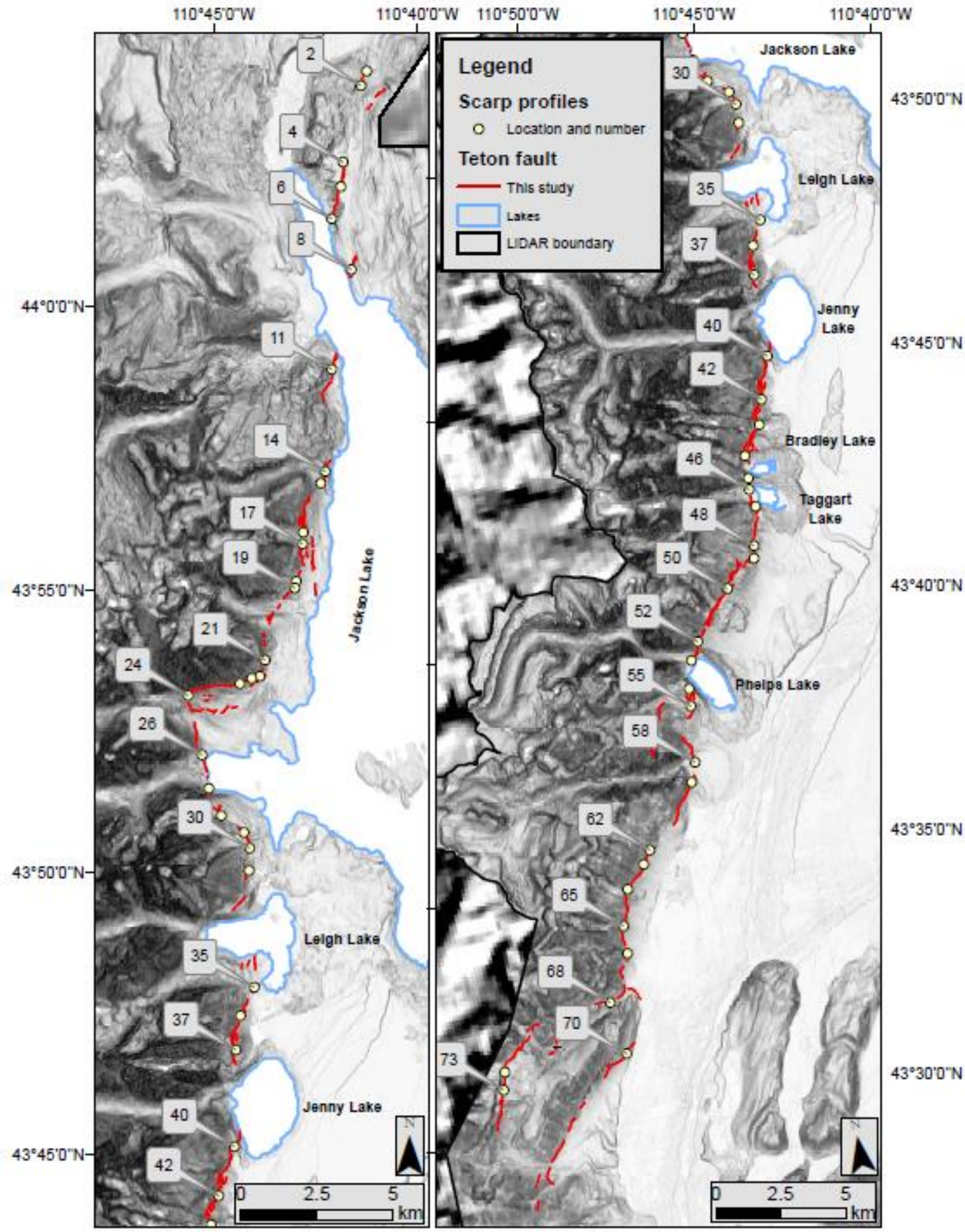

Figure 6. Forty-two fault scarp topographic profiles were extracted from the DEM at approximately 1-km intervals along the Teton fault. Profile numbers (in gray boxes) generally correspond to kilometers south along the fault. Profiles were generated at all locations shown and profiles are numbered sequentially from north to south; some labels omitted for image clarity.

Vertical separation and simple scarp height

Simple scarp height and vertical separation were calculated at fifty scarp profiling locations along the fault. Simple scarp height is defined as the vertical distance between the highest and lowest points across the fault scarp, while vertical separation is defined as the restored vertical distance between the tectonically undeformed footwall and hanging wall surfaces. Simple scarp height was calculated from the highest and lowest points on the fault scarp. Vertical separation was calculated by projecting the pre-faulted surfaces across the scarp and measuring the distance between the projected surfaces at a horizontal position halfway across the fault scarp, following the methods Thompson et al. (2002) and Amos et al. (2010) (Figure 7). Simple scarp height is expected to exceed vertical separation across scarps where the footwall and hanging wall surface slopes are undeformed, providing a simple quality check for the profiling data.

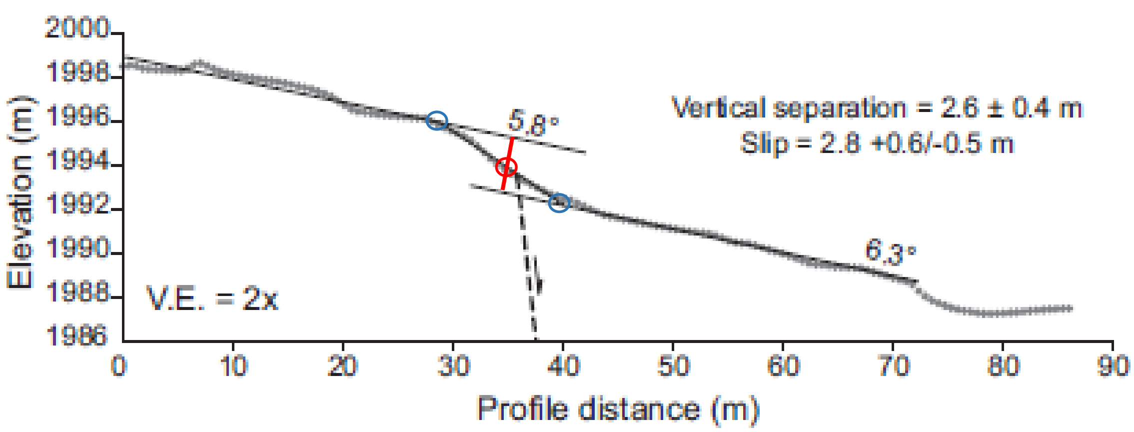

Figure 7. Topographic profile with linear regressions through the footwall and hanging wall surfaces. Vertical separation (red line) is calculated as the distance between the regression lines (straight black lines in center) at the midpoint along the scarp (red circle). Simple scarp height is calculated as the elevation difference between the lowest and highest points (blue circles) on the fault scarp. Modified from Amos et al. (2010), figure 4.

Linear regression lines were projected along the footwall and hanging wall landform surfaces offset by the scarp at each profile location. The slope angle of each surface was calculated from the arctangent of the slope of the best-fit line for each surface (Equation 1). The vertical separation was calculated at the midpoint of the scarp (McCalpin, 1996).

Equation 1: Formula for calculating the slope of the best-fit linear regression line for points defining the footwall and hanging wall surfaces:

$$\textit{Slope angle in degrees} = \arctan(m),$$

where m is the slope of the linear regression line through the surface being considered

Profiles with similar slope angles on both the footwall and hanging wall surfaces provide the best estimate of vertical separation across scarps by reducing measurement error (Figure 8). Where slope angles are equal, the location of vertical separation measurement relative to the scarp is inconsequential, while the vertical separation measurement varies substantially across scarps with strong contrast in footwall-hanging wall slope angles.

Sturge's Rule provides a formula for determining an appropriate number of bins and bin division values for data displayed in histogram format (Scott, 2009). The profiles were classified as low-, moderate-, and high-quality based on similarity of the slope angle between the footwall and hanging wall by applying Sturge's Rule (Equation 2). Profiles classified as low quality ($n=4$) and where calculated vertical separation exceeded simple scarp height ($n=4$) were eliminated from further analyses. Errors associated with these measurements include uncertainty in the placement of points marking the top and bottom of the scarp (e.g., scarp geometric variation), variations in surface roughness or other variation in the landform surface, and uncertainty introduced by the ArcGIS profiler tool used to extract topographic data across the fault scarps. Areas with multiple scarps or antithetic faults were also omitted. The presence of multiple scarps along a profile transect requires an additive approach to simple scarp height and vertical separation analyses, complicating the process and potentially introducing additional error to the measurements.

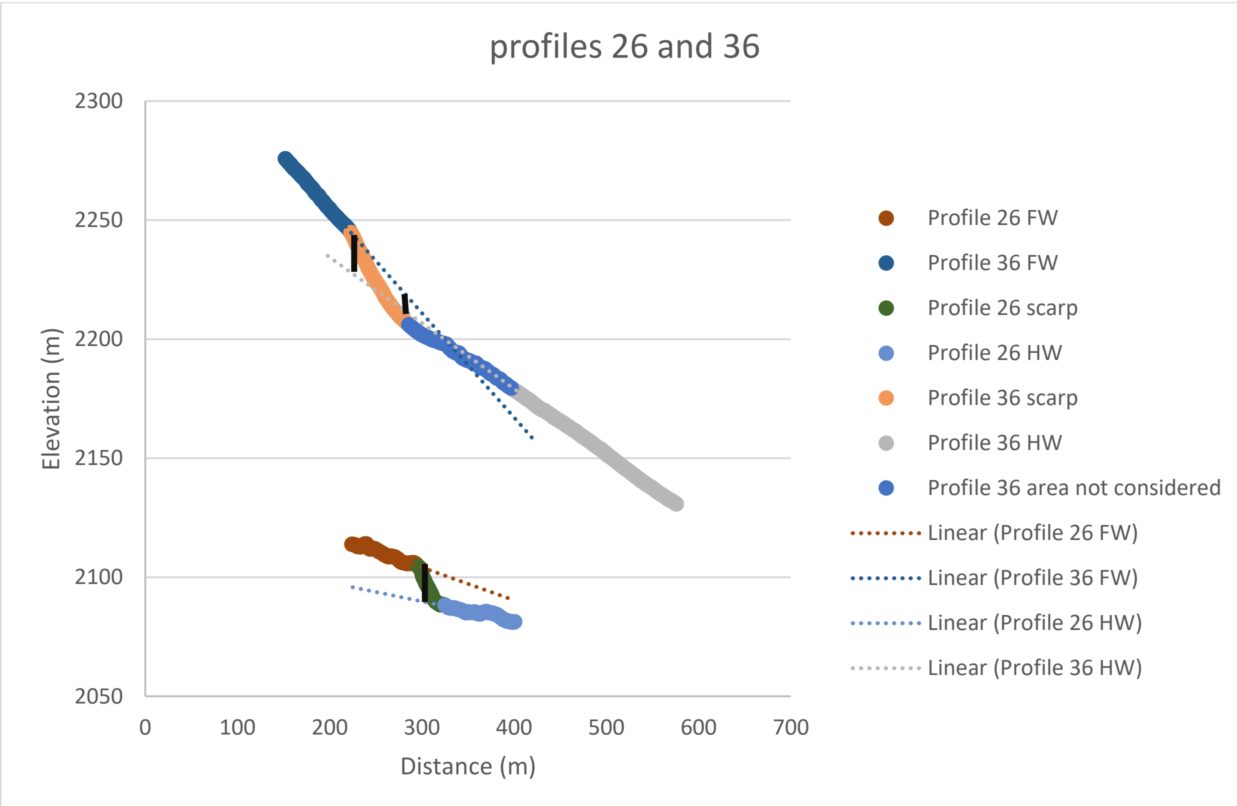

Figure 8. Example of scarp profile with similar footwall and hanging wall surface slopes (profile 26, bottom) and dissimilar footwall and hanging wall surface slopes (profile 36, top).Vertical black lines indicate vertical separation at different points across the scarp, highlighting the error associated with profiles where footwall and hanging wall surface slopes have large variation between them. Dashed lines are linear regression lines extended from the footwall and hanging wall surface slopes. Vertical separation is calculated at the point halfway across the scarp face; differences in footwall and hanging wall surface slope can impact vertical separation measurements.

Equation 2. Sturge's Rule:

$$\text{Number of bins} = 1+3.322*\log(n)$$

where n is the number of data points being considered

Scarps cutting glacial sediment and landforms were further subdivided into Bull Lake, Pinedale-3, Pinedale-2, and Pinedale-1 age based on the work of previous authors (Love et al., 1992; Licciardi and Pierce, 2008; Licciardi et al., 2014b, 2014a, 2015).

Field mapping

Field mapping was conducted in selected areas along the fault over the summer of 2019. Field mapping was used to locate and characterize the extent of hillslope processes within the fault zone and confirm the relationships between scarps, slope failure deposits, and other geomorphic features which were digitally mapped. Field mapping also constrains the spatial distribution and relative magnitude of slope failure events.

Results

Fault scarp mapping

The Teton fault is expressed at the surface as a series of range front-parallel scarps that offset glacial and alluvial landforms. The predominant trend of the Teton fault is north-northeast although individual scarp orientations range from north-northwest to east-northeast. Single-strand and multi-strand areas are common throughout the fault zone, and where multiple scarps are present, they generally parallel one another in close proximity (<0.2 km). In two locations in the southern and central sections of the fault, scarps show a distinct, right-stepping, en echelon pattern (e.g., approximately 2 km south of Granite Canyon and 2.3 km south of Taggart Lake), suggesting a component of dextral shear. In the northern part of the study area, scarps generally parallel the Teton Range except north of Wilcox Point, where the fault lies on the east side of Jackson Lake, 3 to 5 km east of the range front (Figure 1). The scarps offset glacial outwash deposits and moraines of Pinedale age and Holocene alluvial and slope failure deposits. Antithetic scarps within 1 km of the main scarp were mapped northeast of Jackson Lake and across lateral moraines at Taggart and Bradley Lakes (Figure 3). The southern 10 km of the fault zone is characterized by a bifurcation of the main fault into two separate strands, the Phillips Valley fault to the west, and the Teton fault to the east, which are separated by ~2.6 km (Figure 1).

Scarps show a clear and consistent sense of normal, down-to-the-east displacement along the entire fault zone. Simple scarp height ranges from 7 m to 70 m and vertical separation ranges from 1.0 m to 54.4 m across profiles at forty-two locations along the fault (Figure 10). Five of the measured scarps offset glacial drumlins constructed by the GYGS outlet glacier at the end of Pd-3 time (14.4 ±08 ka; Licciardi and Pierce, 2018).

Scarp profile analysis

Simple scarp height and vertical separation were measured across fifty scarp profiles (Table 2). The footwall and hanging wall surface slope was measured at each profile location, and the difference between the footwall and hanging wall surface slopes was calculated. The slope angle differences were binned into seven classes based on the results of the Sturge's Rule calculation (Figure 9). Surface angle contrasts <3.46˚ were classified as high quality (i.e., lower uncertainty in the vertical separation measurement) (green, Figure 9), those with surface angle contrast between 3.46˚ and 10.27˚ were classified as moderate quality (yellow, Figure 9), and those with surface angle contrast >10.27˚ were classified as low quality (i.e., higher uncertainty in the vertical separation measurement) (red, Figure 9).

Table 2. Summary of fault scarp profiles data. Difference in slope was used to classify profiles into low-, moderate-, and high-quality. Low quality profiles and those where calculated vertical separation exceeded that of simple scarp height were eliminated from further analyses.

Profile number	Latitude	Longitude	Simple scarp height (m)	VS (m)	Footwall surface slope (degrees)	Hanging wall surface slope (degrees)	Surface slope contrast (degrees)	Classification
1	-110.687404	44.069354	7.0	1.0	-4.5	-5.9	1.4	High
2	-110.689769	44.065044	7.0	1.7	-8.7	-10.6	1.9	High
4	-110.697244	44.042536	16.0	8.7	-1.9	-6.9	5.0	Moderate
5	-110.701925	44.025826	10.0	10.7	-6.9	-24.3	0.2	High
6	-110.693963	44.010798	10.9	5.8	-10.0	-13.2	3.2	High
8	-110.702147	43.981375	17.0	6.0	-2.4	-2.9	0.5	High
11	-110.704922	43.951281	29.0	12.4	-12.6	-12.3	0.3	High
14	-110.706785	43.947838	44.0	14.3	-8.4	-3.9	4.5	Moderate
15	-110.714036	43.933296	27.9	14.3	-8.6	-8.0	0.5	High
16	-110.714372	43.929925	46.0	28.6	-1.2	-2.5	1.3	High
17	-110.716953	43.918897	23.0	13.9	-6.6	-6.7	0.1	High
18	-110.717507	43.916924	54.9	21.3	-19.1	-12.1	7.0	Moderate
19	-110.729731	43.895712	47.0	17.6	-19.2	-19.7	0.6	High
21	-110.731836	43.890946	36.0	12.8	-7.0	-10.3	3.3	High
22	-110.740026	43.888792	24.0	11.9	-7.2	-10.1	2.9	High
23	-110.761168	43.885312	52.0	18.3	-23.6	-20.8	2.7	High
24	-110.755539	43.867789	20.0	6.2	-10.7	-10.4	0.3	High
26	-110.752819	43.857879	26.0	13.6	-7.7	-5.4	2.3	High
27	-110.747795	43.849847	23.0	6.4	-10.4	-10.7	0.3	High
28	-110.738543	43.844841	22.9	9.3	-16.4	-19.6	3.2	High
29	-110.736233	43.840219	69.9	32.0	-19.1	-13.4	5.7	Moderate
30	-110.736526	43.833645	40.0	24.7	-10.8	-10.9	0.1	High
31	-110.734572	43.799193	32.9	12.8	-19.2	-20.8	1.6	High
35	-110.740216	43.790844	18.0	1.6	-3.4	-4.0	0.7	High
36	-110.742172	43.780768	62.0	14.1	-23.9	-14.6	9.2	Moderate
37	-110.742815	43.752238	41.9	17.8	-2.2	-13.8	11.6	Low
40	-110.749240	43.737736	30.0	10.3	-5.2	-7.3	2.1	High
42	-110.752459	43.729216	47.9	20.9	-7.8	-7.8	0.1	High
43	-110.761808	43.719456	23.0	9.9	-2.9	-1.9	1.0	High
44	-110.762079	43.711617	20.9	10.9	-2.8	-2.3	0.5	High
45	-110.762676	43.707648	63.5	14.8	-9.4	-3.0	6.4	Moderate
46	-110.761058	43.701485	28.9	10.6	-4.2	-1.8	2.4	High
46.5	-110.765136	43.688198	35.0	13.8	-2.0	-2.3	0.3	High
48	-110.766219	43.683865	16.0	7.3	-12.7	-13.0	0.3	High
49	-110.781483	43.675080	51.0	12.9	-11.2	-7.7	3.5	Moderate
50	-110.799723	43.658832	41.0	9.4	-27.6	-15.6	12.0	Low
52	-110.804239	43.652729	39.9	13.0	-27.6	-16.7	10.9	Low
53	-110.807737	43.643202	21.9	6.6	-5.2	-4.7	0.5	High
55	-110.808397	43.637157	36.9	14.0	-4.9	-3.5	1.4	High
58	-110.811079	43.617773	52.0	13.0	-10.9	-8.0	2.9	High
59	-110.814383	43.611141	33.0	12.9	-9.6	-7.8	1.9	High
62	-110.839755	43.590482	14.7	17.3	-43.1	-42.6	0.4	High
63	-110.843839	43.585957	20.2	33.3	-47.9	-40.6	7.3	Moderate
64	-110.853436	43.578388	41.5	44.0	-50.4	-44.1	6.3	Moderate
65	-110.858418	43.566074	37.8	28.0	-58.4	-47.5	10.9	Low
66	-110.858866	43.556457	45.1	29.7	-50.2	-47.0	3.2	High
68	-110.871125	43.540705	58.8	28.9	-30.5	-30.2	0.3	High
70	-110.867630	43.522328	70.9	54.4	-42.9	-33.5	9.5	Moderate
72	-110.926418	43.523322	17.5	17.5	-6.4	-6.6	0.3	High
73	-110.928463	43.517285	17.5	13.6	-29.7	-27.6	2.0	High

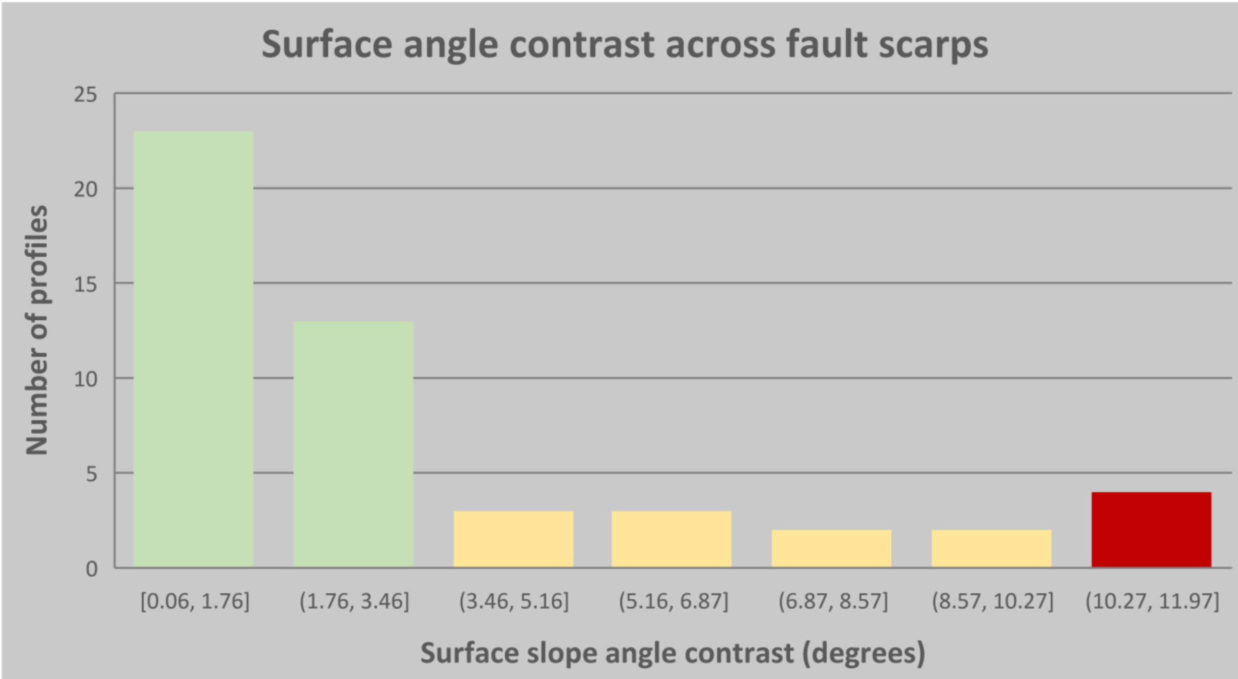

Figure 9. Histogram of Sturge's Rule results. Sturge's Rule was used to define the difference in slope values where fault scarp profiles should be divided into low- (red), moderate- (yellow), and high-quality (green). Low-quality profiles (i.e., those with higher uncertainty in the vertical separation measurement) were removed from further analysis.

The average vertical separation across the forty-two high- and medium-quality profiles is 14.5 m (and 15.4 m across all of the profiles) (Figure 10). At a broad scale, vertical separation is greatest along the southern fault. At a finer scale, vertical separation is less at the ends of the fault and at three locations within the central fault zone, and higher between these areas.

Applying a four- to seven-point moving average trendline to the vertical separation data points highlights the finer pattern of height variability. The dashed gray line in Figure 10 shows the four-point moving average of vertical separation values. The four-point average highlights broader variability while also representing local anomalies. The trendline suggests that vertical separation increases toward the central portion of four separate areas along the fault. These areas are each separated by several scarps with low vertical separation. From north to south, these areas are termed: 1) the Eagle Rest Peak section, from the north end of the fault to Moran Bay; 2) the Mount Moran section, from Moran Bay to the south end of Jenny Lake; 3) the Middle Teton section, from south of Jenny Lake to Granite Canyon; and 4) the Rendezvous Peak section, from Granite Canyon to Teton Pass (Figure 10Figure 10). These sections are discussed in detail in Interpretation and Discussion portion of this paper below .

At the south end of the Teton Range, the Teton fault is hypothesized to intersect the east-west trending Cache Creek thrust fault, a remnant of the early Tertiary Laramide thrust faulting (Lageson, 1992; Smith et al., 1993; Byrd, 1995). Five profiles along the fault have vertical separation greater than 25 m. Three of these highest scarps are located in the southern 10 km of the study area, including the scarp with the greatest vertical separation (54.4 m; Figure 10Figure 10 and Table 3). In that area, the Teton fault is hypothesized to intersect the east-west trending Cache Creek thrust fault, a remnant of early Tertiary Laramide thrust faulting (Lageson, 1992; Smith et al., 1993; Byrd, 1995).

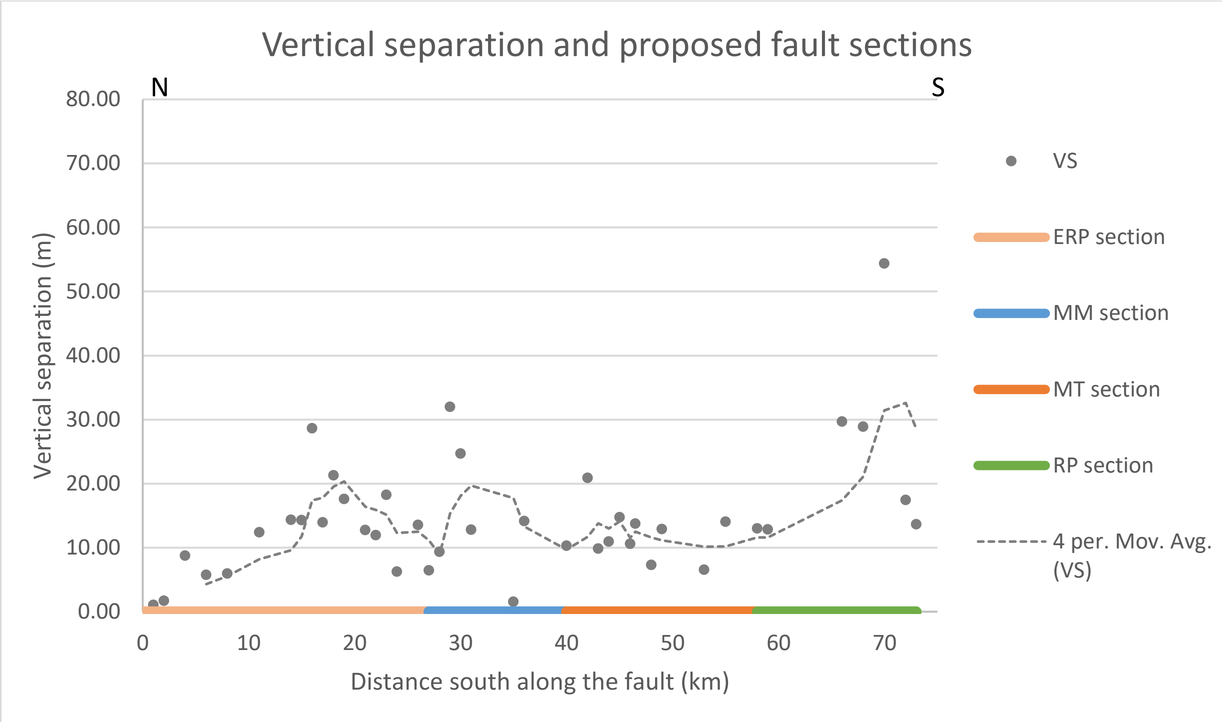

Figure 10. Vertical separation across the forty-two scarp profiles and the extent of the four proposed fault sections. The dashed line is a four-point moving average trend line that highlights the overall pattern of vertical separation along the Teton fault. Increasing the number of points in the moving average function to as many as seven highlights the four areas of vertical separation that follow the expected pattern of normal fault behavior.

Slope failure deposits

Both large- and small-scale slope failure deposits are evident in the study area (Figure 11). Translational and flow deposits of earth, rock, and debris range in size up to 2.3 km^2, although the vast majority of deposits cover <0.1 km^2. Along the fault, slope failures typically run out in an easterly direction. In east-west oriented deglaciated valleys, deposits follow the north and south facing slope directions, often diverting toward the east as they reach the Jackson Hole valley floor (Figure 11). The majority of slope failures occur in Pinedale-age glacial deposits and along deglaciated valley walls, although they are also found on steep slopes of varying orientation and rock type. Several areas where multiple slope failure events have taken place within the boundary of a single, larger slope failure deposits are noted between Jackson and Phelps Lakes (Figure 11b).

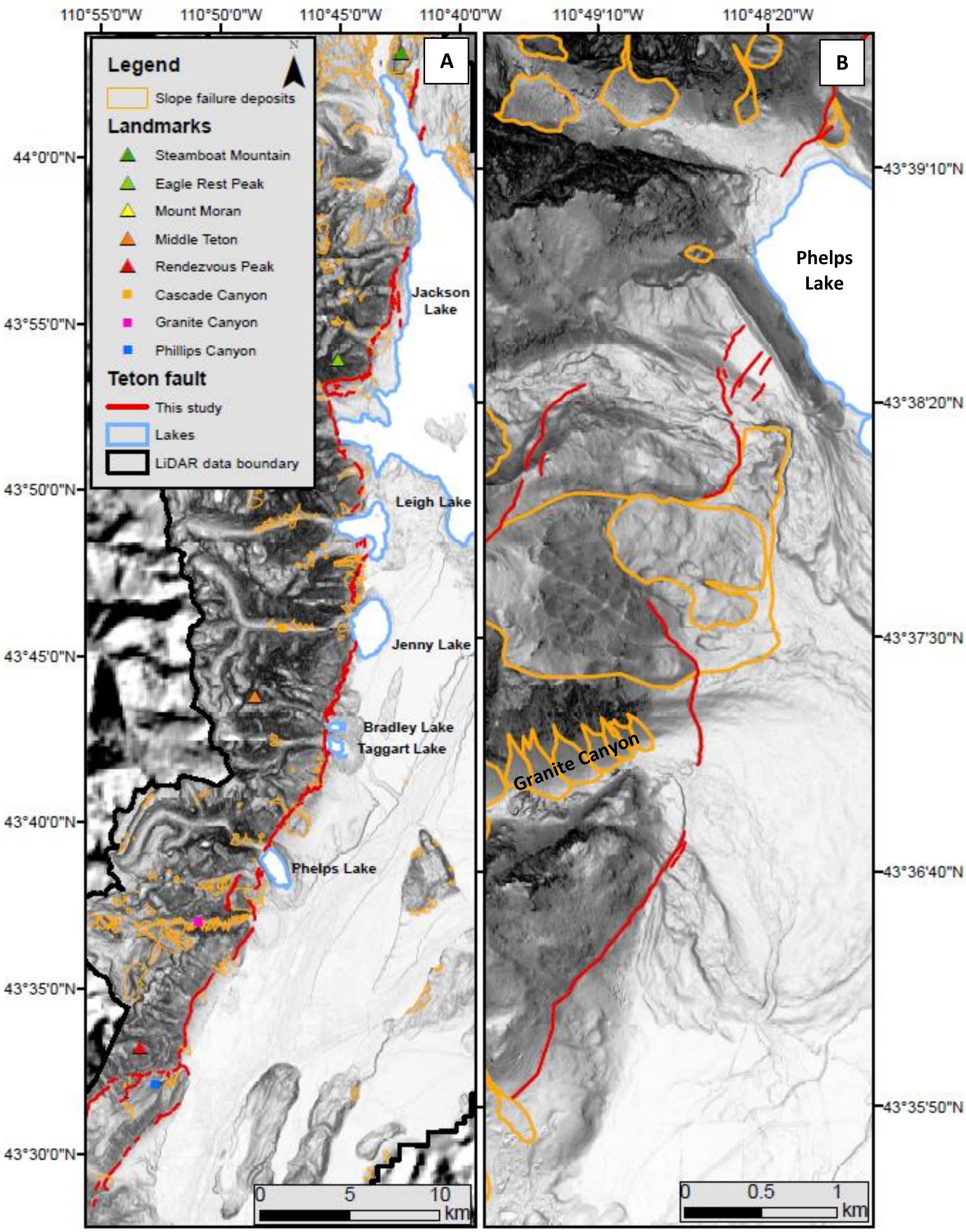

Figure 11. Slope failure map. Deposits are common throughout the Teton Range and along the range front (A, left). An example of an overlapping slope failure deposit (B, center of map) and densely spaced debris flow deposits along the south facing slope of Granite Canyon, south of Phelps Lake (B, right).

Field mapping

Field mapping of select areas resulted in adjustments to the location of digitally mapped fault scarps and slope failure deposits, clarified relationships between features, provided insight that was applied to digital mapping throughout the study area, and improved the accuracy of final map products. The areas selected for field mapping are shown in Figure 12.

In field area A, several digitally mapped fault scarps were eliminated based on surface expression in the field, where they were interpreted as glacial features. Several fault scarps mapped by Zellman et al. (2019a) were also eliminated based on lack of field evidence for surface faulting (Figure 13, 14). In field areas A and B, scarps mapped by Zellman et al. (2019a) were eliminated after geomorphic evidence led to new interpretations of the lineaments (Figure 15, 16). In field areas C and D, mapping clarified the extent of fault scarps.

Rock unit descriptions

Rock units exposed at the surface were correlated to those mapped by Love et al. (1992). Soil and dense vegetation along the range front limit surface exposures of bedrock units in much of the study area. Deposits of glacially transported material and alluvium are common and cover much of the area. Geologic units mapped in the study area are described below.

Quaternary alluvium (Qal)

Gravel, sand, and silt found along modern stream channels, flood plains, and fans.

Quaternary glacial drift (Qg4)

Deposits deposited by Quaternary and possibly older glaciations. Primarily composed of Precambrian rocks from the Teton range and quartzite cobbles and boulders from the Harebell Formation, these deposits are typically mantled by soil and vegetation. Northeast of Jackson Lake, this unit is primarily composed of quartzite roundstones of the Harebell Formation with a sand and gravel matrix. Along the Teton range front, glacial drift deposits form ice-parallel ridges, lateral and end moraines primarily composed of Precambrian rocks from the Teton Range.

Pliocene Huckleberry Ridge Tuff (Th)

Rhyolitic ashfall tuff, typically gray to brown in color. This densely welded rock is typically devitrified, contains abundant phenocrysts of quartz, sanidine, and plagioclase with minor amounts of fine- to medium-grained clinopyroxene and opaque minerals. The unit is divided into Members A, B, and C, with Member C exposed northeast of Jackson Lake.

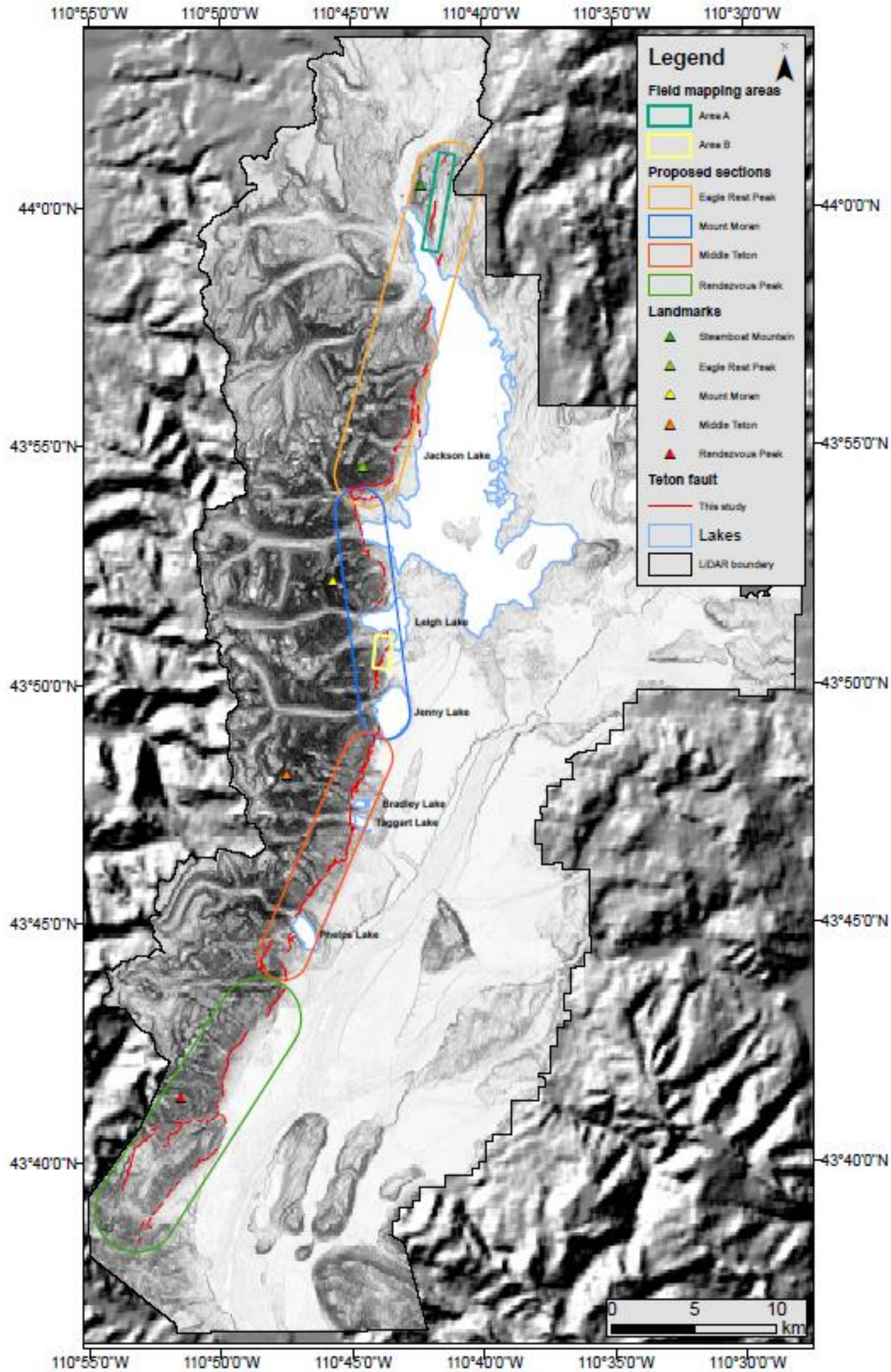

Figure 12. Areas selected for field mapping, proposed fault sections, and landmarks along the Teton Range.

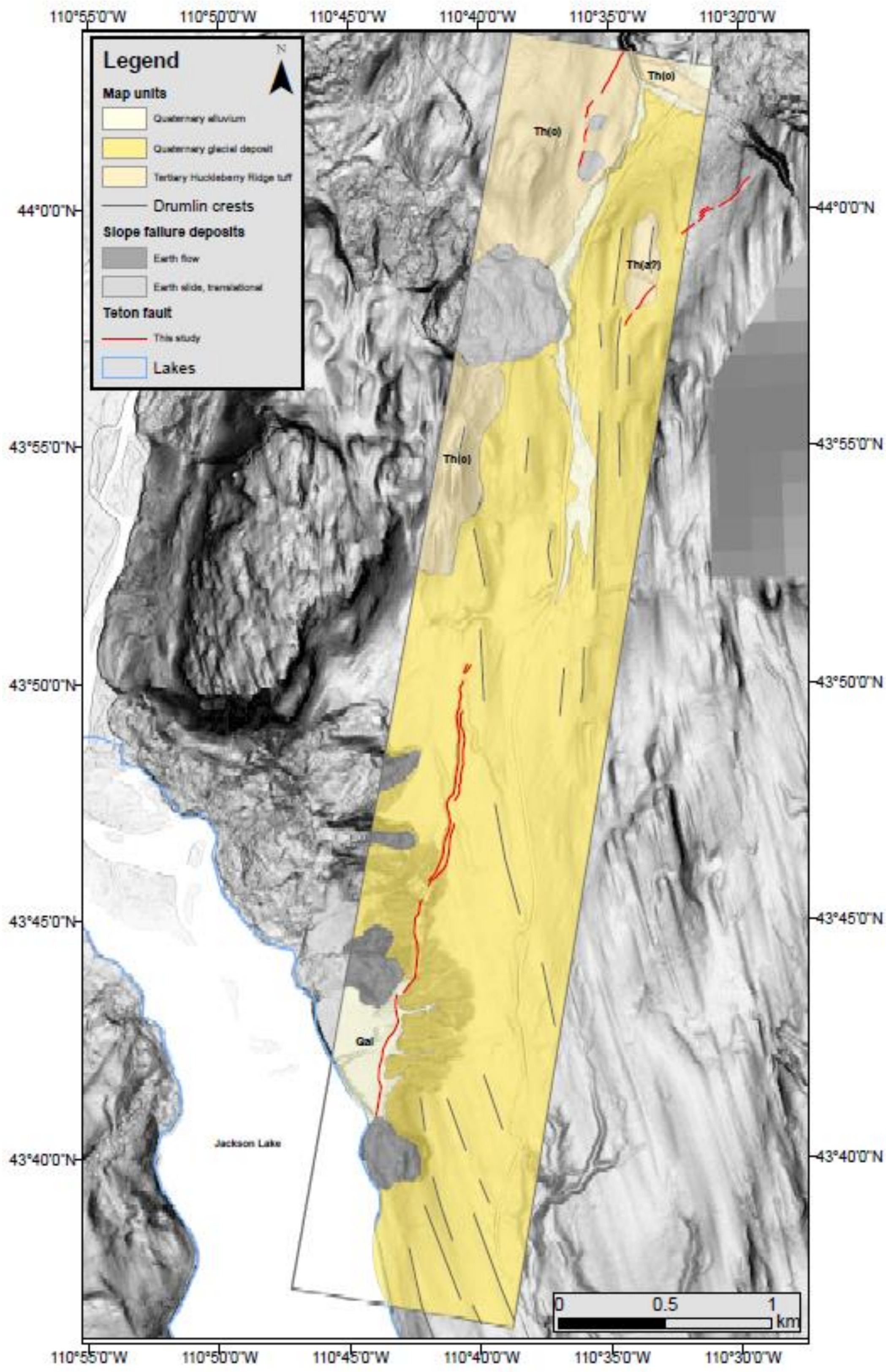

Figure 13. Digitized field map of field area A, northeast of Jackson Lake. This area is within the proposed Eagle Rest Peak section of the Teton fault. NNE-striking fault scarps cross the S- to SE-trend of the drumlin ridges. Translational slides and earth flows are common, particularly along the shore of Jackson Lake.

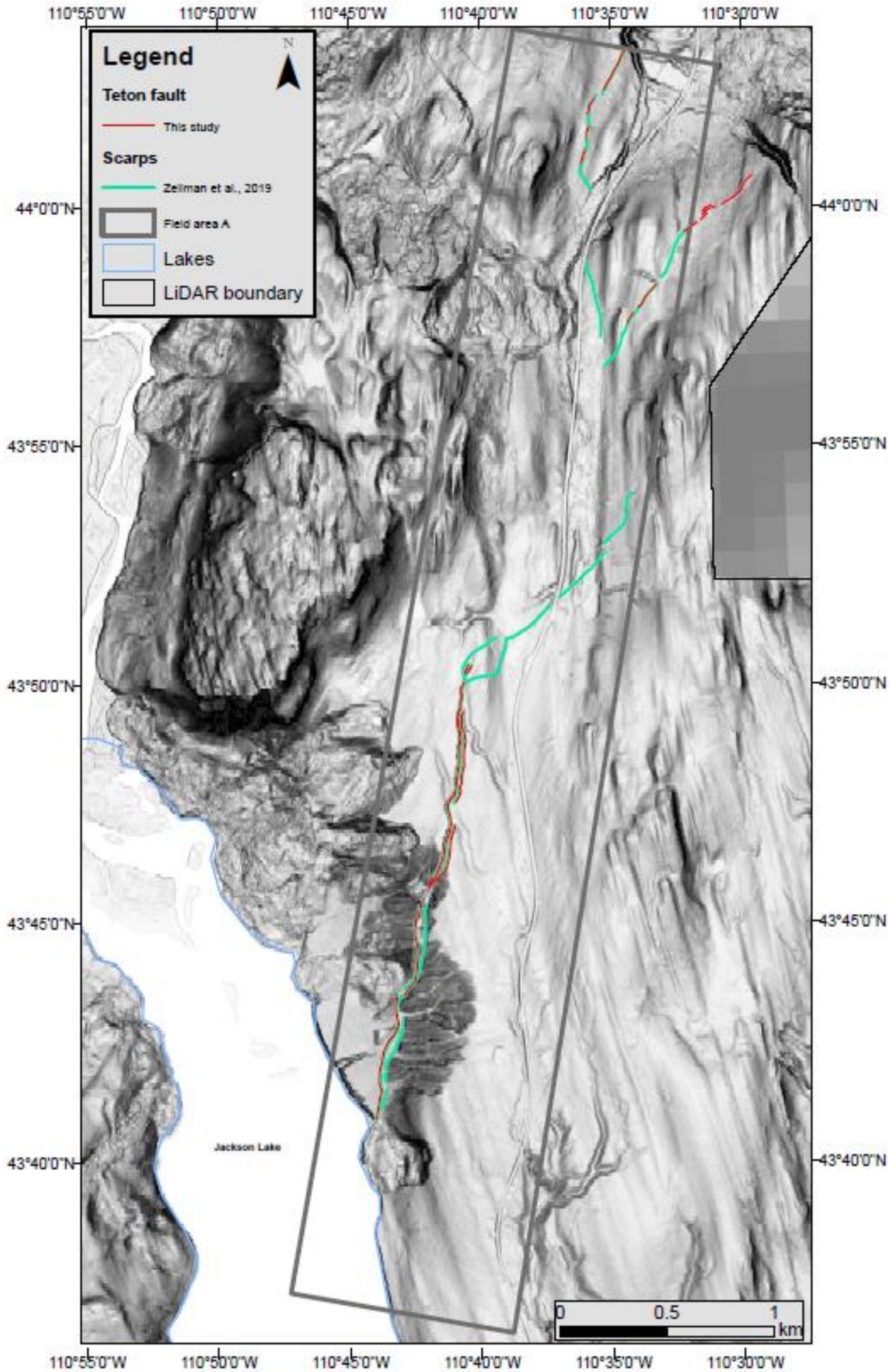

Figure 14. Field and digital mapping in field area A resulted in revision to the fault scarps previously mapped by Zellman et al. (2019). Scarps mapped as part of this project (red) and scarps shown on the Teton Fault map by Zellman et al. (green).

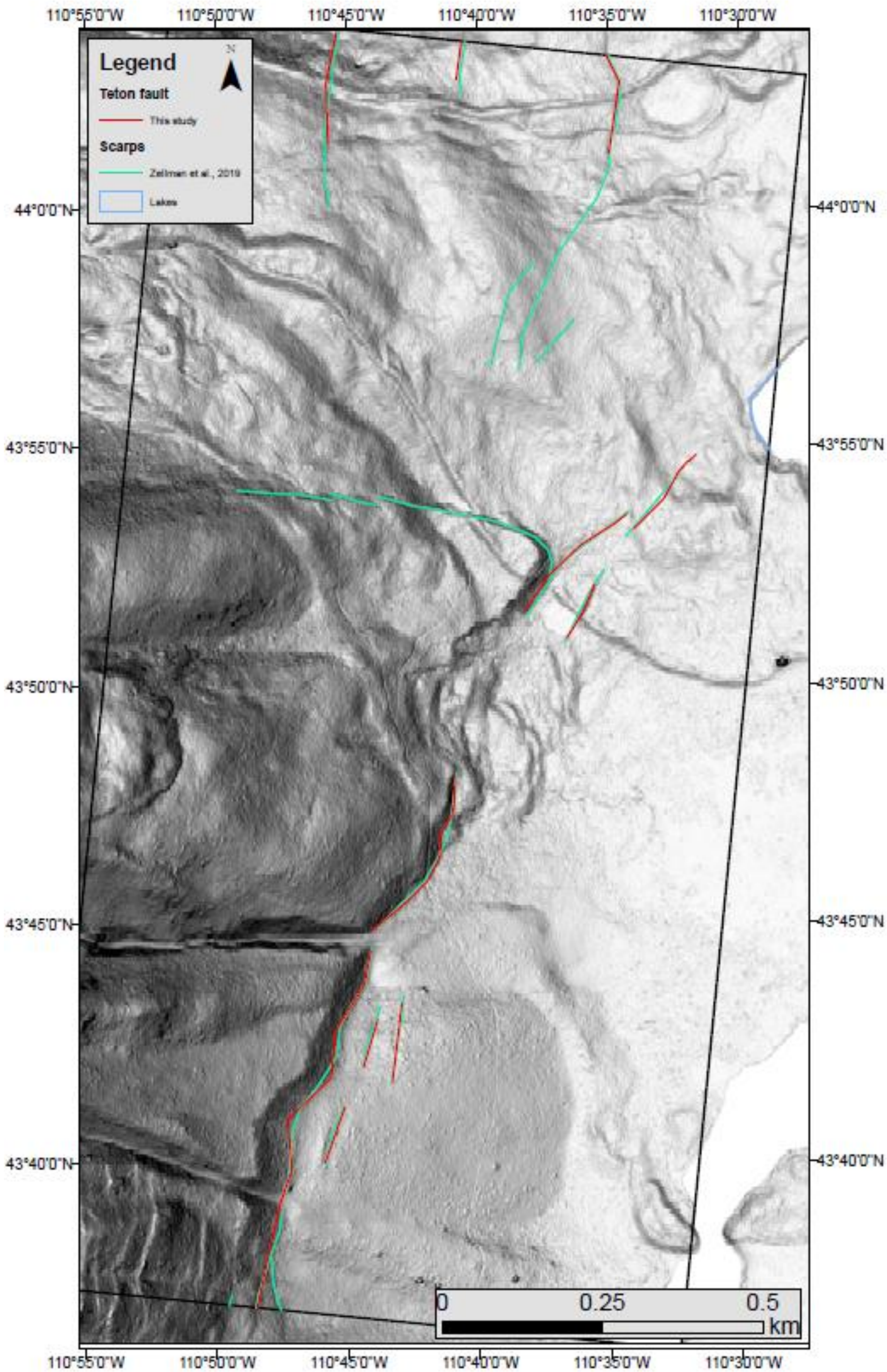

Figure 15. Field and digital mapping in field area B resulted in revision to the fault scarps previously mapped by Zellman et al. (2019). Scarps mapped as part of this project (red) and scarps shown on the Teton Fault map by Zellman et al. (green).

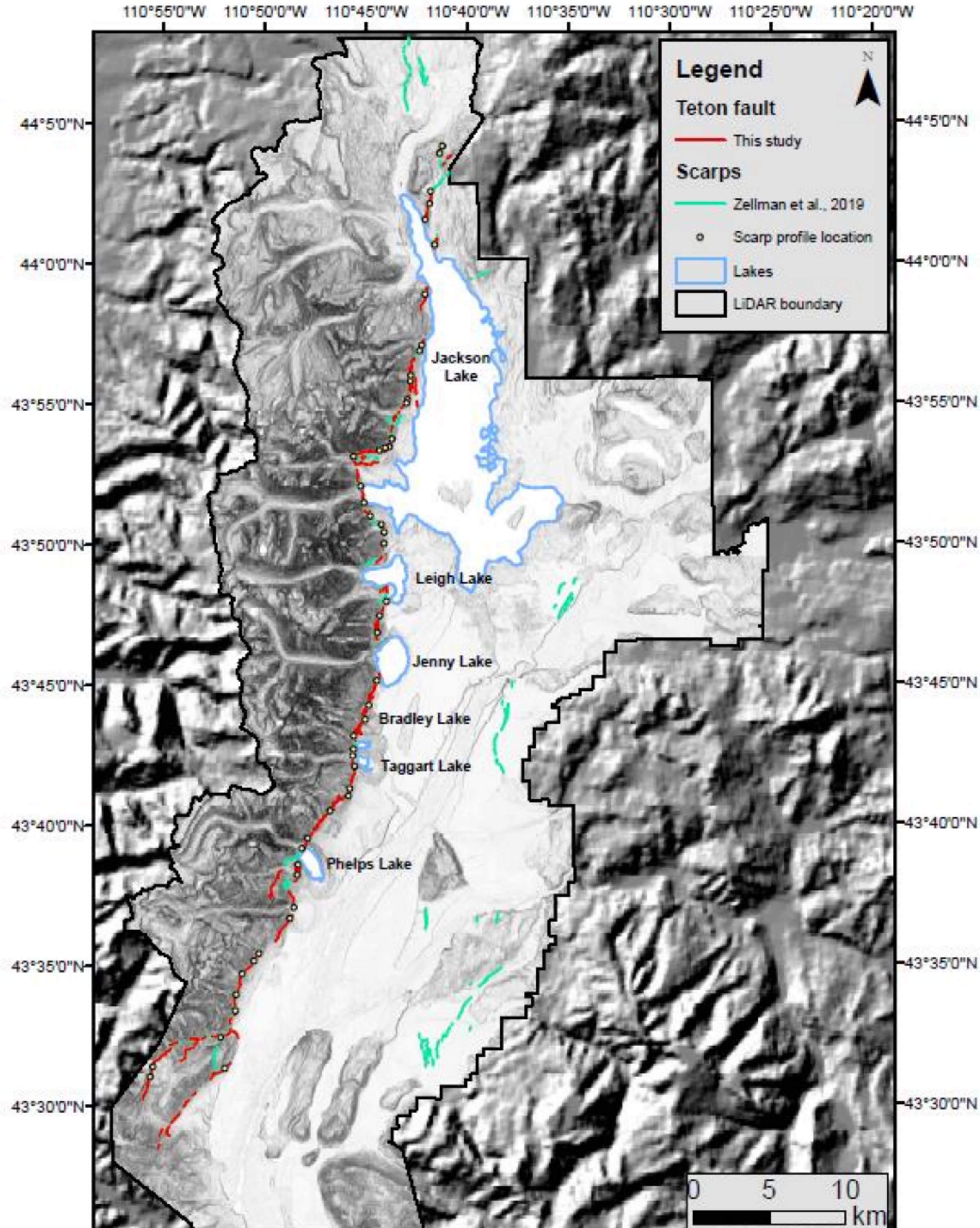

Figure 16. Comparison of fault scarps mapped in this study and those of Zellman et al. (2019). Note that this study was confined to the Teton fault, and the work of Zellman et al. (2019) included mapping scarps north of the Teton fault and other scarps in the Jackson Hole valley.

Interpretation and Discussion

The more detailed dataset of vertical separation presented here indicates that previous fault section interpretations (refer to Chapter I, Previous Work; Susong et al., 1987; Smith et al., 1993) can be improved by considering the expected behavior of normal faults. Here, we propose a four-section model of the Teton fault based on vertical separation analysis and expected patterns of fault behavior. The identification and characterization of fault section and segment boundaries has important implications for hazards assessment. In this context, a fault section is an area along a fault which is typically identifiable from generalized characteristics, while a fault segments represent individual parts of a fault which may rupture independently of one another during an earthquake event. This work indicates that a four-section, or possibly segment, model of the fault should be considered.

Simple scarp height and vertical separation

Simple scarp height across scarps reflect fault offset rates and the surface slope of landforms cut by normal faults. Geometric relationships between surface slope and fault offset lead to higher scarps where the slope of preexisting surfaces is steep (Figure 8). Measurements of vertical separation account for this effect. Thus, measurements of vertical separation across scarps provide a better understanding of offset patterns along fault systems. Vertical separation varies along the length of the Teton fault (Figure 10). Individual scarps are vertically separated by up to 54.4 m (average 14.5 m), and the highest scarps are found along the southern range front and Phillips Canyon.

Along-strike variation in scarp height and vertical separation may be the result of 1) along-strike, variable offset rates of the Teton fault; 2) variable erosion of the fault scarp by Pleistocene glacial processes; 3) variable ages of landforms; 4) erosion and deposition by slope failure and alluvial processes that have occurred since deglaciation; or 5) some combination of these factors, and possibly others.

1) Along-strike variable offset rates

Along strike estimations of offset rate along the fault suggests that variable scarp height may be the result of variable offset rate along the Teton fault. The offset rate may vary between sections and within sections of the fault. Vertical separation across fault scarps combined with surface exposure ages of deglacial landforms can be used to estimate vertical separation rates. Using the average vertical separation measurement across five scarp profiles and the age of the deglacial surface (14.4±0.8 ka; Licciardi and Pierce, 2018), we calculate a vertical separation rate of 0.32±0.01 m/k.y. for the area northeast of Jackson Lake (Figure 17 and Table 4).

Thackray and Staley (2017) calculated a vertical separation rate of 0.82 ±0.13 m/k.y. over the past 14.7 k.y. from valley floor offsets of well-constrained deglacial age in the central portion of the fault but found these values to be inconsistent with data from higher, and geomorphically older, landforms. Using data from the Buffalo Bowl and Granite Canyon paleoseismic studies and vertical separation measurements, DuRoss et al. (2019a) calculate a latest Pleistocene (14.4-4.7 ka) closed-interval vertical slip rate of ~1.1 m/k.y. for the southern Teton fault and an early Holocene to present open-ended rate of ~0.6 m/k.y. These values indicate that along-strike variable offset rates could contribute to variable scarp height.

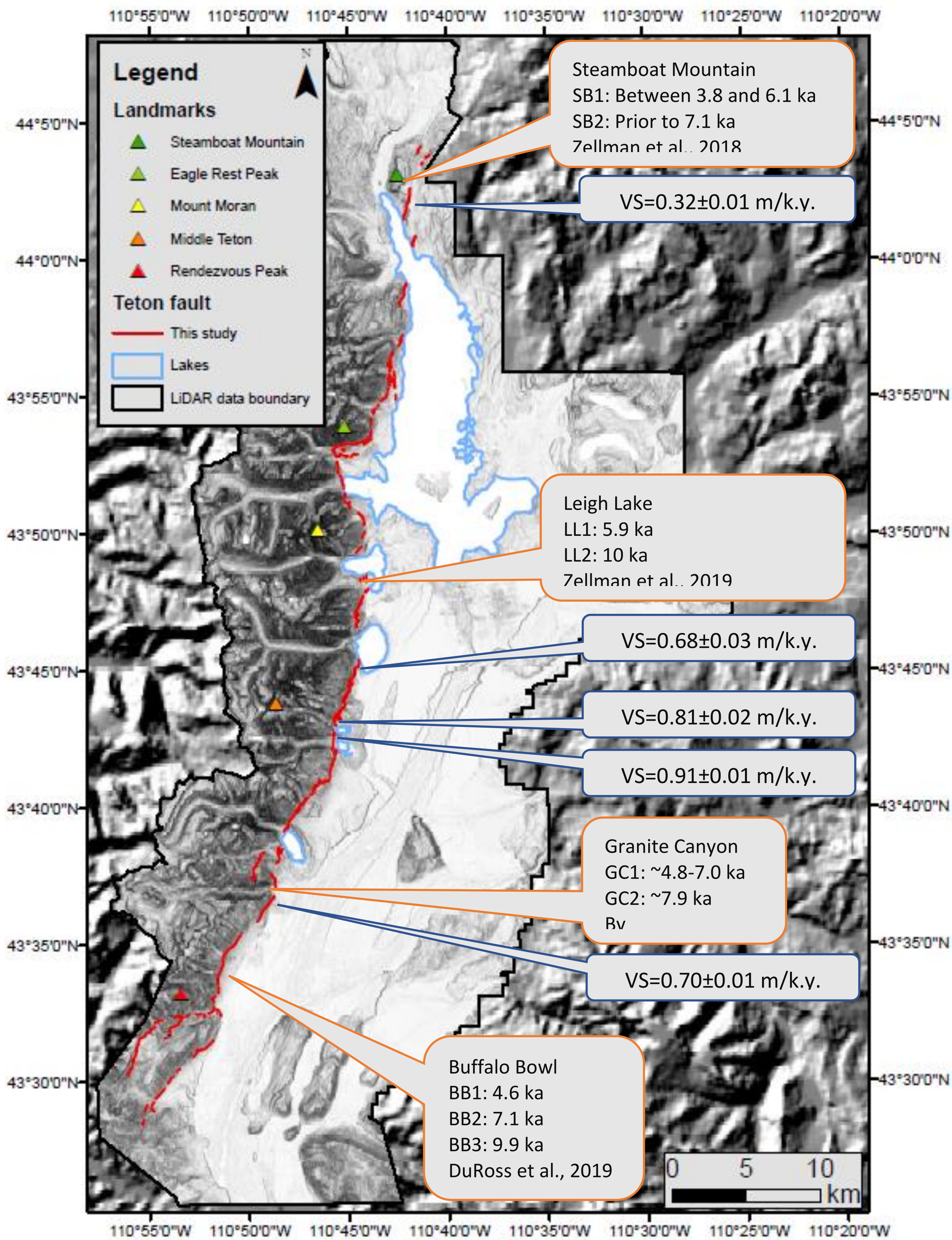

Figure 17. Vertical separation rates and paleoseismic data from previous studies of the Teton fault. Callout boxes with orange borders denote paleoseismic trenching studies, while those with blue borders denote locations of vertical separation rate calculations from this study.

2) variable erosion of fault scarps by Pleistocene glacial processes

Glaciers play a key role in shaping mountain valleys through sediment production, transportation, and deposition (Hallet et al., 1996; Spotila et al., 2004; Brocklehurst and Whipple, 2006; Foster et al., 2010). These factors have likely had a significant impact on erosion and degradation of Teton fault scarps. Because the effects of fault scarp erasure by glacial processes have not been studied in the Teton Range or elsewhere, we assume that glacial erosion and deposition reduced the scarp height to match valley floor topography, effectively erasing the pre-existing vertical separation within glacial valleys.

Assuming this is the case, deglaciated valleys provide an opportunity to compare vertical separation across landforms of assumed similar age. Pinedale age glacial activity is recorded as a series of glacially eroded valleys (on the footwall), sediment filled valleys (on the hanging wall), and lateral and terminal moraines mantling the range front and the fault (Licciardi and Pierce, 2008; Pierce et al., 2018). At the mouth of Glacier Gulch, the valley floor scarp has vertically separation of ~9.9 m. At Phelps Lake, vertical separations of ~6.6 m and ~14.0 m were recorded on the valley floor and right lateral moraines, respectively.

3) variable ages of landforms

The ages of range front landforms and lake sediments have been determined from cosmogenic ^{10}Be surface exposure and radiocarbon dating along the Teton fault (Licciardi and Pierce, 2008; Licciardi et al., 2014a, 2014b, 2015; Larsen et al., 2016; Pierce et al., 2018). Landforms of varying age pose a challenge to addressing fault scarp height variability. Scarps cutting older landforms would likely have experienced a greater number of slip events than those cutting younger landforms, and thus have higher scarps. Landform age plays a critical role in addressing fault scarp height variation.

At Taggart Lake, vertical separation of ~14.7 m and ~12.5 m across the highest fault scarps on the left and right lateral moraines, respectively, allow for evaluation of vertical separation across varying time scales. The moraine ages are 18.2±0.5 ka and 15.1±0.2 ka, respectively, based on preliminary interpretation of cosmogenic ^{10}Be surface exposure dating (Licciardi et al., 2019; Licciardi, pers. comm.). Using these values, both the left and right lateral moraines have undergone similar rates of vertical separation (0.81±0.02 m/k.y. and 0.91±0.01 m/k.y., respectively) (Table 4). Variable landform age appears to explain the difference in vertical separation across these moraines. The valley floor is vertically separated by ~10.6 m and, the presence of this smaller offset indicates that the higher scarps on lateral moraines are likely an artifact of landform age, rather than variable offset rate.

4) erosion and deposition by slope failure and alluvial processes that have occurred since deglaciation

Slope failure events have taken place throughout the study area (Figure 11). In some places, slope failure deposits are offset by fault scarps (Figure 18). Translational slide and debris flow deposits affect the surface expression of scarps along the Teton fault (Figure 19). Individual slope failure-affected areas (e.g., slope failure deposits plus the failure scarp area) reach up to 2.4 km^2, but most deposits cover <0.1 km^2 in the study area. The majority of slope failure deposits have been transported east or southeast, following the general range front topography. In the walls of formerly glaciated valleys and along moraines, deposits are typically transported downslope in the north or south direction.

Approximately 16% of the Teton fault intersects with slope failure deposits. Where slope failure events initiate above and cross fault scarps, the surface expression of the scarp is reduced or entirely obscured by the deposit, effectively reducing the height of scarps in slope failure affected areas (Figure 19, top inset map). Approximately 7% of the fault is buried by slope failure deposits that are uncut by fault scarps. Few slope failure deposits are cut by scarps of the Teton fault; however, there are notable exceptions to this pattern north of Leigh Lake and south of Phelps Lake, where fault scarps are vertically separated by 42.8 and 14.6 m, respectively (Figure 19, center and bottom inset maps). Slope failure deposits are offset by fault scarps along approximately 9% of the fault length.

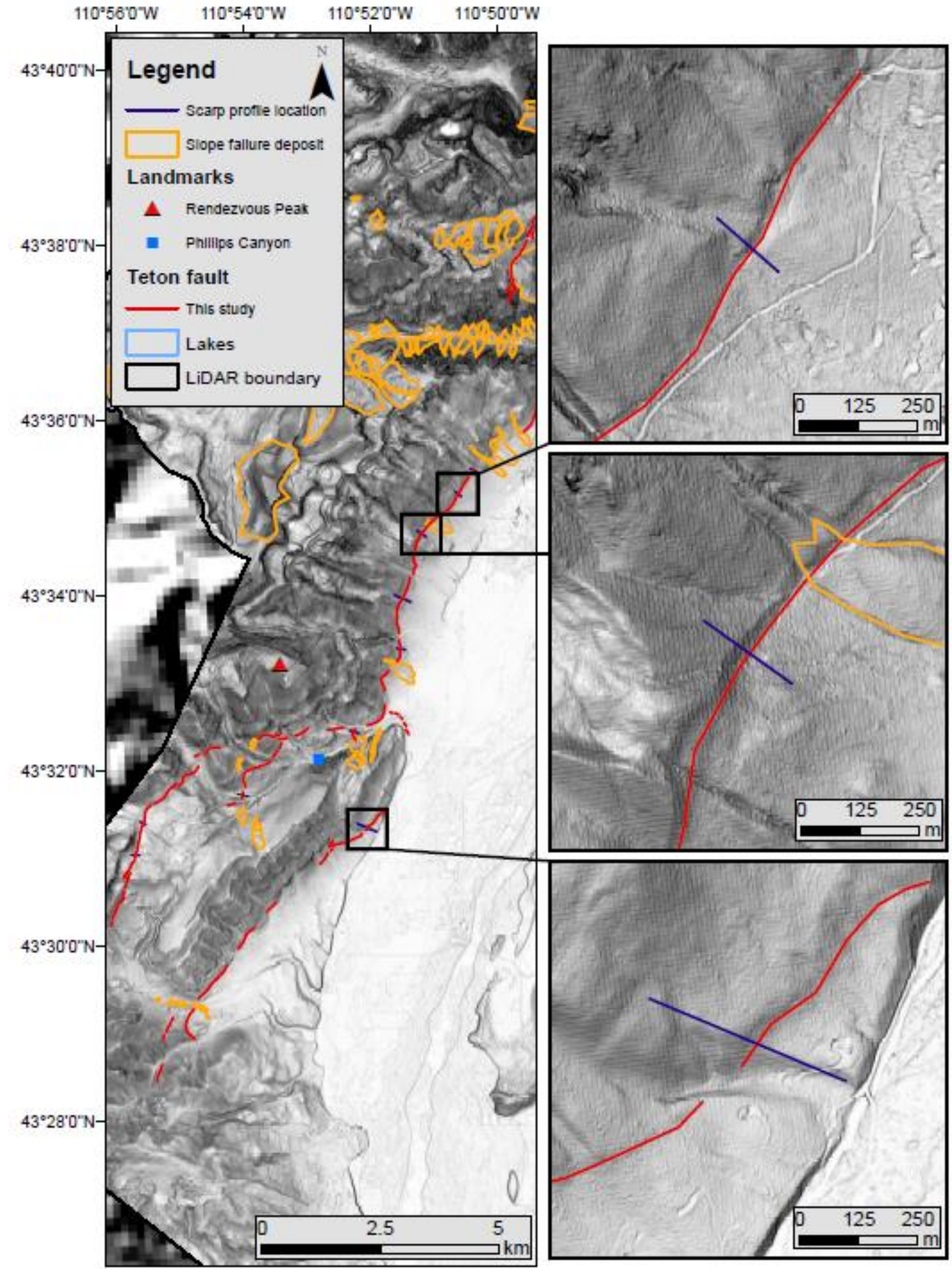

Figure 18. High scarps at southern end of the Teton fault. Inset maps: top- location of profile number 62 (17.3 m vertical separation); center- location of profile number 64 (44.0 m vertical separation) and debris flow deposit cut by the Teton fault; bottom- location of profile 70 (54.4 m vertical separation). Although profiles 62 and 64 were not considered in vertical separation analyses because vertical separation exceeded simple scarp height, they are included here as examples of the high scarps along the southern range front.

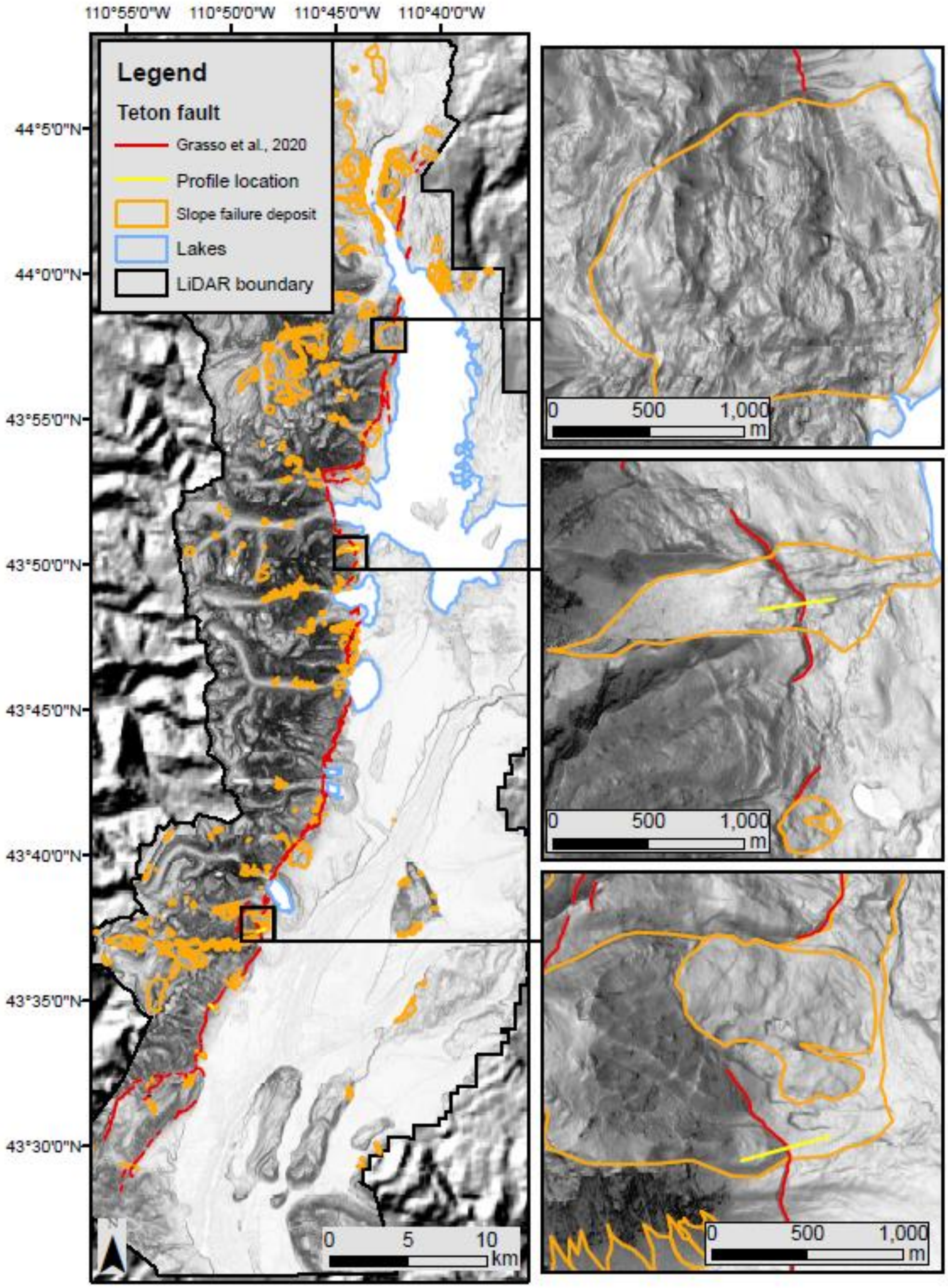

Figure 19. Locations where fault scarps cut slope failure deposits. Insets: top- scarp is buried by a translational slide; center- scarp cuts debris flow deposit; bottom- "nested" translational slides with fault scarp cutting older deposit but not the younger deposit. Yellow lines mark where vertical separation profiles of scarps cutting slope failure deposits were generated.

5) some combination of these factors, and possibly others.

Variable tectonic fault offset rates, variable erosion by Pleistocene glacial processes, and erosion by slope failure and alluvial processes may all influence the size of Teton fault scarps individually or in concert. It is also possible that other factors not identified here (e.g., lithologic, climatic, or hydrologic variations) play a role in fault scarp height variability and sediment flux within the fault zone. Both large- and small-scale landscape disturbance events (e.g., earthquakes, slope failures, and floods) may be triggered by movement of the Teton fault. Erosion and deposition by alluvial processes can reduce fault scarp height. Sediment flux along the fault influences geomorphology, stream character, and flooding along the range front.

Fault sections, fault segments, and their boundaries

The number of segments and the location of segment boundaries along the Teton fault have been the subject of debate, as has the identification and characterization of fault sections and segments in general (Crone and Machette, 1984; Machette et al., 1991; Smith et al., 1993; Faulds and Varga, 1998; O'Connell et al., 2003; DuRoss et al., 2019b). Susong et al. (1987) proposed a three-segment model of the Teton fault based on field mapping and topographic profiling at 17 locations along the fault. Smith et al. (1993) proposed a three-segment model of the Teton fault with segments defined by changes in strike direction, lateral stepping, structural complexities, variation in scarp height, and interpretation of gravity data. However, both of these studies were confined to a limited section of the central portion of the Teton fault.

The three-segment interpretation is contrasted by the work of Ostenaa (1988), who suggested that the gravity anomaly is not concurrent with a fault segment boundary, and interpreted the fault as being divided into two segments. It is important to note that many of the commonly referenced indicators of segmentation are distinctly two-dimensional in nature, and the two-dimensional nature of geologic maps and the limited ability of many study approaches to portray three-dimensional conditions at depth along a fault may contribute to misunderstandings of fault growth and segmentation (Walsh et al., 2003).

Here, we propose a four-section model of the Teton fault based on vertical separation across fault scarps and changes in strike direction (Figure 10 and Figure 20). From north to south, these four sections are the Eagle Rest Peak (ERP), Mount Moran (MM), Middle Teton (MT), and Rendezvous Peak (RP) sections (Figure 20 and Table 3). The ERP section extends from northeast of Jackson Lake south to Moran Bay. The MM section extends from north of Moran Bay to the south end of Jenny Lake. The MT section reaches from south Jenny Lake to Granite Canyon. The RP section extends from Granite Canyon to the south end of the fault at Teton Pass. Vertical separation is greatest toward the central portion of each of these sections and declines toward the ends, following the expected pattern of normal fault behavior.

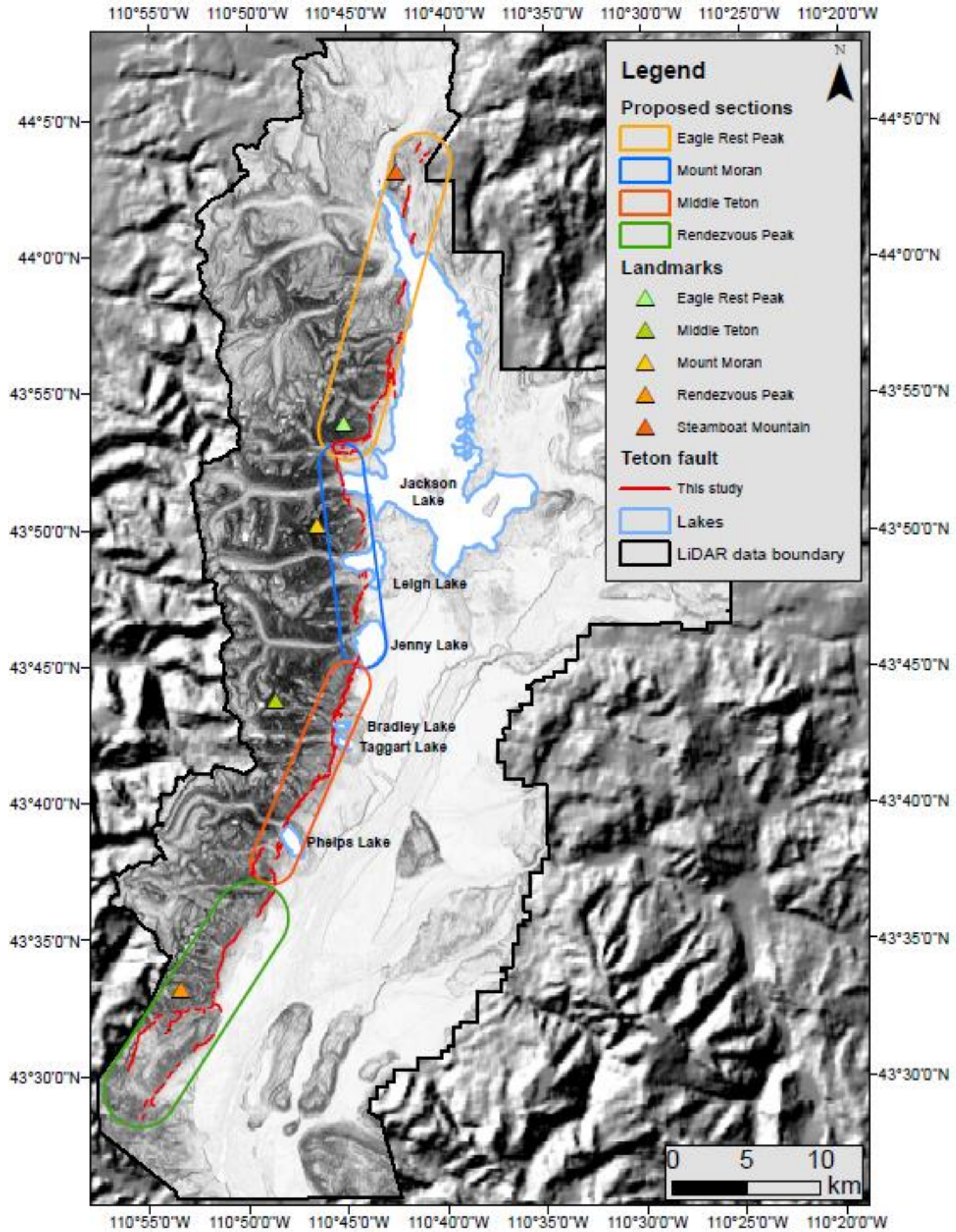

Figure 20. The proposed four-section model of the Teton fault. The model is primarily based on vertical separation across fault scarps. Note that the proposed sections also correspond to changes in strike within the Eagle Rest Peak, Mount Moran, Middle Teton, and Rendezvous Peak sections.

Table 3. Summary of proposed fault sections. Average, maximum, and minimum vertical separation (VS) measurements vary between each section.

Proposed section	Approximate Length (km)	Fault strike	Number of profiles	Average VS (m)	Maximum VS (m)	Minimum VS (m)
Eagle Rest Peak	22	NNE	18	11.9	21.3	1.0
Mount Moran	15	NNE	7	15.0	32.0	1.6
Middle Teton	16	NNE	11	12.2	14.8	6.6
Rendezvous Peak	19	NE	6	26.1	54.4	13.6

The ERP section extends from northeast of Jackson Lake south to Moran Bay. This section is characterized by a NNE-striking fault and vertical separation ranging from 1.0 to 21.3 m (average 11.9 m) based on measurements from 18 scarp profiles distributed along 22 km of the fault (Table 3 and Figure 20). At the northern end of the section, fault scarps cut drumlins sculpted by the Jackson Lake Lobe of the GYGS ice sheet. We calculate a vertical separation rate of 0.32±0.01 m/k.y. using the average vertical separation across the five scarp profiles cutting drumlinoid topography northeast of Jackson Lake and a surface age of 14.4±0.8 ka based on work by Licciardi and Pierce (2018) (Figure 17 and Table 3).

Table 4. Summary of vertical separation rates calculated from scarp profile data and previously published surface age data. Note: the average vertical separation across five scarp profiles was used to estimate vertical separation rates northeast of Jackson Lake. Along the southern range front, the average vertical separation across five scarp profiles, and two surface exposure ages, were used to estimate vertical separation rates in the area. Note: surface ages at Taggart Lake right and left lateral moraines are preliminary ages

Area	Vertical separation (m)	Surface age (ka)	Vertical separation rate (m/k.y.)	Surface age reference
Drumlins NE of Jackson Lake	4.64	14.4+/-0.8	0.32±0.01	Licciardi and Pierce, 2018
Jenny Lake right lateral moraine	10.28	15.2 +/-0.7	0.68±0.03	Licciardi and Pierce, 2018
Taggart Lake right lateral moraine	13.77	15.1+/-0.2	0.91±0.01	Licciardi, pers. comm.
Taggart Lake left lateral moraine	14.76	18.2 +/-0.5	0.81±0.02	Licciardi, pers. comm.
Granite Canyon right lateral moraine	12.85	18.24+/-0.34	0.70±0.01	Licciardi et al., 2014
Southern range front, using Pinedale age surface exposure constraint	28.80	18.24+/-0.34	1.6±0.02	Licciardi et al., 2014
Southern range front, using Bull Lake age surface exposure constraint	28.80	136+/-13	0.21±0.03	Licciardi and Pierce, 2008

The Mount Moran section includes the area from Moran Bay to the southern end of Jenny Lake (Figure 20). This section is characterized by vertical separation ranging from 1.6 m to 32.0 m (average 15.0 m) based on measurements from 7 scarp profiles distributed along 15 km of the fault. In this area, fault scarps offset a variety of landforms including ice cap outlet glacier deposits from the Jackson Lake lobe of the GYGS, slope failure deposits, and the Teton-sourced lateral moraines of Pinedale age at both the north and south ends of Jenny Lake (Figure 21). We calculate a vertical separation rate of 0.68±0.03 m/k.y. across the Jenny Lake right lateral moraine using a surface exposure age of 15.2±0.7 ka from Licciardi and Pierce (2018) (Figure 17 and Table 3).

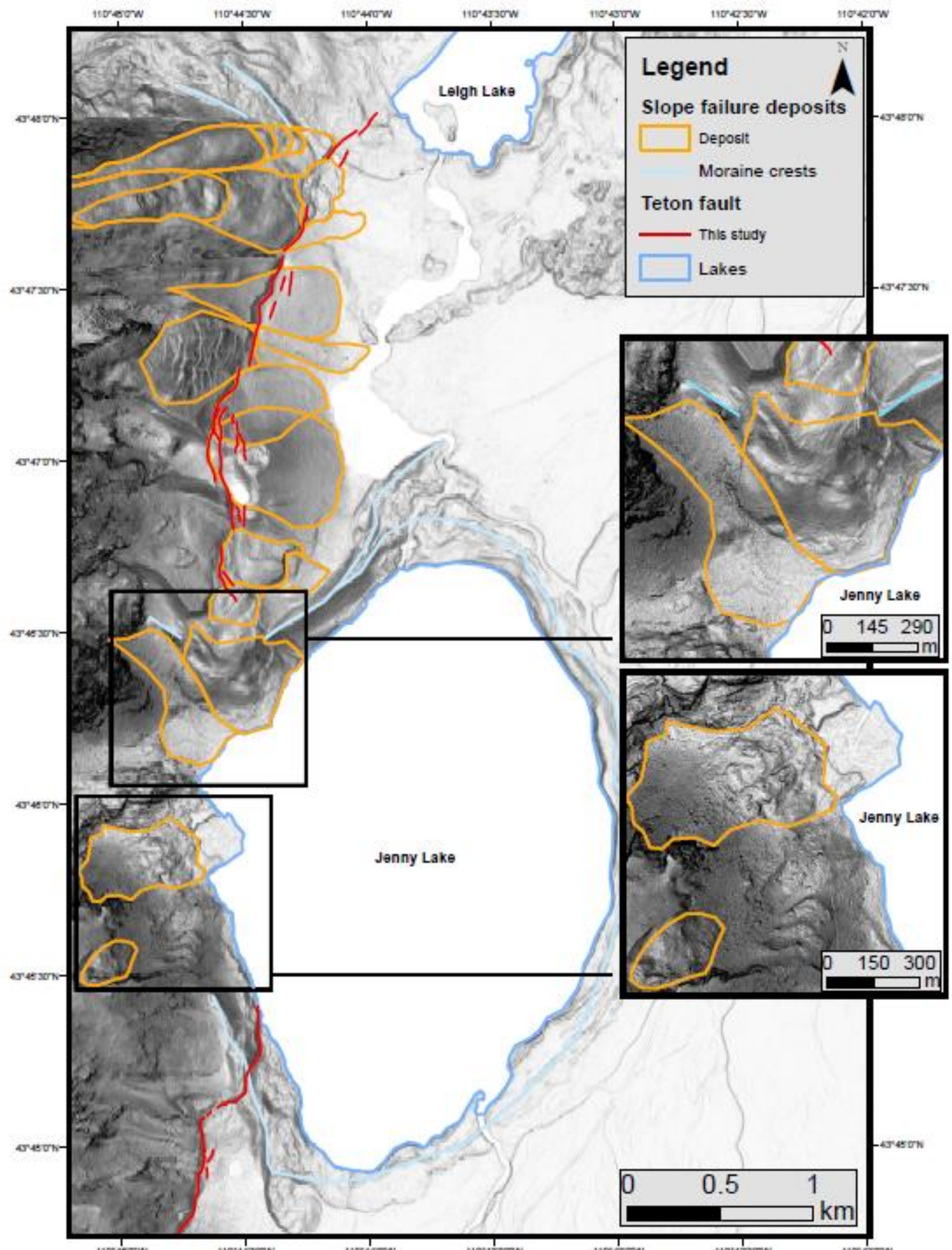

Figure 21. Fault scarps, moraine crests, and slope failure deposits at Jenny Lake. Inset maps: top- slope failure deposits on the left lateral moraine of Jenny Lake conceal the fault scarp; bottom- slope failure deposits along the western shore of Jenny Lake.

The Middle Teton section includes the area from southern Jenny Lake to the north side of Granite Canyon (Figure 10 and Figure 20). This section is characterized by a NNE-striking fault and vertical separation ranging from 6.6 m to 14.8 m (average 12.2 m) based on measurements from 11 scarp profiles distributed along 16 km of the fault (Table 3). Fault scarps offset Pinedale age lateral moraines at Bradley, Taggart, and Phelps Lakes as well as Glacier Gulch. We calculate a vertical separation rate of 0.91±0.01 m/k.y. across the left lateral moraine at Taggart Lake using a surface exposure age of 15.1±0.2 ka from Licciardi (2019) (Table 4). A vertical separation rate of 0.81±0.02 m/k.y. across the right lateral moraine at Taggart Lake using a surface exposure age of 18.2±0.5 ka from Licciardi (2019) (Table 4). Translational slides and a rock glacier deposit are also offset by the fault in this section but remain undated at this time.

The Rendezvous Peak section includes the fault zone from Granite Canyon south to Teton Pass (Figure 10 and Figure 20). This section is characterized by NE-striking a fault and vertical separation ranging from 13.6 to 54.4 m (average 26.1 m) (Table 3 and Figure 20). Within this zone, the fault bifurcates into two semi-parallel strands: the Phillips Valley fault to the west, and the Teton fault to the east. Debris flows and translational slides are common in this section but are infrequently offset by the fault. Anomalously high scarps in this section are found in several locations along both the Phillips Valley and Teton fault strands. These high scarps may be the result of greater landform age, high fault offset rates, structural interactions with the Laramide age Cache Creek and Jackson thrust faults, or some combination of these factors. We calculate a vertical separation rate of 0.70±0.01 m/k.y. across the right lateral moraine at Granite Canyon using a surface exposure age of 18.24±0.34 ka from Licciardi et al. (2014b) (Table 4).

Surface age data are limited in the Rendezvous Peak section, so two distinct vertical separation rates have been calculated using the average vertical separation across the five southernmost scarp profiles (25.8 m) and two assumed ages. The first of these, using the Pinedale surface exposure age from the right lateral moraine at Granite Canyon, provides a vertical separation rate of 1.6±0.02 m/k.y. (Table 4). The second, calculated using a Bull Lake surface exposure age of 136±0.34 ka from boulders in southern Jackson Hole (Licciardi and Pierce, 2008), provides a vertical separation rate of 0.21±0.03 m/k.y. (Table 4). If scarps along the southern range front cut Pinedale age deposits, the vertical separation rate along the southern fault is higher than other, more well-constrained, vertical separation rates calculated along the fault. However, if these scarps cut surface deposits of Bull Lake age, the vertical separation rate along the southern range front is less than the vertical separation rate for scarps cutting Pinedale age deposits to the north. It is also possible that the fault cuts landforms of both ages and that these rates, based on average vertical separation, are not meaningful.

The transition zones between these four distinct areas of the range front may represent boundaries between fault sections or segments. The sections proposed here are based on data that represent the behavior of the fault in Middle to Late Pleistocene time. Data from paleoseismic trenching studies indicates that the most recent surface rupturing event on the Teton fault took place 4-5 ka; this may indicate that sections (or segments) of the fault rupture in unison, or have done so recently (Zellman et al., 2018, 2019c; DuRoss et al., 2019b). However, these studies are bear uncertainty, and further paleoseismic work is needed to better clarify the rupture history and potential for segmentation and segment linkage during earthquake events along the fault.

Uncertainty in these approaches comes from four primary sources: 1) fault scarps cut complex deglacial, alluvial, and hillslope landforms, leading to uncertainty when choosing the top and bottom points of the scarp used for calculating the simple scarp height and vertical separation values; 2) geomorphology along the fault zone is complex and surface age data is limited, such that measuring profiles across isochronous surfaces can be challenging; 3) the ArcGIS profiler tool extracts data from the LiDAR-based DEM at a set resolution, inherently introducing a small level of error in profile measurement; and 4) higher fault scarps increase the uncertainty of both simple scarp height and vertical separation calculations (Thackray and Staley, 2017).

Surface expression of the fault varies across five geomorphic areas

Surface expression of fault scarps varies along the length of the Teton fault. Five geomorphic areas with unique surface expression of the fault have been identified in the study area: 1) drumlins in Pinedale age ice cap outlet lobe deposits northeast of Jackson Lake; 2) scarps cutting glacial outwash and alluvial fans between Jackson and Jenny Lakes; 3) Pinedale-age lateral moraines; 4) Pinedale-age deglaciated valley floors; and 5) the southern range front, where the age of surface deposits remains largely unknown (Figure 22 and Table 5).

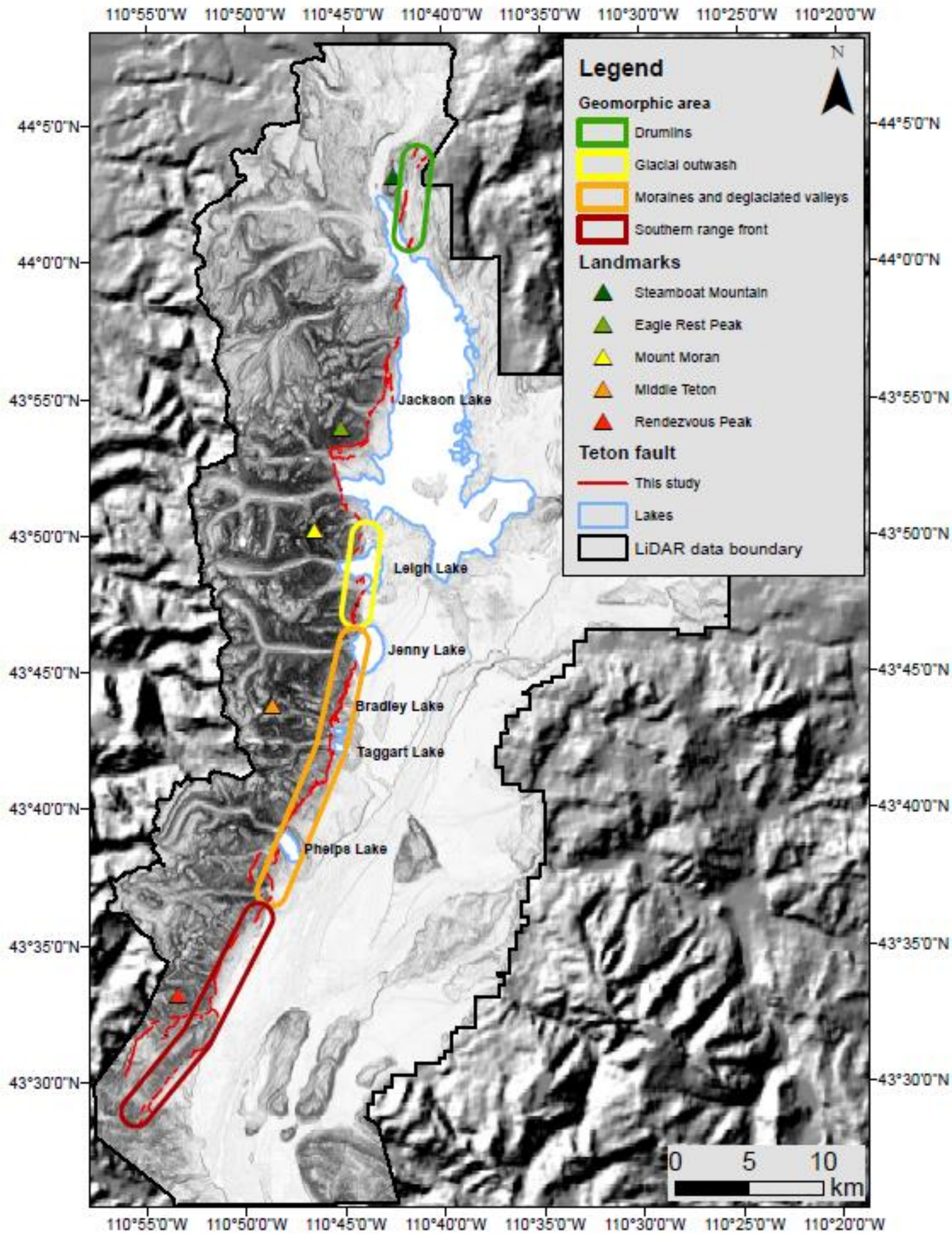

Figure 22. Five geomorphic areas identified along the Teton fault.

Table 5. Summary of fault behavior through the five geomorphic areas. Average and maximum vertical separation across scarps (VS) are included for comparison.

Geomorphic Area	Extent	Fault strike	Average VS (m)	Maximum VS (m)
Drumlins	Northeast of Jackson Lake	NNE	4.6	8.7
Pinedale outwash	Jackson Lake to south Jenny Lake	NNW	15.7	32.0
Pinedale lateral moraines	Leigh Lake to Granite Canyon	NE to N	12.9	14.8
Pinedale deglacial valleys	Leigh Lake to Granite Canyon	NNE to NE	10.2	13.0
Southern range front	Granite Canyon to Teton Pass	NE	28.8	54.4

Slope failures tend to be larger in the northern half of the study area and smaller and more common in the southern half of the study area

Slope failure deposits along the Teton range front generally fall into two categories: translational slides and debris flows. North of Leigh Lake, translational slide deposits are more common than debris flow deposits. Slide deposits tend to be larger in this area than those found in the southern half of the study area, covering up to 2.4 km^2. South of Leigh Lake, translational slide deposits up to 2.3 km^2 were mapped, but most deposits are <0.5 km^2. Several of the larger slide deposits contain smaller slides within their borders. The majority of debris flow deposits are found within the southern half of the study area (Figure 23).

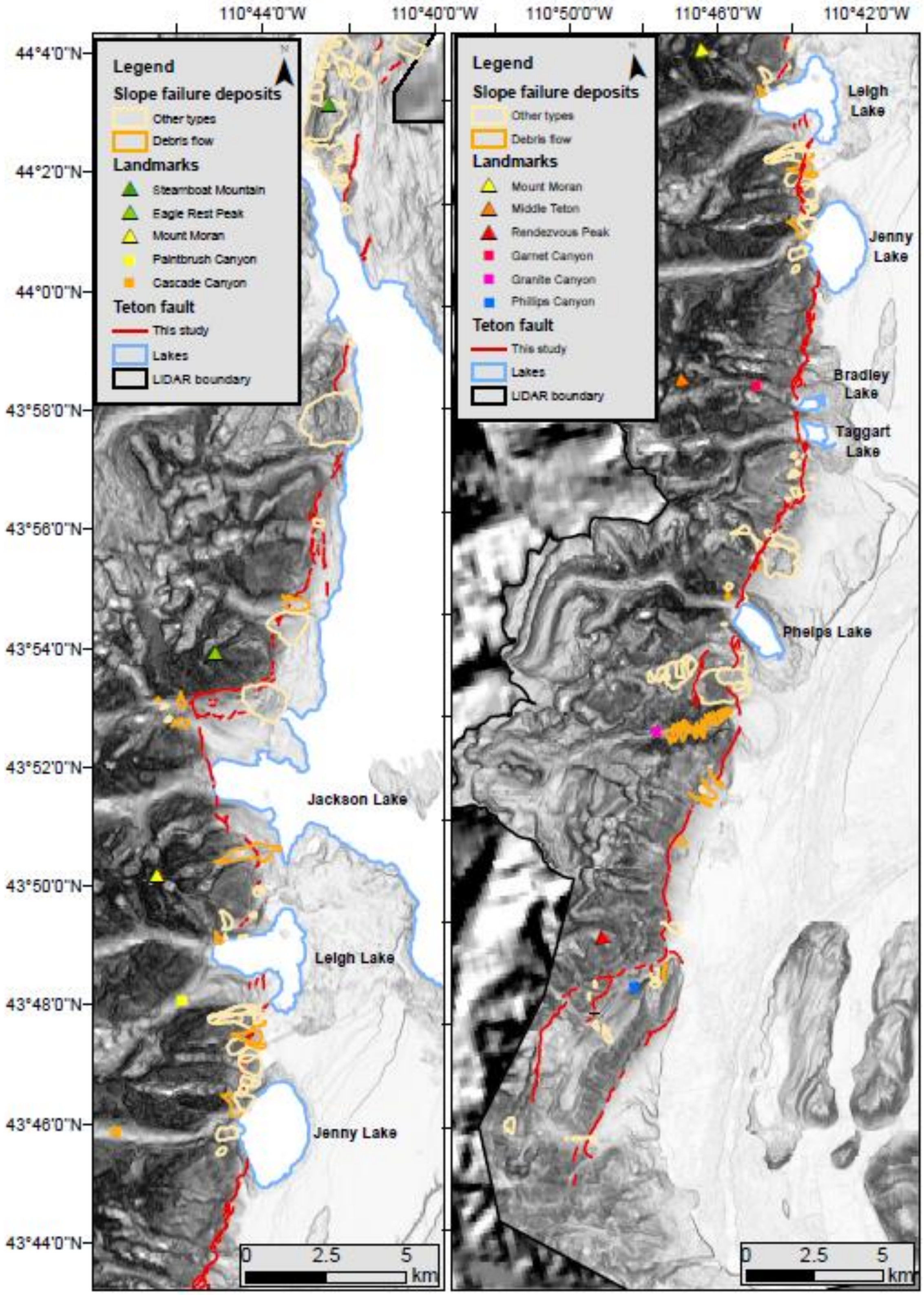

Figure 23. Debris flows and other slope failure deposits in the northern and southern halves of the study area. Translational slide deposits are more common in the north, particularly along the shores of Jackson Lake, while debris flow deposits are more common along the southern half of the study area and on the south-facing slopes of deglaciated valleys.

Conclusions

Along the 75-km Teton fault, fault scarps are well-expressed geomorphically and vary in height by up to tens of meters over short (<1 km) and longer distances. LiDAR data reveal these scarps and provide an opportunity to explore the surface expression of scarps across varying geomorphic areas, use vertical separation across fault scarps to address questions surrounding fault section or segment boundaries, and explore questions of glacial erosion fault processes. Scarp height has been influenced by glacial (e.g., erosion and deposition), hillslope (e.g., translational slope failures and debris flows), and alluvial processes (e.g., floods, channelized drainage), as well as apparent slip rate variations, resulting in variable fault scarp height along the length of the Teton fault.

Variable scarp height indicates a four-section model of the Teton fault should be considered

Previously proposed models of the Teton fault suggest that it is composed of two to three segments (Ostenaa, 1988; Smith et al., 1993). The greatest slip rate is expected to be concentrated within the central portions of normal faults, resulting in a systematic increase in vertical separation toward the central portion of the fault (Cowie and Roberts, 2001; Densmore et al., 2007).

Vertical separation analyses from profiles at forty-two locations along the Teton fault indicate that the fault does not, as a whole, follow this expected pattern of behavior. However, the expected pattern of fault behavior is observed within four discrete sections of the fault. Based on this pattern of vertical separation, we propose a four-section model of the Teton fault with section boundaries at Moran Bay, south Jenny Lake, and Granite Canyon (Figure 20). Each of these sections are characterized by a pattern of vertical separation across fault scarps which increases toward the central portion of the area (Figure 10 and Table 3). The transition zones between these four distinct areas of the range front may represent boundaries between fault sections or segments.

Scarps at the southern end of the fault are high

South of Granite Canyon, fault scarps with anomalously large (>15 m) vertical separation are common (Figure 10). These anomalously high scarps may reflect greater landform age, variable fault slip rate, or a combination of these factors. Dating of these landforms would clarify the vertical separation rates in this southern area and their relationship to the rest of the fault system.

Slope failures tend to be larger in the northern half of the study area and smaller and more common in the southern half of the study area

Translational slope failure deposits are more common along the northern Teton fault, while debris flow deposits and smaller translational slope failures are more common along the southern range front. Along deglaciated valley walls, south-facing slopes are more prone to debris flow activity than north-facing slopes.

LiDAR-based mapping combined with field confirmation in selected areas allows rapid reconnaissance of the fault zone

LiDAR-based identification of fault scarps and vertical separation profiling are useful tools in fault zone analyses, particularly where thick vegetation, rough terrain, or other concerns make field mapping difficult. LiDAR-based mapping of fault scarps, glacial features, and slope failure deposits, coupled with field confirmation in select areas, allowed for rapid reconnaissance of the study area, which spanned an approximately 1-km wide area straddling the fault. This approach can improve mapping accuracy and reduce the time and expense associated with traditional field mapping approaches.

Chapter III: Field Mapping

Abstract

Geomorphological field approaches were used to map fault scarps and slope failure deposits in targeted areas along the Teton fault. The targeted areas were selected based on the results of initial digital mapping from LiDAR-derived digital elevation, hillshade, and slope models of the Teton range front. Field mapping focused on four targeted areas of complex geomorphic relationships identified from the initial digital mapping effort. The field investigation resulted in redefinition of lineaments previously interpreted as fault scarps, adjustment of landform boundaries initially interpreted from LiDAR-based mapping, and reinterpretation of slope failure deposit materials. This study emphasized the effectiveness of coupling digital mapping approaches with field-checking with traditional mapping techniques in selected areas.

Digital mapping of fault scarps and slope failure deposits from LiDAR-derived digital elevation (DEM), hillshade and slope models coupled with field mapping in targeted areas allows rapid reconnaissance of large study areas and field sites where dense vegetation or difficult terrain make traditional field mapping approaches unrealistic.

Introduction

The morphological evolution of the landscape along the Teton fault is of primary importance to understanding fault behavior and assessing the risks of natural hazards within the fault zone. Where the fault intersects landforms of known age, estimates of the fault slip rate can be made using the vertical separation across fault scarps and landform ages. Fault slip estimates and slope failure characteristics are key elements in assessing the potential for natural hazards mitigating their effects. The reader is referred to Chapter I: Introduction for a review of early mapping in the Teton Range and surrounding area.

Geomorphological field mapping in this case provides a field-check for landform elements and patterns identified in digital maps and helps refine the identification and characterization of features. Areas chosen for detailed field mapping were selected based on the results of digital mapping efforts and focused on areas where landform relationships or boundaries were uncertain.

Field investigation was used to locate and characterize the extent of hillslope processes within the fault zone and field-check digital mapping of scarps, slope failure deposits, and other geomorphic features. Field mapping also helps constrain the spatial distribution and relative magnitude of slope failure events where deposit boundaries are difficult to discern from digital maps. Field mapping efforts corrected location errors associated with fault scarp mapping, adjusted slope failure deposit boundaries, and helped clarify relationships between tectonic and geomorphic features within the study area. The insights gained were applied to digital mapping throughout the study area after field mapping was complete.

Methods

Field mapping was carried out during the summer of 2019. Four areas were selected for field mapping (Figure 24). Areas where the Teton fault intersects lateral moraines, drumlinoid topography, and slope failure deposits were mapped at a scale of 1:6,000 using slope imagery base maps generated from LiDAR data (Figure 13 through 15). The Geologic Map of Grand Teton National Park (Love et al., 1992) was used as reference when identifying bedrock and surficial deposits. Landform features were identified from their geomorphic characteristics, location and relationship to the Teton fault and surrounding landscape, and insight from the digital mapping.

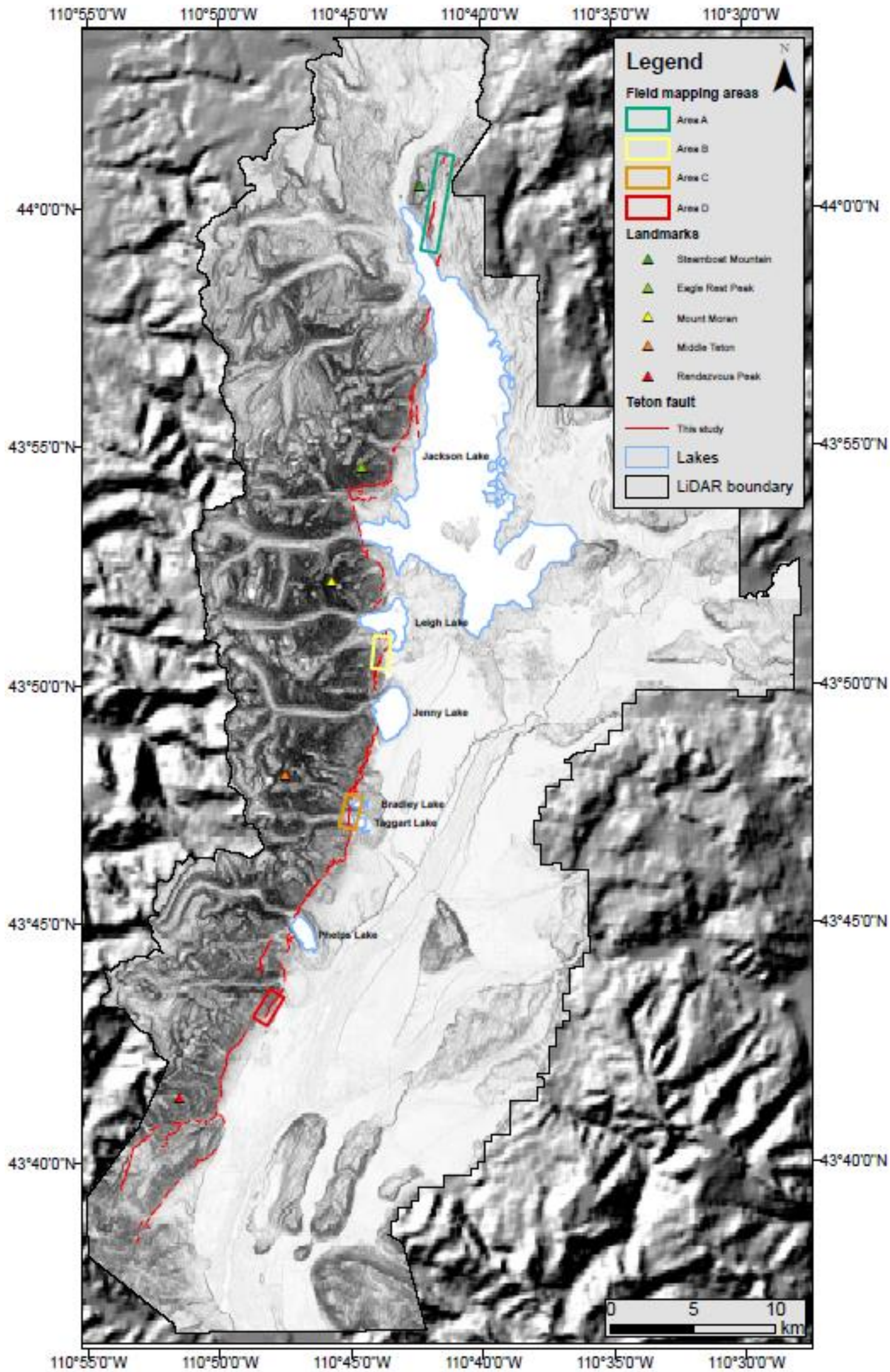

Figure 24. Field areas A, B, C, and D were selected for field mapping.

Description of Mapped Features

Fault scarps

Fault scarps were mapped where linear features several meters in length or longer vertically offset surficial deposits or pre-existing landform features, typically by several meters or more.

Slope failure deposits

Slope failures are defined as mass movements that involve outward or downward movement of a mass of slope-forming material under the influence of gravity (Goudie, 2004). Slope failures generally fall into two categories: translational slides, and debris flows.

Translational slides consist of poorly consolidated surficial material which has detached from the slope it occupies in a shift of position. The deposits of translational slides are distinguished from other forms of slope failure by their distinct boundaries, hummocky topography, and surficial profiles with an overall convex up morphology. In the study area, the vegetation covering deposits of this type typically includes trees, grasses, and mossy boulders up to approximately 2 m in diameter. The rupture scarp formed by translational slides in the study area is typically curvilinear at the surface and dips steeply to the area where the deposit accumulates.

Debris flows are transitional between landslides and sediment-laden water floods. They commonly occur in tectonically active areas subject to rapid uplift and erosion (Goudie, 2004). Debris flow deposits were identified by their characteristic elongated and lobate shape, convex-up morphology, clear boundaries where they contact surrounding landforms and surficial deposits. Debris flows are typically matrix-supported, and their deposits are often pockmarked with depressions <1 m in diameter in the study area.

Glacial features

Glacially sculpted drumlins, deglacial valleys, lateral moraines, and ice sheet deposits were identified and mapped in the study area. Drumlins were identified on the eastern flank of Jackson Lake as approximately 0.1-1.0 km-long elongate hill forms largely composed of glacial debris, in this case the quartzite roundstones in a matrix of sand and gravel of Pinedale age (Pierce et al., 2018).

Deglacial valleys in the Teton Range are likely the result of repeated glacial cycles of mountain glacier advance and retreat. Glacially carved valleys extend from high in the Teton Range to the range front and were identified by their U-shaped cross-sectional profiles, relationship to moraine deposits, and insight from the scientific literature on the glacial history of the area.

Lateral moraines form high ridges extending onto the Jackson Hole valley floor at the foot of the Teton Range. They were identified and mapped based on their linear hill forms and relationships to the surrounding topography (e.g., extending out onto the valley floor from deglacial valleys), with insight from the scientific literature on the glacial history of the area.

Glacial deposits are common along the Teton range front and are primarily the result of Bull Lake and Pinedale age ice advance and retreat. Ice sheet deposits were identified from their rounded to sub-rounded grains ranging in size from fine sand to large boulders, their relationships to other landforms and surficial deposits, and insight from the scientific literature and existing geologic maps of the area.

Rock unit descriptions

Rock units exposed at the surface were correlated to those mapped by Love et al. (1992). Soil and dense vegetation along the range front limit surface exposures of bedrock units in much of the study area. Deposits of glacially transported material and alluvium are common and cover much of the area. Mapped units correspond to those mapped by Love et al. (1992). The following rock unit descriptions correspond to those shown on the Geologic Map of Grand Teton National Park and are summarized from Love et al. (1992).

Quaternary alluvium (Qal)

Gravel, sand, and silt found along modern stream channels, flood plains, and fans.

Quaternary glacial drift deposit (Qg4)

Deposits deposited by Quaternary and possibly older glaciations. Primarily composed of Precambrian rocks from the Teton range and quartzite cobbles and boulders from the Harebell Formation, these deposits are typically mantled by soil and vegetation. Northeast of Jackson Lake, this unit is primarily composed of quartzite roundstones of the Harebell Formation with a sand and gravel matrix. Along the Teton range front, glacial drift deposits form ice-parallel ridges, lateral and end moraines primarily composed of Precambrian rocks from the Teton Range.

Pliocene Huckleberry Ridge Tuff (Th)

Rhyolitic ashfall tuff, typically gray to brown in color. This densely welded rock is typically devitrified, contains abundant phenocrysts of quartz, sanidine, and plagioclase with minor amounts of fine- to medium-grained clinopyroxene and opaque minerals. The unit is divided into Members A, B, and C, with Member C exposed northeast of Jackson Lake.

Early Proterozoic Mount Owen quartz monzonite and associated pegmatite (Xmo)

This unit primarily consists of fine- to medium-grained, light colored, massive to weakly flow-banded biotite quartz monzonite with masses of muscovite- and biotite-bearing pegmatite.

Archean Rendezvous Metagabbro (Wr)

Gray to green coarse-grained, weakly foliated metagabbro. Consists of dark green to black hornblende grains 2-5 cm long surrounded by a matrix of light gray plagioclase grains.

Archean layered gneiss and migmatite (Wgm)

Medium- to fine-grained biotite gneiss and schist interlayered with quartz and plagioclase gneiss. Layers are typically 1-10 cm thick.

Results

Four areas were mapped, each representing unique characteristics of the four fault sections proposed by this project (Chapter II; Figure 12). Field mapping identified previously unrecognized features and landform characteristics in each of these areas, which are described below.

Field area A

In the northern end of the proposed Eagle Rest Peak section, northeast of Jackson Lake, NNE- to NE-striking fault scarps offset S to SE trending drumlins carved by Pinedale age ice advance and retreat (Figure 13). The fault is expressed as a series of relatively low scarps (1.0 to 21.3 m vertical separation) that offset surface material primarily composed of rounded quartzite cobbles and smaller material. Field and digital mapping resulted in elimination of several scarps previously mapped as part of the Teton fault by Zellman et al. (2019) which are shown in Figure 14. At the northern end of this area, the fault bifurcates into two strands, one striking NNE and the other turning to the NE. The average vertical separation across scarps in this area is 5.7 m, while the average simple scarp height is 11.3 m. Several slope failure deposits were mapped in the area. Translational slide deposits are common along the eastern shore of Jackson Lake and the Snake River corridor, where outcrops of the Tertiary (Pliocene) Huckleberry Ridge tuff are covered by glacial deposits and loosely consolidated soil and vegetation. Earth flow deposits were interpreted at the southern end of the area along the eastern shore of Jackson Lake, and the scarps of these deposits are cut by the Teton fault in several places along the lakeshore.

Field area B

Field area B, within the proposed Mount Moran fault section and at the southern end of Leigh Lake, is characterized by GYGS-derived glacial deposits, exposures of Archean layered gneiss and migmatite bedrock, and slope failure deposits (Figure 15). The fault strikes north to NE in this area. Field mapping reinterpreted an east-west striking lineament as the edge of a translational rockslide rather than a fault scarp, as previously mapped by Zellman et al., (2019) (Figure 15). Additional slope failure deposits mapped in the area include several translational rockslides and debris flows.

Rockslide deposits consist of large (>2 m) rock blocks covered by a boulder-strewn surface with relatively thin soils that support smaller trees, brush, and grasses. Larger rockslide deposits are accompanied by overriding smaller translational rockslides that displace portions of the underlying larger slide material. Water seeps and springs are common along the edges of these deposits and form small drainages that flow northeast toward String Lake. Several debris flow deposits were also mapped in the area, and a singular rotational slide deposit was located in the southwest corner of the field area.

Field area C

Field area C, in the proposed Middle Teton fault section, is characterized by some of the highest fault scarps in the study area. Here, north-striking fault scarps offset lateral and medial moraines at Bradley and Taggart Lakes and Glacier Gulch (Figure 25). Vertical separation and simple scarp height across fault scarps averages 12.1 m and 36.6 m, respectively. The medial moraine between Bradley and Taggart Lakes is vertically separated by 14.8 m and is one of the tallest fault scarps in the study area. Where the fault crosses the Taggart Lake valley floor, alluvial deposits are vertically separated 10.6 m, while vertical separation across the right lateral moraine of Taggart Lake is 12.5 m. Field mapping revealed two offset alluvial terraces in the Taggart Lake valley.

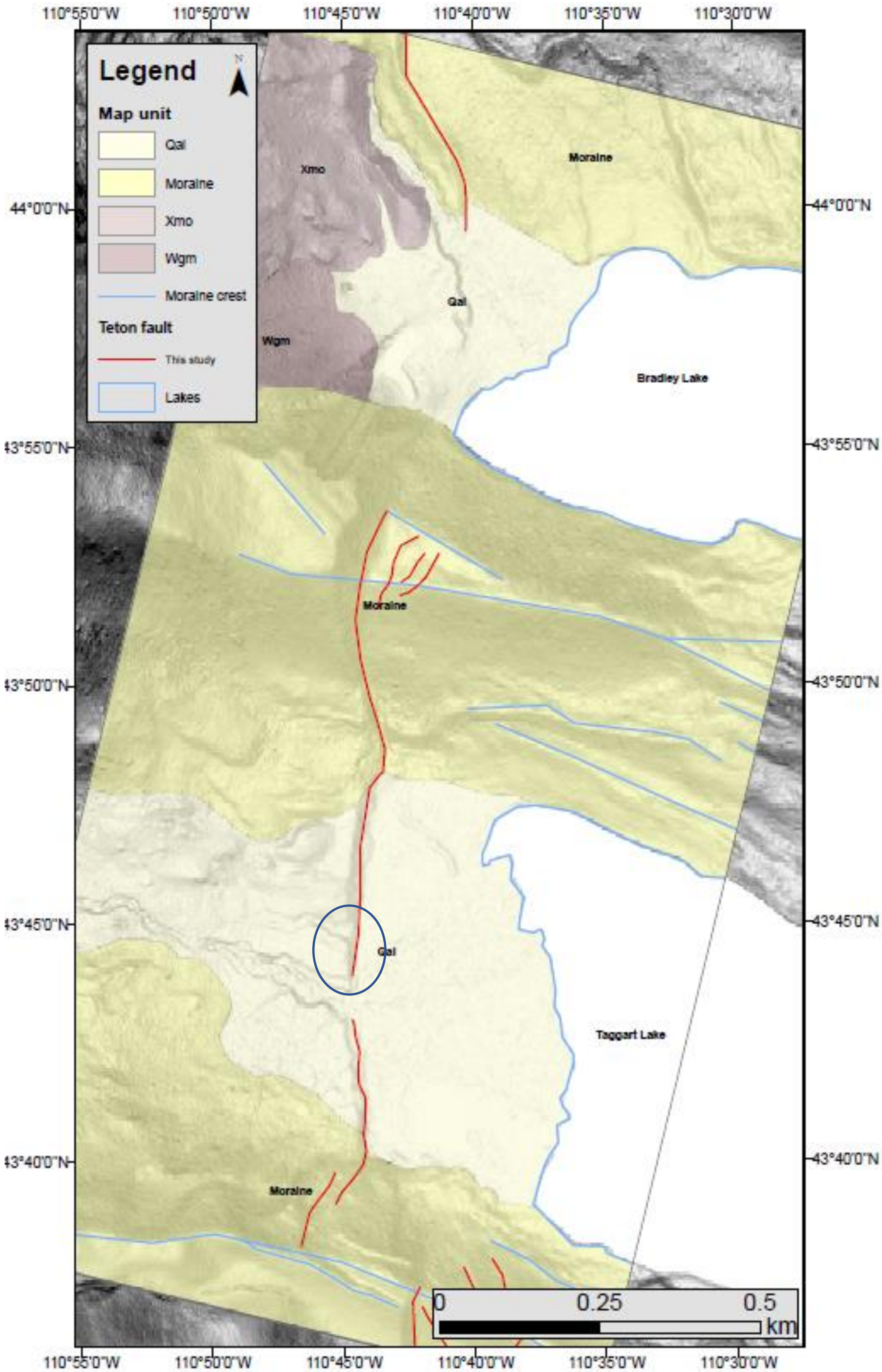

Figure 25. Digitize map of field area C, along the central portion of the Teton fault. Blue oval denotes location of two offset stream terraces.

Field area D

Field area D, in the proposed Rendezvous Peak fault section, is characterized by a well-preserved fault scarp that offsets a heavily vegetated bouldery hillside (Figure 26). Surficial sediment in this area includes angular boulders of Archean Rendezvous metagabbro, glacial deposits, alluvium, and a single debris flow deposit that overlies an older and more diffuse alluvial fan. The area is densely vegetated with trees and brush, particularly on the east side of the fault. In this area, mapping did not adjust the fault mapped by Zellman et al. (2019), but the boundaries of the Rendezvous metagabbro bedrock is shifted from that mapped by Love et al. (1992).

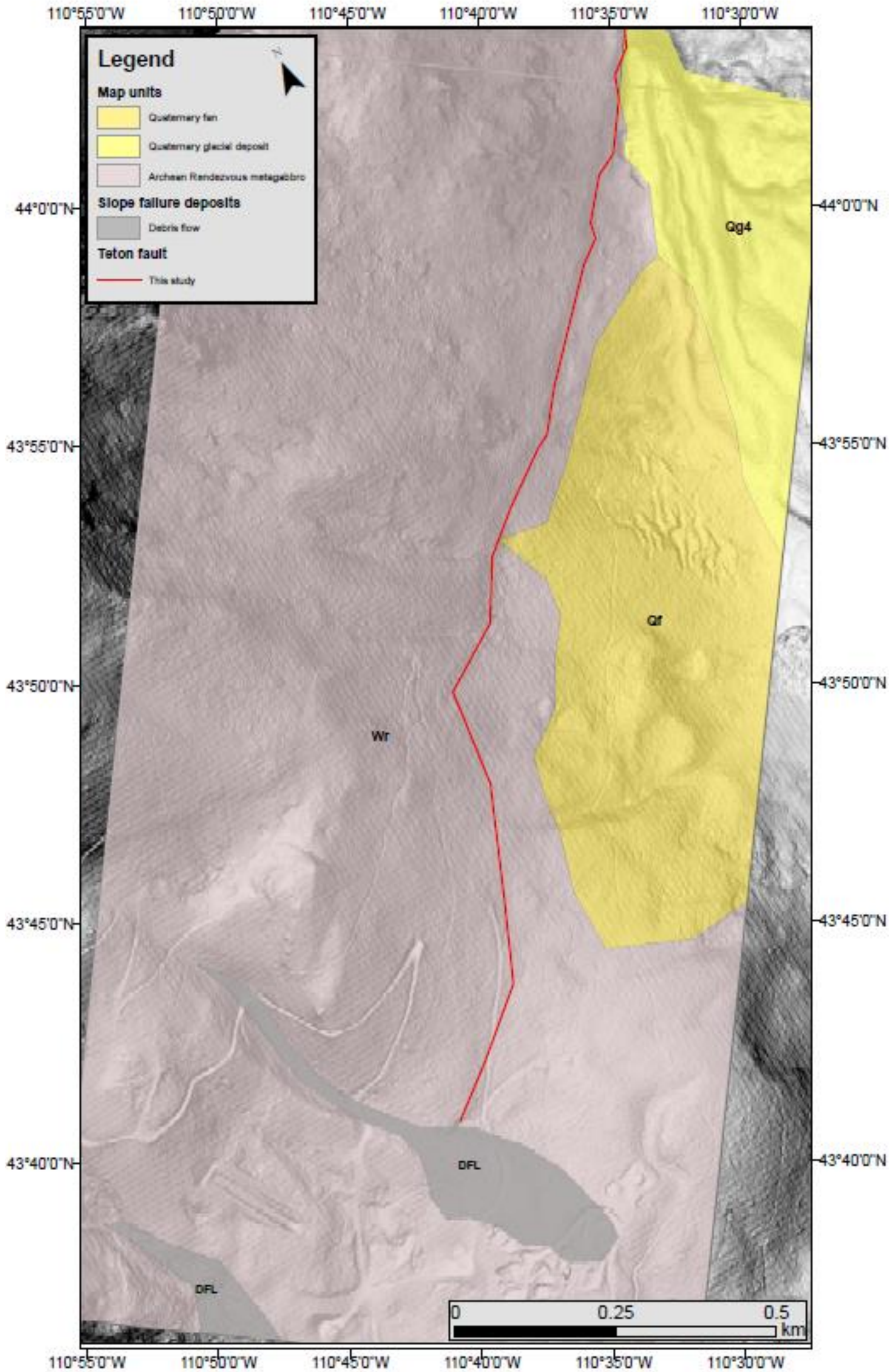

Figure 26. Digitized map of field area D, along the southern range front. Note that the debris flow deposits intersect areas where infrastructure has been developed.

Discussion and conclusions

Field mapping remains a key component in landscape characterization projects that depend on LiDAR-based mapping for initial landform identification or site characterization. Identification of geomorphic features is largely dependent on the scale at which areas are viewed (Pavlopoulos et al., 2009). Field mapping of selected sites throughout a study area that has been digitally mapped provides a quality control check for the study area as a whole and can improve the identification and classification of landforms, geological materials, and other features of interest.

Field mapping of selected areas along the Teton fault (e.g., field area A, northeast of Jackson Lake) resulted in adjustments to the most recently published map of the Teton fault (Zellman et al., 2019b) clarified field relationships between landforms (e.g., the boundaries of slope failure deposits south of Leigh Lake in field area B), identified potentially datable landforms (e.g., offset alluvial terraces in field area C), and emphasized the benefits of LiDAR data and digital mapping capabilities in steep terrain or where vegetation or other conditions make access difficult (e.g., dense vegetation in field area D).

In field area A, northeast of Jackson Lake, field mapping clarified the relationship between two parallel fault scarps, the eastern of which has been interpreted as an antithetic scarp to the Teton fault (Figure 13). The graben between the two scarps forms a boggy area with several sag ponds. The ponds may provide an opportunity for sediment coring studies that could reveal new information about the timing of fault offset in the area. Digital mapping alone would be unlikely to identify these small features on the landscape.

In field area B, field mapping provided a new interpretation of the east-west trending lineament mapped as a fault scarp by Zellman et al. (2019), which is now interpreted as the depositional contact of a translational rockslide deposit that extended onto the GYGS glacial drift depositional surface (Figure 15, 16). Additionally, field mapping revealed the three smaller translational rockslide deposits overlying the larger slope failure, and a complex slope failure deposit with characteristics of both rockslide (e.g., angular boulders exposed at the surface) and translational slide (e.g., little back tilting, numerous water seeps). Debris flows were also mapped in the area. The presence of several slope failure deposits indicates the slopes in this area are particularly prone to failure.

In field area C, field mapping revealed two offset alluvial terraces in the Taggart Lake valley (Figure 25). The terraces could potentially be dated by optically stimulated luminescence methods and may provide constraint on the timing of fault offset in the area.

In field area D, dense brush and closely spaced trees made field mapping very challenging. The fault scarp is well-preserved and easily discernable in LiDAR-derived maps, but field refinement was not possible (Figure 26). Field mapping in this area emphasizes the benefits of LiDAR data for mapping in areas where field access is difficult.

In summary, field mapping of selected areas along the Teton fault resulted in adjustments to the most recently published map of the Teton fault. The effort clarified relationships between glacial landforms, slope failure deposits, and fault scarps, and emphasized the benefits of LiDAR data for mapping areas where field access is challenging.

The recent rise in digital mapping capabilities has not eliminated the need for traditional field mapping approaches. Rather, it emphasizes the continued need for strong foundational knowledge, skills, and ability to efficiently field-check digitally derived mapping data. LiDAR-based mapping is limited in its ability to fully characterize slope failure deposits (Schulz, 2004). Slope- and hillshade-based maps show the surface morphology of slope failure deposits but cannot be used to identify other common indicators of slope failure, including water seeps and distressed vegetation. Field mapping provides an opportunity to evaluate an area for these and other conditions that may indicate the occurrence or potential for slope failure and improve the quality of interpretive classifications, particularly when the type of material involved needs to be identified or characterized.

Chapter IV: Implications for seismotectonic and slope failure hazards assessments

Abstract

The approximately 75-km long Teton normal fault is capable of producing large magnitude (M>6) earthquakes which could cause significant shaking and other hazards along the Teton range front and surrounding area. High resolution LiDAR data, digital mapping, and field confirmation were used to identify and characterize fault scarps and slope failure deposits in the Teton fault zone. Based on vertical separation analysis and the expected behavior and surface expression of normal faults, we proposed a four-section model of the Teton fault. The proposed sections may represent segment boundaries with potentially important implications for seismotectonic and slope failure hazards assessment. Slope failure deposits indicate that larger, and likely less frequent, slope failures take place north of Leigh Lake, while smaller, and likely more frequent slope failures occur to the south. The results of slope failure mapping have important implications for manmade infrastructure along the range front. The high-resolution data and combined digital and field mapping approach used here allowed for efficient and effective reconnaissance of the study area, particularly in areas where dense vegetation and steep slopes make traditional geomorphic field mapping difficult.

Introduction

The Teton fault represents a potentially significant source of earthquake and associated natural hazards. Slope failures can be triggered by seismic events and are common in tectonically active areas subject to rapid uplift and erosion (Goudie, 2004; Highland and Bobrowsky, 2008). The Teton range front is no exception, and many slope failures have taken place throughout the study area and may or may not have been triggered by seismic activity. Here, we present results of LiDAR-based digital mapping of fault scarps and slope failure deposits and propose a four-section model of the Teton fault based on vertical separation across the scarp. The following review of relevant scientific literature provides context and background on fault segmentation, hazards assessment, and the effectiveness of LiDAR-based digital mapping in identifying and characterizing slope failure hazards.

Segmentation and hazards

Both Susong et al. (1987) and Smith et al. (1993) suggested three-segment models of the Teton fault, that earthquakes may be associated with individual segments, and that segment boundaries may be important in rupture initiation and termination. The three-segment models are based on the extent of similarly aged faulting, changes in fault trend, changes in range topography, lateral variations in fault strike and footwall structures, and inferences from gravity anomaly data. However, the study was confined to a limited section within the central portion of the Teton fault and failed to analyze the entire Teton fault zone (Figure 2). The gravity anomaly and segment boundary interpretation was challenged by Ostenaa, (1988), who suggested the southern and central portions of the Teton fault belong to a single, continuous segment. Fault segmentation has important implications for seismic hazards assessment, particularly in regard to variation in rupture length and earthquake magnitude.

Seismic hazards can be strongly influenced by the rupture length associated with a given earthquake event (DePolo et al., 1991; DuRoss et al., 2016). Earthquakes may rupture along a single segment or across multiple fault segments (DePolo et al., 1991; DuRoss et al., 2016). As faults grow in size (length and rupture surface area), the potential earthquake magnitude associated with the fault also increases (Cowie and Scholz, 1992). Normal faults are expected to accumulate the greatest vertical displacement toward the central portion of the fault (Cowie and Scholz, 1992; Cowie and Roberts, 2001; Densmore et al., 2007). Here, we propose a four-section model of the Teton fault which is based on patterns of vertical separation across fault scarps. The section boundaries proposed may represent segment boundaries or important structural discontinuities that have previously been overlooked in studies of the Teton fault.

Slope failure and hazards

The effects of slope failure hazards vary widely and are influenced by material type, degree of consolidation, particle size, slope angle, geomorphology, soil type, and other factors including the presence of manmade structures and population centers (Highland and Bobrowsky, 2008). Slope failures can have significant socio-economic impacts, particularly in populated areas where urbanization and development take place on steeply sloping ground (Aleotti and Chowdhury, 1999). Thus, identifying slopes that are prone to failure is an essential element of hazard assessment work, which is a growing professional field in the United States and abroad (Petley, 1998; Mora et al., 2015; Guthrie, 2017).

Both qualitative and quantitative hazard assessments are applied in areas prone to slope failure. Qualitative assessment focuses on locating and mapping hazard-prone areas and is heavily dependent on expert knowledge and site-specific experience, while quantitative assessment is dependent on statistical and deterministic approaches based on engineering principles (Aleotti and Chowdhury, 1999; Silva et al., 2008). Little work has been done to characterize the potential for slope failure hazards along the Teton range front. Gilbert et al (1983) suggested that seismically induced slope failure was a potential hazard near the Jackson Lake Dam, but the most recent ground motion evaluation (O'Connell et al., 2003) did not address the potential for slope failure hazards in-depth. Here, we present a qualitative assessment of slope failure deposits along the Teton range front and characterize the areas most prone to slope failure within the study area.

Hazards mapping

Both digital and traditional, field-based mapping play key roles in assessing earthquake and slope failure hazards (Seijmonsbergen and de Graaff, 2006; Burns and Madin, 2009). Because hazards assessment and risk management are largely dependent on expert knowledge and the ability to apply critical thinking to theoretical models of hazard potential, coupling digital- and field-based mapping is common in hazard assessment work (Harding, 2000; Silva et al., 2008; Burns and Madin, 2009; Crawford, 2012; Mora et al., 2015). High-resolution LiDAR data has proven particularly effective for identifying and characterizing fault scarps and areas prone to slope failure. Hillshade, slope, and slope aspect models derived from LiDAR data are useful for locating and mapping faults and geomorphic features of slope failures (Harding, 2000; Glenn et al., 2006; Burns and Madin, 2009; Crawford, 2012). Combining high-resolution remotely sensed data, digital mapping, and field-checking at targeted sites, allows for rapid reconnaissance of sites where dense vegetation, challenging terrain, or other conditions make access and traditional mapping approaches difficult to utilize.

Methods

Detailed methods are provided in Chapter II, and the following is a brief summary of the methods used as they apply to the implications for seismotectonic and slope failure hazards addressed in this study.

The LiDAR-based DEM was used to generate slope and hillshade models of the study area. The models were used to locate and map fault scarps and slope failure deposits throughout the study area. The variation in vertical separation along the Teton fault was analyzed from scarp-normal topographic profiles generated from the DEM at forty-two locations along the fault.

Results

Detailed results are provided in Chapter II, and the following is a brief summary of the results as they apply to the implications for seismotectonic and slope failure hazards addressed in this study. Mapping identified scarps of the Teton fault along an approximately 75-km stretch of the Teton range front and northeast of Jackson Lake (Figure 1). Vertical separation across the fault scarp indicates that four sections of the fault follow an expected pattern of normal fault behavior (Figure 10). Slope failure deposits were mapped along the range front (Figure 11). Combining digital mapping with field mapping in targeted areas clarified relationships between fault scarps and landforms along the range front (Figure 13, 14, 15, 24, and 25), allowing rapid reconnaissance of the study area and qualitative characterization of slope failure deposits.

Interpretation and Discussion

A strong earthquake on the Teton fault could impact buildings, roadways, and trail systems in the area. The Jackson Lake dam, originally constructed in 1907, includes earthfill and concrete sections. The dam has undergone several rebuilds and was reinforced in 1989 after a preliminary seismic hazard assessment was completed by Gilbert et al., (1983) (O'Connell et al., 2003). The most recent ground motion evaluation for the Jackson Lake Dam modeled scenarios in which ruptures took place on a single segment, two independent segments, or three fault segments. The study indicates that rupture of the northern segment of the Teton fault (as proposed by Smith et al., 1993) would likely produce a M 6.9 to M 7.0 earthquake, depending on the dip of the fault, and simultaneous rupture of multiple fault segments would likely be associated with larger magnitude earthquakes. However, abundant new data have been collected from the fault zone since then, and the new findings about the fault history and rupture patterns should be incorporated into seismic hazard analyses.

Segmentation and hazards

Fault segmentation has important implications for seismic hazard assessment, particularly in regard to variation in rupture length, earthquake magnitude and frequency (Crone and Machette, 1984; DePolo et al., 1991; Faulds and Varga, 1998; DuRoss et al., 2016). One- two- and three-segment models of the Teton fault have been based on varying definitions of segmentation (Ostenaa, 1988; Smith et al., 1993; O'Connell et al., 2003).

Here, we propose a four-section model of the Teton fault based on vertical separation across fault scarps and changes in strike direction (Figure 10 and Figure 20). Vertical separation is greatest in the central portion of each of these sections and tapers toward each end, following the expected pattern of normal fault behavior (Cowie and Scholz, 1992; Cowie and Roberts, 2001; Densmore et al., 2007). The transition zones between these four areas may represent boundaries between fault sections or segments.

Although the fault appears to be seismically quiescent at local magnitude (M_L) >3 (White et al., 2009), paleoseismic studies at Steamboat Mountain, Leigh Lake, Buffalo Bowl, and Granite Canyon indicate the surface rupturing events have taken place along the fault during Holocene time (Byrd, 1995; Zellman et al., 2018, 2019c; DuRoss et al., 2019b). The most recent event revealed by paleoseismic work is recorded in the trench walls at Buffalo Bowl, and occurred ~4.6±0.4 ka (DuRoss et al., 2019b). Offset landforms and post-glacial deposits along the range front record a history of large scarp-forming earthquakes along the fault (Licciardi and Pierce, 2008). Paleoseismic trenching studies reveal evidence of surface rupturing earthquakes at ~3.8-6.1 ka and prior to 7.1 ka at Steamboat Mountain, ~5.9 and ~10 ka south of Leigh Lake, ~4.6 ka, ~7.1 ka, and ~9.9 ka at Buffalo Bowl, and at ~5.9 ka and ~7.9 ka at Granite Canyon (Table 1) (Byrd, 1995; Zellman et al., 2018, 2019c; DuRoss et al., 2019b). While the age ranges of some past events overlap between segments, the dating uncertainties preclude determination of simultaneous rupture between segments.

Paleoseismic data indicate that the most recent paleoseismic event may have ruptured the surface at the Steamboat Mountain, Leigh Lake, Granite Canyon, and Buffalo Bowl sites, though the age uncertainties preclude clear determination of synchroneity. If this is the case, the most recent event may have ruptured along the entire length of the Teton fault. The oldest event inferred from the Leigh Lake paleoseismic study (LL2, 9.7-10.4 ka) overlaps in age range with the oldest event recorded at the Buffalo Bowl site (BB3, 9.4-10.4 ka) but no event of similar timing was interpreted from the Granite Canyon trench. Taken together, these data indicate that the Teton fault is active and that sections of the fault may rupture individually or in concert. Thus, questions about fault sections, segments, and hazard potential along the Teton fault remain important and open for debate.

Slope failure and hazards

Slope failure deposits were mapped along the range front (Figure 11) and are interpreted as translational slides and debris flows based on geomorphology, evidence for source areas, surface appearance (roughness), and the presence of head- and flank-scarps. Translational slides move as coherent blocks of earth material, while flow activity is characterized by rapid downslope movement of unconsolidated material, often of varying size and composition. Slope failure deposits range in size, with larger deposits being more common north of Leigh Lake. Slope failure size may be related to degree of material water saturation, variable material consolidation or type, slope angle, or some combination of these or other factors (Petley, 1998; Aleotti and Chowdhury, 1999; Highland and Bobrowsky, 2008).

North of Leigh Lake, slope failures appear to be primarily single-event occurrences forming singular deposits. In this area, the majority of slope failure deposits take place in the glacial deposits and sedimentary bedrock units. Glacial deposits are composed of unconsolidated sand, gravel, cobbles, and boulders. Translational slide deposits are larger (up to 2.4 km^2)in this area than those found south of Leigh Lake (generally <1.0 km^2), and debris flow deposits appear to be far less common. This area appears prone to larger, slope failure events.

South of Leigh Lake, the majority of slope failures take place within Pinedale age glacial outwash and on Pinedale age moraines. Debris flows are common, forming elongate fans that frequently overlap along the range front. The north walls of deglaciated valleys appear to be more susceptible to debris flow than do the south walls (e.g., Granite Canyon), with debris flow deposits accumulating to form fans along the deglaciated valley floors (Figure 11). Where translational slides are identified, smaller deposits are frequently found overlapping and within the boundaries of larger deposits (e.g., south of Phelps Lake), but this pattern was only observed on translational slide deposits south of Leigh Lake. The area south of Leigh Lake appears to be prone to smaller slope failure events than areas to the north.

Relatively little manmade infrastructure exists along the range front north of Granite Canyon. South of the canyon, housing and resort-style developments along the range front are built on older slope failure deposits. Several debris flow deposits, identified by their elongate fan-shaped deposits and the relatively straight and narrow flow paths leading to them, were mapped in the area, and these appear to overlie older alluvial fan surfaces at the base of steep, rocky slopes with narrow drainages. Here, the Teton fault does not appear to offset debris flow deposits, and they are thus interpreted to be younger than the most recent surface rupturing earthquake event evident from the Granite Canyon paleoseismic trench, which occurred ~5 ka (Byrd, 1995).

Hazards mapping

Digital fault scarp and slope failure deposit mapping and characterization were improved by field mapping in selected areas along range front. LiDAR-derived digital elevation, hillshade, and slope models provide a unique approach to identifying hazard-prone areas, particularly where dense vegetation make field access difficult. The ability to quickly visualize multiple factors that impact scarp and slope failure deposit identification makes digital mapping efficient and effective for mapping these features. Field-checking features identified from LiDAR data in targeted areas provided a quality control check on digitally mapped features and clarified relationships between fault scarps, slope failure deposits, and other features on the landscape. The value of combining these methods is particularly high in large study areas and where field access is challenging (Harding, 2000; Glenn et al., 2006; Burns and Madin, 2009; Clift and Springston, 2012; Crawford, 2012; Mora et al., 2015). For this study, combining high-resolution LiDAR data, digital mapping approaches, and field checking in selected areas allowed rapid reconnaissance of the study area and improved the characterization and analysis of fault scarps and areas prone to slope failure throughout the study area.

Conclusions

We propose a four-section model of the Teton fault based on vertical separation analysis (Figure 10 and Table 3). Each of the sections proposed is characterized by a pattern of vertical separation across fault scarps, which increases toward the central portion of sections and decreases at section boundaries, as is expected for individual normal faults (Table 3) (Cowie and Scholz, 1992; Cowie and Roberts, 2001; Densmore et al., 2007). This work indicates a four-section model should be considered and further work is needed in order to clarify whether or not the Teton fault is truly segmented, to determine whether surface rupturing earthquake events occur only in individual sections, or if ruptures cross section/segment boundaries along the fault, and to better characterize the seismic hazards of such events, including the potential for seismically-triggered slope failures.

Slope failures are common along the Teton range front (Figure 11). Slope failures generally fall into two categories: translational earth- and rock-slides, and debris flows. North of Leigh Lake, slope failures appear to be primarily single-event occurrences forming singular deposits which result almost entirely in translational slide deposits. While translational slide deposits are found throughout the study area, debris flow deposits are nearly absent along the range front north of Leigh Lake.

South of Leigh Lake, slope failure deposits are generally smaller and more closely spaced than to the north. Debris flows are common in this area and frequently overlap one another as well as older alluvial fan deposits. Debris flows commonly evolve into alluvial fan deposits over time as water transports sediment down the debris flow path; in fact, debris flows can be considered a primary process by which alluvial fans accumulate material over time (Goudie, 2004). We interpret these data to indicate that larger and less frequent slope failures generally take place to the north, and smaller and more frequent slope failures generally take place to the south of Leigh Lake, and that debris flows along the southern range front likely accumulate over time, developing into broader geomorphological landforms and may eventually transition into alluvial fans.

This work indicates that slope failures are common along the Teton range front, are larger and less common north of Leigh Lake and are smaller and likely more common south of Leigh Lake. Although relatively little manmade infrastructure exists along the range front north of Granite Canyon, Teton Village sits atop older alluvial fan surfaces and debris flow deposits at the foot of steep, rocky slopes (Figure 26). The debris flow deposits are not offset by the Teton fault, indicating that they are likely younger than ~5 ka based on evidence for the most recent surface rupturing earthquake event from the Granite Canyon paleoseismic trench (Byrd, 1995). Further work exploring the timing of slope failure and correlation to paleoseismic trench study data and lake coring work would help determine whether slope failure hazards are triggered by earthquakes on the Teton fault.

This study emphasizes the applicability of high-resolution LiDAR data, digital mapping, and field checking to the identification and characterization of fault scarps and slope failure deposits. Further, the application of GIS software provides unique insight into the variability in slope failure susceptibility and allows for rapid reconnaissance of large study areas or sites where dense vegetation and difficult terrain make access and traditional geomorphic mapping difficult. Because hazard assessment and risk management remain largely dependent upon expert knowledge (Silva et al., 2008) and the ability to apply critical thinking to theoretical models of hazard potential, this combined approach using digital and field observations can improve landscape and geomorphological interpretations.

Chapter V: Extended Conclusions

Based on vertical separation analysis and the expected pattern of vertical separation across normal faults, we propose a four-section/segment model of the Teton fault. The four sections proposed are: 1) the Eagle Rest Peak section, from the north end of the fault to Moran Bay; 2) the Mount Moran section, from Moran Bay to the south end of Jenny Lake; 3) the Middle Teton section, from south of Jenny Lake to Granite Canyon; and 4) the Rendezvous Peak section, from Granite Canyon to Teton Pass (Figure 20). Section boundaries are located at Moran Bay, south Jenny Lake, and Granite Canyon. Each of the sections proposed here are characterized by a pattern of vertical separation across fault scarps which follows the expected behavior of normal faults (Figure 10, 20).

Variable fault scarp height indicates a four-section model of the Teton fault should be considered

Fault segmentation and the criteria for identifying fault segments has been the subject of debate (Swan et al., 1980; Crone and Machette, 1984; Schwartz and Coppersmith, 1984; DePolo et al., 1991; Machette et al., 1991; DuRoss et al., 2016). Segment boundaries are commonly defined based on three broad categories of data: structural characteristics of the fault zone, geometric relationships of surface scarps, and fault behavior (e.g., slip rate). It is important to note that both the criteria used to identify fault segments and the scale at which those criteria are assessed both need to be considered as well. Swan et al. (1980) estimated the number of potential fault segments along the Wasatch fault zone could be as high as ten based on Holocene and Pleistocene surface ruptures interpreted from paleoseismic trenching work, but did not identify segment boundaries. Schwartz and Coppersmith (1984) utilized paleoseismic, geophysical, and geodetic data to propose six major fault segments along the Wasatch fault in northern Utah. Paleoseismic, geophysical, geometric, structural, behavioral, and geomorphic data have also been cited as potential indicators of fault segmentation (DePolo et al., 1991). Crone and Machette (1984) suggested that gaps in surface faulting and variation in throw along the length of rupture resulting from the 1983 Borah Peak earthquake on the Lost River fault in central Idaho indicate that the fault system may include a major segment boundary which was crossed during surface rupture.

DuRoss et al. (2016) suggest that multi-segment, single-segment, partial-segment, and segment boundary spillover ruptures are possible along faults. Multi-segment ruptures involve two or more segments and extend across primary segment boundaries; single-segment ruptures affect the complete length of a single fault segment; a partial-segment fault rupture offsets only a portion of a single fault segment; and spillover ruptures cross primary segment boundaries. Secondary, or sub-segment, structures and boundaries may also exist within primary fault segments (DuRoss et al., 2016). However, the uncertainty associated with paleoseismic data makes differentiating between rupture of adjacent segments and earthquake events that occur closely in time (i.e., decades or less) challenging (DuRoss and Hylland, 2015).

Susong et al. (1987) and Smith et al. (1993) suggested a three-segment model of the Teton fault (Figure 2 and Figure 27). Segment boundaries were proposed south of Taggart Lake and north of Moran Bay. However, that study suggested that the southern section of the fault terminates north of Phillips Canyon and the north end of the fault terminates south of the confluence of the Snake River with Jackson Lake. The most recently published map of the Teton fault, and the present study, indicate that the Teton fault continues approximately 8 km south of Phillips Canyon to the

Cache Creek thrust system and approximately 7 km northeast of Jackson Lake (Zellman et al., 2019; Figure 1, this study). These northern and southern extents of the fault could be included with the southern and northern segments, or possibly considered individual fault segments, by the approach of Smith et al. (1993). In any discussion of fault segmentation, the identification and interpretation of segment boundaries is an important consideration.

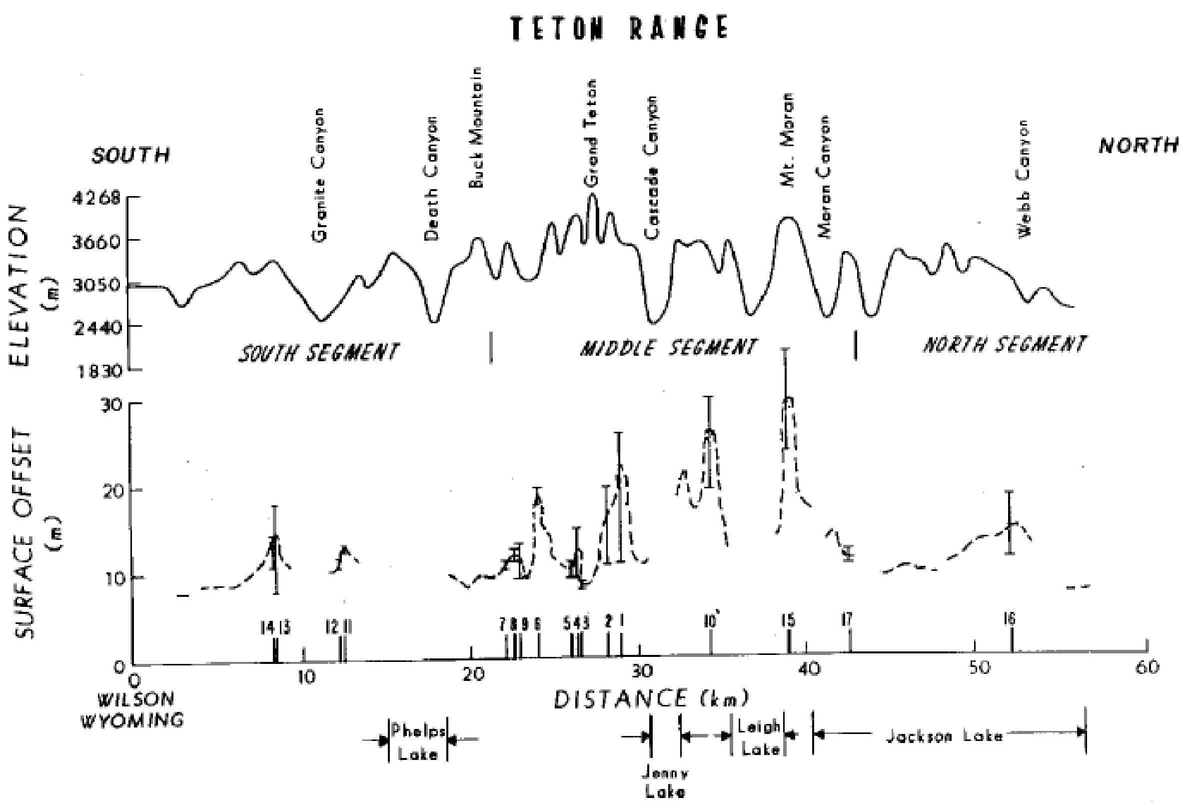

Figure 27.The three-segment model of the Teton fault proposed by Susong et al. (1987) and built upon in work by Smith et al. (1993). Modified from Smith et al., 1993. Previous studies of vertical separation across fault scarps have inferred section boundaries where vertical separation across scarps decreases and corresponds to decreased elevation along the range crest.

Smith et al. (1993) proposed that the boundary between the southern and middle segments of the fault lies north of Taggart Lake. Their suggested boundary is based on vertical separation across the fault, gravity anomaly interpretation, and changes in fault strike. Their vertical separation data from 25 topographic profiles measured between northern Jackson Lake and the north side of

Phillips Canyon indicate an area of low vertical separation at the proposed segment boundary. Their gravity anomaly and segment boundary interpretations were contrasted by Ostenaa (1988), who suggested that the southern and central portions of the fault belong to one continuous segment. Changes in fault strike may indicate segment boundaries, and Smith et al. (1993) note that the fault strikes NE through the proposed southern segment and N through the proposed middle segment. However, changes in strike are largely a matter of scale, and the vertical separation analysis carried out in this study indicates that the fault includes four sections which follow the expected pattern normal fault behavior (Cowie and Scholz, 1992; Cowie and Roberts, 2001; Densmore et al., 2007).

Vertical separation is greatest toward the central portion of each of the four proposed fault sections. Section boundaries are characterized by vertical separation lows. Smith et al. (1993) note that the average vertical separation across scarp profiles at five locations within their proposed southern segment is 13 m; however, when scarps south of Phillips Canyon are considered, the average vertical separation south of Taggart Lake increases to 21.2 m when topographic profiles at 9 sites are considered (Figure 28).

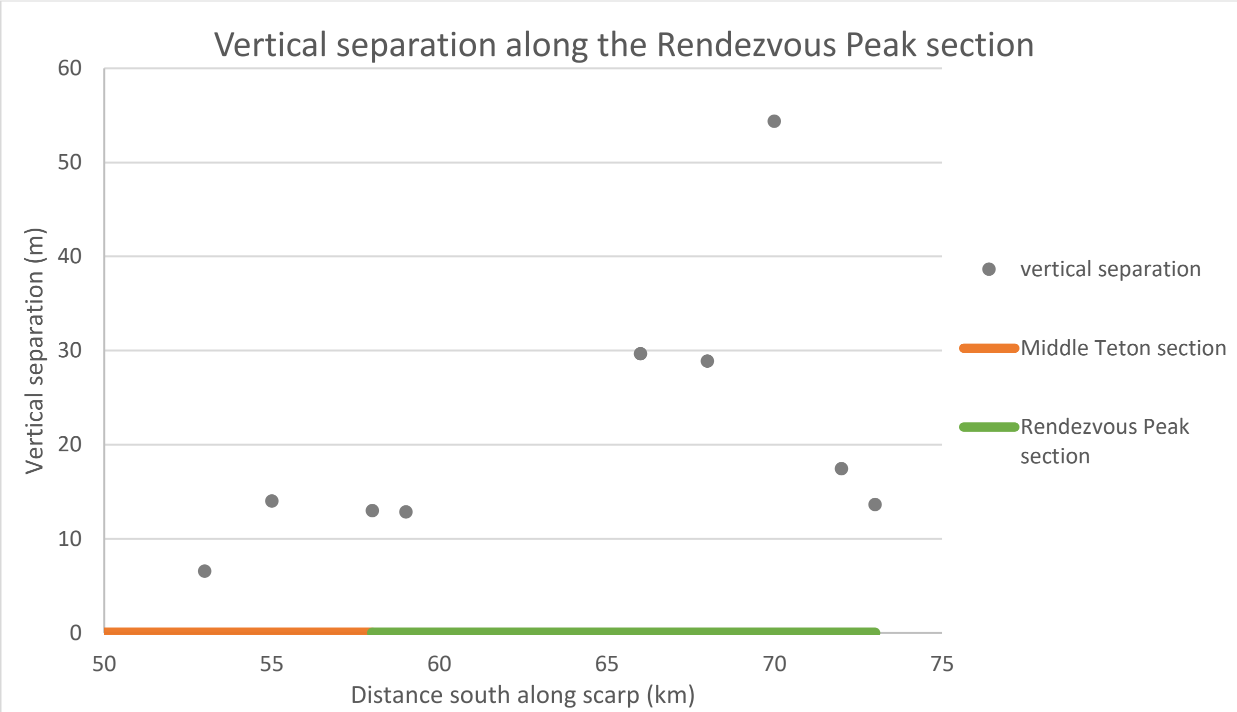

Figure 28. Vertical separation along the southern range front. Average vertical separation over the entire area is 21.2 m when scarp profiles at 9 locations are considered. The proposed Middle Teton and Rendezvous Peak sections proposed here are included for geographical reference to other figures in this report.

South of Granite Canyon, fault scarps with anomalously high (>15 m) vertical separation are common (Figure 10, 20). The high scarps in this area contradict the expected behavior of normal fault systems (Cowie and Roberts, 2001; Densmore et al., 2007). These anomalously high scarps are likely the result of greater landform age, higher fault slip rate, or a combination of these factors. Because surficial deposits in the area remain undated, a need for further work in the area persists.

Landform age is of primary concern when considering potential fault sections or segments. The timing of glacial retreat through surface exposure ages provide the best available data for constraining the timing of fault offset in the study area. The timing of Pinedale ice maxima varied across the Yellowstone-Teton region from approximately 18.8 to 16.5 ka (Licciardi and Pierce, 2008).

Northeast of Jackson Lake, glacial deposits cut by the fault were deposited by the Snake River lobe of the GYGS during Pinedale-3 time, 14.4±0.8 ka based on outwash relationships with the inner Jenny Lake moraine (Licciardi and Pierce, 2018). Scarps in this area have an average vertical separation of 4.6 m. Using the average vertical separation and a surface age of 14.4±0.8 ka, the average vertical separation rate in this area is 0.32±0.01 m/k.y. over the past 14.4 ka (Table 4).

Preliminary results from the trenching study at Steamboat Mountain indicate two Holocene earthquake events on the Teton fault northeast of Jackson Lake (Zellman et al., 2018). The earliest event, SM2, occurred prior to 7.1 ka, while the later event, SM1, occurred between 3.8 and 6.1 ka based on preliminary results of radiocarbon dating samples from two trenches; vertical offset data from the trenching project has not yet been published (Zellman et al., 2018).

At Jenny Lake, the inner moraine along the northern side of the lake has been dated to 13.5±1.1 ka by cosmogenic ^{10}Be exposure dating of 13 boulders (Licciardi and Pierce, 2018). Slope failure deposits appear to have covered the fault across this moraine, but on the south side of Jenny Lake the inner moraine is vertically offset by approximately 10.3 m (profile 40, Figure 6). Lateral moraines at Glacier Gulch, Bradley and Taggart Lakes have been sampled for cosmogenic ^{10}Be surface exposure dating, but the final results have not been published at this time. Forthcoming publications will document the surface exposure ages of fault offset lateral moraines along the range front (Licciardi, pers. comm.). At Phelps Lake, the left lateral moraine has a cosmogenic ^{10}Be exposure age of 21.62 ± 2.04 ka from two samples (Licciardi et al., 2014b). Variable landform age appears to explain the difference in vertical separation across these moraines. The valley floor scarp is lower than the scarps crossing the lateral moraines at Phelps Lake, and the presence of this smaller offset indicates that the higher scarps on lateral moraines are likely an artifact of landform age and scarp inheritance rather than variable offset rate.

Variable fault scarp height may reflect variable erosion by glacial processes

This and other studies assume that pre-existing fault scarps are fully erased by advancing and retreating glacial ice (Thackray and Staley, 2017). However, quantifying the degree of glacial erosion along valley floors is difficult and has not been studied in the Teton Range. If glacial erosion does not effectively reduce pre-existing fault scarps to valley floor topography, inherited scarp height may influence vertical separation rate calculations.

At Taggart Lake, the left lateral moraine, valley floor, and right lateral moraine scarps are vertically separated by 14.8 m, 10.6 m, and 12.5 m, respectively. The variation in vertical separation across the area may be the result of variable landform age, variable slip rate along the fault, or a combination of these factors. However, the calculated vertical separation rate across the right lateral moraine at Taggart Lake is 0.91±0.01 m/k.y., while across the left lateral moraine it is 0.81±0.02 m/k.y., indicating that variable landform age is likely the dominating factor in producing the high scarps in the area, rather than variation in slip rate, which is similar across the area (Table 4).

Cosmogenic ^{10}Be exposure age samples have been collected from the lateral moraines, but final results remain unpublished (Licciardi, pers. comm.). Field mapping of the area confirmed the presence of two small stream terraces cut by the fault scarp crossing the valley (Figure 26). If datable, these terraces could provide useful insight into the timing and rate of fault offset in the area.

Surface expression of the fault varies across five geomorphic areas

Five geomorphic areas with unique surface expression of the fault have been identified in the study area: 1) drumlins in Pinedale age ice sheet deposits northeast of Jackson Lake; 2) scarps cutting Pinedale age glacial outwash between Jackson and Jenny Lakes; 3) Pinedale age lateral moraines; 4) Pinedale age deglacial valleys; and 5) the southern range front, where the age of surface deposits remains largely unknown (Figure 22 and Table 5).

Drumlinoid topography

The first of these areas, northeast of Jackson Lake, is characterized by NNE-striking scarps that cut across the S to SE surficial fabric created by drumlinoid topography. Here, vertical separation of scarps averages 4.6 m based on fault scarp profiles at five locations, the lowest average vertical separation in any of the geomorphic areas identified (profiles 1-8; Figure 6). In this area, translational slide deposits are common along the eastern shore of Jackson Lake. The fault scarp passes through slope failure head scarps near the lake but does not offset slope failure deposits (Figure 13).

Pinedale age glacial outwash between Jackson and Jenny Lakes

Scarps that cut Pinedale age glacial outwash deposits between Jackson and Jenny Lake strike north and have an average vertical separation of approximately 15.7 m based on fault scarp profiles at six locations in the area (profiles 28-36; Figure 6). Translational rockslides, debris flows, and alluvial fan surfaces are common along the fault in this area, and slope failure deposits are offset by fault scarps in most locations (Figure 19).

Pinedale age lateral moraines

Pinedale age lateral moraines are characteristically offset by NE to N striking fault scarps. The vertical separation across lateral moraines ranges from 10.3 to 14.7 m, with an average of 12.69 m based on fault scarp profiles measured at Jenny Lake, Granite Canyon, Bradley and Taggart lakes (Figure 6, Table 3). Translational rockslide and debris flow deposits were mapped along the fault at Jenny Lake but are notably absent from the moraines of Glacier Gulch, Bradley and Taggart Lakes (Figure 11).

Pinedale age deglacial valleys

In deglacial valleys with Pinedale age valley floor deposits, the fault strikes NNE. Vertical separation across fault scarps ranges from approximately 6.6 to 13.0 m, with an average of 10.2 m based on fault scarp profiles measured at Glacier Gulch, Taggart Lake, Phelps Lake, and Granite Canyon (profiles 43, 46, 53, 58; Figure 1, Figure 6). Fault scarps are absent from the deglacial valley floors at Leigh and Jenny Lakes (Figure 1). At Jenny Lake, debris and rock flows from the north and south valley walls have formed deposits along the valley floor. Several debris flow deposits have been mapped along Granite Canyon, primarily initiating on the northern canyon wall. Slope failure deposits are notably absent from the other Pinedale age deglacial valley floors considered here.

The southern range front

The southern range front is characterized by several anomalously high (>15 m vertical separation) scarps (Figure 6, Figure 10). Vertical separation ranges from approximately 13.6 m to 54.4 m (average 28.8 m) across six profiles (Table 3). These are the highest recorded values for any of the five geomorphic areas. The fault strikes NE through the area and bifurcates into two strands at Phillips Canyon. Slope failure deposits are relatively uncommon in this area. North of Phillips Canyon, debris flow deposits that intersect the trace of the Teton fault are vertically offset in some locations and undisturbed in others (Figure 23).

Slope failures tend to be larger in the northern half of the study area and smaller and of greater number in the southern half of the study area

High-resolution LiDAR data can be used to identify and characterize the morphological components of slope failure deposits, provide insight into the materials involved in slope failure, and aid in identifying slope failure activity (Glenn et al., 2006). The toe, body, upper block, internal scarps, compression (transverse) ridges, head and flank scarps, and the initiation point and travel path of deposits are identifiable in LiDAR-derived maps (Glenn et al., 2006; Highland and Bobrowsky, 2008; Burns and Madin, 2009; Clift and Springston, 2012).

Identification of slope failure deposits from LiDAR data is largely dependent on the scale of observation, and mapping at multiple scales often provides an effective approach to slope failure inventory mapping (Glenn et al., 2006; Burns and Madin, 2009; Burns et al., 2012). A scale of 1:8,000 to 1:3,000 is commonly used and was effective for this study (Burns and Madin; Glenn et al., 2006; Seijmonsbergen and de Graaff, 2006; Burns et al., 2012; Burns and Mickelson, 2016).

Slope failure deposits along the Teton range front were mapped at a scale of 1:3,000 using ArcGIS 10.7 and LiDAR-derived hillshade and slope maps (Figure 11). The mapped deposits generally fall into two movement classifications: slides and flows. The materials involved are typically rock, earth, debris, or some combination of these materials. North of Leigh Lake, translational slide deposits are more common than debris flow deposits. Slide deposits tend to be larger in this area than those found in the southern half of the study area, covering up to 2.4 km^2. South of Leigh Lake, translational slide deposits up to 2.3 km^2 were mapped, but the majority of deposits are <0.5 km^2. Several of the larger slide deposits contain smaller slides within their borders, indicating that the southern half of the study area is prone to more frequent slope failure events than the northern half. Most debris flow deposits are also found along the southern half of the study area and typically occur on south-facing slopes of steeply sided canyons (e.g., Granite Canyon; Figure 23).

LiDAR-based mapping combined with field confirmation in selected areas allows rapid reconnaissance of the fault zone

LiDAR-based identification of fault scarps, slope failures, and other geomorphic features is particularly useful in areas where thick vegetation, rough terrain, or other concerns make field mapping difficult (Harding and Berghoff, 2000; Glenn et al., 2006; Burns and Madin, 2009; Amos et al., 2010; Clift and Springston, 2012; Haddon et al., 2016). Bare-earth topographic models reveal surface features that might otherwise not be observed using traditional field mapping approaches. This study coupled together LiDAR-based mapping of fault scarps, glacial features, and slope failure deposits, and traditional geomorphic field mapping in selected areas to identify and characterize landform elements throughout the study area. This approach very effective at reducing mapping errors and clarifying landform identification while reducing the time and effort required to map the study area. In addition to reducing the time and effort required to map features in difficult terrain, LiDAR- and GIS-based mapping offers an effective approach to understanding the relationships between topography, geology, soils, vegetation, hydrological data, and other factors that are key to addressing slope failure and other natural hazards (Seijmonsbergen and de Graaff, 2006; Burns and Madin, 2009; Amos et al., 2010; Haddon et al., 2016; Thackray and Staley, 2017). Coupling LiDAR data, GIS-based mapping, and field reconnaissance can improve mapping accuracy and reduce the time and expense associated with traditional field mapping approaches.

References

Aleotti, P., and Chowdhury, R., 1999, Landslide hazard assessment: summary review and new perspectives: Bulletin of Engineering Geology and the Environment, v. 58, p. 21–44, doi:10.1007/s100640050066.

Amos, C.B., Kelson, K.I., Rood, D.H., Simpson, D.T., and Rose, R.S., 2010, Late Quaternary slip rate on the Kern Canyon fault at Soda Spring, Tulare County, California: Lithosphere, v. 2, p. 411–417, doi:10.1130/L100.1.

Arrowsmith, J.R., Rhodes, D.D., and Pollard, D.D., 1998, Morphologic dating of scarps formed by repeated slip events along the San Andreas Fault, Carrizo Plain, California: Journal of Geophysical Research: Solid Earth, v. 103, p. 10141–10160, doi:10.1029/98JB00505.

Ballantyne, C.K., 2002, A general model of paraglacial landscape response: The Holocene, v. 3, p. 371–376.

Barrientos, S.E., Stein, R.S., and Ward, S.N., 1987, Comparision fo the 1959 Hebgen Lake, Montana and the 1983 Borah Peak, Idaho, earthquakes from geodetic observations: Bulletin of the Seismological Society of America, v. 77, p. 784–808.

Brocklehurst, S.H., and Whipple, K.X., 2006, Assessing the relative efficiency of fluvial and glacial erosion through simulation of fluvial landscapes: Geomorphology, v. 75, p. 283–299, doi:10.1016/j.geomorph.2005.07.028.

Brown, S.J., Thigpen, J.R., Spotila, J.A., Krugh, W.C., Tranel, L.M., and Orme, D.A., 2017, Onset Timing and Slip History of the Teton Fault, Wyoming: A Multidisciplinary Reevaluation: Timing of Onset of the Teton Fault: Tectonics, v. 36, p. 2669–2692, doi:10.1002/2016TC004462.

Bucknam, R.C., and Anderson, R.E., 1979, Estimation of fault-scarp ages from a scarp-height-slope-angle relationship: Geology, v. 7, p. 11–14.

Burbank, D.W., Leland, J., Fielding, E., Anderson, R.S., Brozovic, N., Reid, M.R., and Duncan, C., 1996, Burbank et al., 1996. Bedrock incision, rock uplift and threshold hillslopes in the northwestern Himalayas: Nature, v. 379, p. 505–510.

Burns, W.J., and Madin, I.P., 2009, Protocol for Inventory Mapping of Landslide Deposits from Light Detection and Ranging (lidar) Imagery: Oregon Department of Geology and Mineral Industries Special Paper 42, 36 p., https://www.oregongeology.org/pubs/dds/slido/sp-42_onscreen.pdf.

Burns, W.J., Madin, I.P., and Mickelson, K.A., 2012, Protocol for shallow-landslide susceptibility mapping.pdf: Oregon Department of Geology and Mineral Industries Special Paper 45, 38 p.

Byrd, J.O.D., 1995, Neotectonics of the Teton fault, Wyoming [Dissertation]: University of Utah, 215 p.

Byrd, J.O.D., Smith, R.B., and Geissman, J.W., 1994, The Teton fault, Wyoming: Topographic signature, neotectonics, and mechanisms of deformation: Journal of Geophysical Research, v. 99, p. 20095–20122.

Clift, A.E., and Springston, G., 2012, Protocol for Identification of Areas Sensitive to Landslide Hazards in Vermont: Vermont Geological Survey Technical Report, p. 1-102.

Cowie, P.A., and Roberts, G.P., 2001, Constraining slip rates and spacings for active normal faults: Journal of Structural Geology, v. 23, p. 1901–1915, doi:10.1016/S0191-8141(01)00036-0.

Cowie, P.A., and Scholz, C.H., 1992, Growth of faults by accumulation of seismic slip: Journal of Geophysical Research, v. 97, p. 11085, doi:10.1029/92JB00586.

Crawford, M.M., 2012, Using LiDAR to Map Landslides in Kenton and Campbell Counties, Kentucky: Kentucky Geological Survey Report of Investigations, p. 1–12.

Crone, A.J., and Machette, M.N., 1984, Surface faulting accompanying the Borah Peak earthquake and segmentation of the Lost River fault, central Idaho: Geology, v. 12, p. 664–667.

Densmore, A.L., Gupta, S., Allen, P.A., and Dawers, N.H., 2007, Transient landscapes at fault tips: Journal of Geophysical Research, v. 112, p. 16, doi:10.1029/2006JF000560.

DePolo, C.M., Clark, D.G., Slemmons, B.D., and Ramelli, A.R., 1991, Historical surface faulting in the Basin and Range province, western North America: implications for fault segmentation: Journal of Structural Geology, v. 13, p. 123–136, doi:10.1016/0191-8141(91)90061-M.

Doser, D.I., and Smith, R.B., 1983, Seismicity of the Teton-Southern Yellowstone Region, Wyoming: Bulletin of the Seismological Society of America, v. 73, p. 1369–1394.

DuRoss, C.B., Gold, R.D., Briggs, R.W., Delano, J.E., Ostenaa, D.A., Zellman, M.S., Cholewinski, N., Wittke, S.J., and Mahan, S.A., 2019a, Holocene earthquake history and slip rate of the southern Teton fault, Wyoming, USA: GSA Bulletin, doi:10.1130/B35363.1.

DuRoss, C.B., Gold, R.D., Briggs, R.W., Delano, J., Ostenaa, D., Zellman, M., Cholewinski, N., Wittke, S., and Mahan, S., 2019b, Paleoseismic history and slip rate of the Teton fault at the Buffalo Bowl site: Seismological Society of America Annual Meeting, April 27-30, Albuquerque, New Mexico.

DuRoss, C.B., and Hylland, M.D., 2015, Synchronous Ruptures along a Major Graben-Forming Fault System: Wasatch and West Valley Fault Zones, Utah: Bulletin of the Seismological Society of America, v. 105, p. 14–37, doi:10.1785/0120140064.

DuRoss, C.B., Personius, S.F., Crone, A.J., Olig, S.S., Hylland, M.D., Lund, W.R., and Schwartz, D.P., 2016, Fault segmentation: New concepts from the Wasatch Fault Zone, Utah, USA: Journal of Geophysical Research: Solid Earth, v. 121, p. 1131–1157, doi:10.1002/2015JB012519.

Faulds, J.E., and Varga, R.J., 1998, The role of accommodation zones and transfer zones in the regional segmentation of extended terranes, in Accommodation zones and transfer zones; the regional segmentation of the Basin and Range Province: Geological Society of America, Special Paper 323, p. 1-45, doi:10.1130/0-8137-2323-X.1.

Fossen, H., and Rotevatn, A., 2016, Fault linkage and relay structures in extensional settings- a review: Earth Science Reviews, v. 154, p. 14–28, doi:10.1016/j.earscirev.2015.11.014.

Foster, D., Brocklehurst, S.H., and Gawthorpe, R.L., 2010, Glacial-topographic interactions in the Teton Range, Wyoming: Journal of Geophysical Research, v. 115, p. F01007, doi:10.1029/2008JF001135.

Foster, D., Brocklehurst, S.H., and Gawthorpe, R.L., 2008, Small valley glaciers and the effectiveness of the glacial buzzsaw in the northern Basin and Range, USA: Geomorphology, v. 102, p. 624–639, doi:10.1016/j.geomorph.2008.06.009.

Gilbert, J.D., Ostenaa, D., and Wood, C., 1983, Seismotectonic study, Jackson Lake Dam and Reservoir, Minidoka Project, Wyoming: U.S. Bureau of Reclamation Seismotectonic Report 83–8, 122 p.

Glenn, N.F., Streutker, D.R., Chadwick, D.J., Thackray, G.D., and Dorsch, S.J., 2006, Analysis of LiDAR-derived topographic information for characterizing and differentiating landslide morphology and activity: Geomorphology, v. 73, p. 131–148, doi:10.1016/j.geomorph.2005.07.006.

Goudie, A. (Ed.), 2004, Encyclopedia of geomorphology: London; New York, Routledge : International Association of Geomorphologists, v. 1, 1202 p.

Guthrie, R., 2017, The emergence of geohazards as a profession in North America: Geotechnical News,.

Haddon, E.K., Amos, C.B., Zielke, O., Jayko, A.S., and Burgmann, R., 2016, Surface slip during large Owens Valley earthquakes: Geochemistry Geophysics Geosystems, v. 17, p. 2239–2269, doi:10.1002/2016GC006406.

Hadley, J.B., 1978, Madison Canyon Rockslide, Montana, U.S.A., *in* Developments in Geotechnical Engineering, Elsevier, v. 14, Part A, p. 167–180, doi:10.1016/B978-0-444-41507-3.50012-X.

Hallet, B., Hunter, L., and Bogen, J., 1996, Rates of erosion and sediment evacuation by glaciers: A review of field data and their implications: Global and Planetary Change, v. 12, p. 213–235, doi:10.1016/0921-8181(95)00021-6.

Hampel, A., Hetzel, R., and Densmore, A.L., 2007, Postglacial slip-rate increase on the Teton normal fault, northern Basin and Range Province, caused by melting of the Yellowstone ice cap and deglaciation of the Teton Range? Geology, v. 35, p. 1107–1110, doi:10.1130/G24093A.1.

Harding, D.J., 2000, Fault scarp detection beneath dense vegetation cover: airborne LiDAR mapping of the Seattle fault zone, Bainbridge Island, Washington State, *in* Proceedings of the American Society of Photograpmmetry and Remote Sensing Annual Conference, Washington, D.C., American Society of Photogrammetry and Remote Sensing, p. 11.

Havenith, H.B., Vanini, M., Jongmans, D., and Faccioli, E., 2003, Initiation of earthquake-induced slope failure: influence of topographical and other site specific amplification effects: Journal of Seismology, v. 7, p. 397–412.

Highland, L.M., and Bobrowsky, P., 2008, The Landslide Handbook- A guide to Understanding Landslides: United States Geological Survey Circular Handbook, 42 p.

Keefer, D.K., 1984, Landslides caused by earthquakes: Geological Society of America Bulletin, v. 95, p. 406–421.

Kim, G., Yune, C.Y., Paik, J., and Lee, S.W., 2016, Analysis of debris flow behavior using airborne LiDAR and image data: International Archives of the Photogrammetry, Remote Sensing and Spatial Information Sciences - ISPRS Archives, v. 41, p. 85–88, doi:10.5194/isprsarchives-XLI-B8-85-2016.

King, G., 1983, The accommodation of large strains in the upper lithosphere of the earth and other solids by self-similar fault systems: the geometrical origin of b-Value: Pure and Applied Geophysics PAGEOPH, v. 121, p. 761–815, doi:10.1007/BF02590182.

Lageson, D.L., 1992, Possible Laramide influence on the Teton normal fault, western Wyoming.pdf, *in* Regional Geology of Eastern Idaho and Western Wyoming, Geological Society of America, Memoir, v. 179, 14 p.

Larsen, D.J., Crump, S.E., Abbott, M.B., Harbert, W., Blumm, A., Wattrus, N.J., and Hebberger, J.J., 2019, Paleoseismic Evidence for Climatic and Magmatic Controls on the Teton Fault, WY: Geophysical Research Letters, v. 46, p. 13036–13043, doi:10.1029/2019GL085475.

Larsen, D.J., Finkenbinder, M.S., Abbott, M.B., and Ofstun, A.R., 2016, Deglaciation and postglacial environmental changes in the Teton Mountain Range recorded at Jenny Lake, Grand Teton National Park, WY: Quaternary Science Reviews, v. 138, p. 62–75, doi:10.1016/j.quascirev.2016.02.024.

Leopold, E.B., Liu, G., Love, J.D., and Love, D.W., 2007, Plio-Pleistocene climatic transition and the lifting of the Teton Range, Wyoming: Quaternary Research, v.67, 11p., doi:10.1016/j.yqres.2006.10.006.

Licciardi, J.M., and Pierce, K.L., 2008, Cosmogenic exposure-age chronologies of Pinedale and Bull Lake glaciations in greater Yellowstone and the Teton Range, USA: Quaternary Science Reviews, v. 27, p. 814–831, doi:10.1016/j.quascirev.2007.12.005.

Licciardi, J.M., and Pierce, K.L., 2018, History and dynamics of the Greater Yellowstone Glacial System during the last two glaciations: Quaternary Science Reviews, v. 200, 33 p., doi:10.1016/j.quascirev.2018.08.027.

Licciardi, J., Pierce, K.L., Finkel, R.C., and Zimmerman, S.H., 2014a, Expanded chronology of Late Pleistocene glacial events in the greater Yellowstone and Grand Teton regions: Geological Society of America, v. Rocky Mountain (66th Annual) and Cordilleran (110th Annual) Joint Meeting, 1 p.

Licciardi, J.M., Pierce, K.L., Finkel, R.C., and Zimmerman, S.H., 2014b, Timing of late Pleistocene glacier culminations and retreat in Grand Teton National Park: Geological Society of America 2014 Annual Meeting Abstracts with Programs, v. 46, no. 6.

Licciardi, J.M., Pierce, K.L., Thackray, G.D., Finkel, R.C., and Zimmerman, S.R.H., 2015, Cosmogenic 10Be Chronologies of Moraines and Glacially Scoured Bedrock in the Teton Range, with Implications for Paleoclimatic Events and Tectonic Activity: AGU Fall Meeting Abstracts, v. 51, p. PP51E-02.

Licciardi, J., Pierce, K., Thackray, G., Zellman, M., Larsen, D., and Schweinsberg, A., 2019, Late Pleistocene glacier chronologies and fault slip rates in the Teton Range, USA, revealed by 10Be dating of fault-displaced moraines: International Union for Quaternary Research, Dublin, Ireland, https://app.oxfordabstracts.com/events/574/program-app/submission/91357.

Love, J.D., 1977, Summary of upper Cretaceous and Cenozoic stratigraphy, and of tectonic and glacial events in Jackson Hole, Northwestern Wyoming.pdf: Rocky Mountain Thrust Belt Geology and Resources 29th Annual Field Conference Guidebook, p. 585–593.

Love, J.D., Reed, J.C., and Christiansen, A.C., 1992, Geologic Map of Grand Teton National Park, Teton County, Wyoming: United States Geological Survey, 1 p.

Love, D.J., Reed, J.C., Jr., and Pierce, K.L., 2003, Creation of the Teton landscape: Moose, WY, Grand Teton History Association in cooperation with the National Park Service, 132 p.

Machette, M.N., Personius, S.F., Nelson, A.R., Schwartz, D.P., and Lund, W.R., 1991, The Wasatch fault zone, Utah—segmentation and history of Holocene earthquakes: Journal of Structural Geology, v. 13, p. 137–149, doi:10.1016/0191-8141(91)90062-N.

Marston, R.A., Weihs, B.J., and Butler, W.D., 2010, Slope Failures and Cross-Valley Profiles, Grand Teton National Park, Wyoming: University of Wyoming National Park Service Research enter, v. 33, p. 15.

McCalpin, J.P. (Ed.), 1996, Paleoseismology: San Diego, California, Academic Press, 588 p.

McColl, S.T., and Davies, T.R.H., 2013, Large ice-contact slope movements: Glacial buttressing, deformation and erosion: Earth Surface Processes and Landforms, v. 38, p. 1102–1115, doi:10.1002/esp.3346.

Mora, O.E., Liu, J., Gabriela Lenzano, M., Toth, C.K., and Grejner-Brzezinska, D.A., 2015, Small Landslide Susceptibility and Hazard Assessment Based on Airborne Lidar Data: Photogrammetric Engineering & Remote Sensing, v. 81, p. 239–247, doi:10.14358/PERS.81.3.239-247.

Morgan, L.A., and McIntosh, W.C., 2005, Timing and development of the Heise volcanic field, Snake River Plain, Idaho, western USA: Geological Society of America Bulletin, v. 117, p. 288, doi:10.1130/B25519.1.

Nash, D.B., 1984, Morphologic dating of fluvial terrace scarps and fault scarps near West Yellowstone, Montana: Geological Society of America Bulletin, v. 95, p. 1413–1424.

O'Connell, D.R.H., Wood, C.K., Ostenaa, D.A., Block, L.V., and LaForge, R.C., 2003, Ground Motion Evaluation for Jackson Lake Dam, Min-min.pdf: Seismotectonics and Geophysics Group, Technical Service Center, Bureau of Reclamation Final Report 2003–2, 493 p.

Ostenaa, D.A., 1988, Late Quaternary behavior of the Teton fault, Wyoming: Geological society of America Abstracts with Programs, v. 20, p. A14.

Pavlopoulos, K., Evelpidou, N., and Vassilopoulos, A., 2009, Mapping geomorphological environments: Heidelberg; New York, Springer, 247 p.

Petersen, M.D. et al., 2014, Documentation for the 2014 Update of the United States National Seismic Hazard Maps: U.S. Geological Survey Open-File Report Open-File Report 2014–1091, 255 p., https://pubs.er.usgs.gov/publication/ofr20141091.

Petley, D.N., 1998, Geomorphological Mapping for Hazard Assessment in a Neotectonic Terrain: The Geographical Journal, v. 164, p. 183–201, doi:10.2307/3060369.

Phillips, F.M., Ayarbe, J.P., Harrison, B.J., and Elmore, D., 2003, Dating rupture events on alluvial fault scarps using cosmogenic nuclides and scarp morphology: Earth and Planetary Science Letters, v. 215, p. 203–218.

Pierce, K.L., and Colman, S.M., 1986, Effect of height and orientation (microclimate) on geomorphic degradation rates and processes, late-glacial terrace scarps in central Idaho: Geological Society of America Bulletin, v. 97, p. 869–885.

Pierce, K.L., and Good, J.D., 1992, Field Guide to the Quaternary Geology of Jackson Hole, Wyoming: United States Geological Survey Open-File Report 92–504, 59 p.

Pierce, K.L., Licciardi, J.M., Good, J.M., and Jaworowski, C., 2018, Pleistocene Glaciation of the Jackson Hole Area, Wyoming: U.S. Geological Survey Professional Paper 1835: U.S. Geological Survey Professional Paper 1835, 68 p.

Pierce, K.L., Muhs, D.R., Fosberg, M.A., Mahan, S.A., Rosenbaum, J.G., Licciardi, J.M., and Pavich, M.J., 2011, A loess-paleosol record of climate and glacial history over the past two glacial-interglacial cycles (~150ka), southern Jackson Hole, Wyoming: Quaternary Research, v. 76, p. 119–141, doi:10.1016/j.yqres.2011.03.006.

Roberts, S.V., and Burbank, D.W., 1993, Uplift and thermal history of the Teton Range (northwestern Wyoming) defined by apatite fission-track dating: Earth and Planetary Science Letters, v. 118, p. 295–309, doi:10.1016/0012-821X(93)90174-8.

Rodríguez-Peces, M.J., García-Mayordomo, J., Azañón, J.M., and Jabaloy, A., 2014, GIS application for regional assessment of seismically induced slope failures in the Sierra Nevada Range, South Spain, along the Padul Fault: Environmental Earth Sciences, v. 72, p. 2423–2435, doi:10.1007/s12665-014-3151-7.

Romeo, R., 2000, Seismically induced landslide displacements: a predictive model: Engineering Geology, v. 58, p. 337–351, doi:10.1016/S0013-7952(00)00042-9.

Schulz, W., 2004, Landslides mapped using LiDAR imagery, Seattle, Washington: U.S. Geological Survey Open-File Report 2004–1396.

Schwartz, D.P., and Coppersmith, K.J., 1984, Fault behavior and characteristic earthquakes: Examples from the Wasatch and San Andreas Fault Zones: Journal of Geophysical Research: Solid Earth, v. 89, p. 5681–5698, doi:10.1029/JB089iB07p05681.

Scott, D.W., 2009, Sturges' rule: Wiley Interdisciplinary Reviews: Computational Statistics, v. 1, p. 303–306, doi:10.1002/wics.35.

Seijmonsbergen, A.C., and de Graaff, L.W.S., 2006, Geomorphological mapping and geophysical profiling for the evaluation of natural hazards in an alpine catchment: Natural Hazards and Earth System Science, v. 6, p. 185–193, doi:10.5194/nhess-6-185-2006.

Shroder, J.F.Jr., and Weihs, B.J., 2017, Mass-Movement Disturbance Regime Landscapes, Hazards, and Water Implications: Grand Teton National Park: v. 36, p. 15.

Silva, F., Lambe, T.W., and Marr, W.A., 2008, Probability and Risk of Slope Failure: Journal of Geotechnical and Geoenvironmental Engineering, v. 134, p. 1691–1699, doi:10.1061/(ASCE)1090-0241(2008)134:12(1691).

Smith, R.B., Byrd, J.O.D., and Susong, D.D., 1993, The Teton Fault, Wyoming; seismotectonics, Quaternary history, and earthquake hazards: Geological Survey of Wyoming Memoir, v. 5, p. 628–667.

Spotila, J.A., Buscher, J.T., Meigs, A.J., and Reiners, P.W., 2004, Long-term glacial erosion of active mountain belts: Example of the Chugach–St. Elias Range, Alaska: Geology, v. 32, p. 501, doi:10.1130/G20343.1.

Susong, D.L., Smith, R.B., and Bruhn, R.L., 1987, Earthquake Hazards of the Grand Teton National Park Emphasizing the Teton Fault: v. 11, p. 26.

Swan, F.H.I., Schwartz, D.P., and Cluff, L.S., 1980, Swan et al., 1980. Recurrence of moderate to large magnitude earthquakes produced by surface faulting on the Wasatch fault zone, Utah.pdf: Bulletin of the Seismological Society of America, v. 70, p. 1431–1462.

Thackray, G.D., Rodgers, D.W., and Streutker, D., 2013, Holocene scarp on the Sawtooth fault, central Idaho, USA, documented through lidar topographic analysis: Geology, v. 41, p. 639–642, doi:10.1130/G34095.1.

Thackray, G.D., and Staley, A.E., 2017, Systematic variation of Late Pleistocene fault scarp height in the Teton Range, Wyoming, USA: Variable fault slip rates or variable landform ages? Geosphere, v. 13, p. 287–300, doi:10.1130/GES01320.1.

Thompson, S.C., Weldon, R.J., Rubin, C.M., Abdrakhmatov, K., Molnar, P., and Berger, G.W., 2002, Late Quaternary slip rates across the central Tien Shan, Kyrgyzstan, central Asia: SLIP RATES ACROSS THE KYRGYZ TIEN SHAN: Journal of Geophysical Research: Solid Earth, v. 107, p. ETG 7-1-ETG 7-32, doi:10.1029/2001JB000596.

Tranel, L.M., Spotila, J.A., Binnie, S.A., and Freeman, S.P.H.T., 2015, Quantifying variable erosion rates to understand the coupling of surface processes in the Teton Range, Wyoming: Geomorphology, v. 228, p. 409–420, doi:10.1016/j.geomorph.2014.08.018.

Tranel, L.M., Spotila, J.A., Kowalewski, M.J., and Waller, C.M., 2011, Spatial variation of erosion in a small, glaciated basin in the Teton Range, Wyoming, based on detrital apatite (U-Th)/He thermochronology: Spatial variation of erosion in a small, glaciated basin in the Teton Range, Wyoming: Basin Research, v. 23, p. 571–590, doi:10.1111/j.1365-2117.2011.00502.x.

Tranel, L.M., and Strow, M.L., 2017, 10Be analysis of amalgamated talus pebbles to investigate alpine erosion, Garnet Canyon, Teton Range, Wyoming: Geosphere, v. 13, p. 36–48, doi:10.1130/GES01297.1.

Tucker, G.E., McCoy, S.W., Whittaker, A.C., Roberts, G.P., Lancaster, S.T., and Phillips, R., 2011, Geomorphic significance of postglacial bedrock scarps on normal-fault footwalls: Journal of Geophysical Research, v. 116, p. 14, doi:10.1029/2010JF001861.

Valagussa, A., Marc, O., Frattini, P., and Crosta, G.B., 2019, Seismic and geological controls on earthquake-induced landslide size: Earth and Planetary Science Letters, v. 506, p. 268–281, doi:10.1016/j.epsl.2018.11.005.

Wallace, R.E., 1977, Wallace, 1977. Profiles and ages of young fault scarps, north-central Nevada.pdf: Geological Society of America Bulletin, v. 88, p. 1267–1281.

Walsh, J.J., Bailey, W.R., Childs, C., Nicol, A., and Bonson, C.G., 2003, Formation of segmented normal faults: a 3-D perspective: Journal of Structural Geology, v. 25, p. 1251–1262, doi:10.1016/S0191-8141(02)00161-X.

White, B.J.P., 2006, Seismicity, Seismotectonics and Preliminary Earthquake Hazard Analysis of the Teton Region, Wyoming [PhD Thesis]: University of Utah.

White, B.J.P., Smith, R.B., Husen, S., Farrell, J.M., and Wong, I., 2009, Seismicity and earthquake hazard analysis of the Teton-Yellowstone region, Wyoming: Journal of Volcanology and Geothermal Research, v. 188, p. 277–296, doi:10.1016/j.jvolgeores.2009.08.015.

Woolpert, Inc., 2015, Grand Teton and National Elk Refuge Airborne LiDAR Task Order Report: LiDAR data report, 48 p.

Wyoming Geographic Information Science Center, 1997, Digital Elevation Model for Wyoming 90 meter: Wyoming Geographic Information Science Center Digital, https://www.geospatialhub.org/datasets/58d88faf67c34677b94a69a6daba4d7c.

Zellman, M., DuRoss, C., and Thackray, G., 2019a, The Teton Fault Teton County, Wyoming: Wyoming Geological Survey Open File Report 2019–1, 1 p.

Zellman, M.S., DuRoss, C.B., and Thackray, G.D., 2019b, The Teton Fault, Teton County, Wyoming: Wyoming Geological Survey Map.

Zellman, M.S., DuRoss, C.B., Thackray, G.D., Briggs, R.W., Cholewinski, N., Reyes, T., Patton, N., and Mahan, S.A., 2018, A Paleoseismic Investigation of the Northern Teton Fault at the Steamboat Mountain Trench Site, Grand Teton National Park, Wyoming: https://www.researchgate.net/publication/328475804_Paleoseismic_Investigation_of_the_Teton_Fault_at_Leigh_Lake.

Zellman, M.S., DuRoss, C.B., Thackray, G.D., Personius, S.F., Reitman, N.G., Mahan, S.A., and Brossy, C.C., 2019c, Holocene Rupture History of the Central Teton Fault at Leigh Lake, Grand Teton National Park, Wyoming: Bulletin of the Seismological Society of America, p. 16, doi:10.1785/0120190129.